THEORETICAL STUDY OF DRUG ACTION IN A SODIUM CHANNEL

THEORETICAL STUDY OF STATE-DEPENDENT ACTION OF TOXINS AND DRUGS IN A VOLTAGE GATED SODIUM CHANNEL

By

DANIEL GARDEN, B. Sc.

A Thesis

Submitted to the School of Graduate Studies

in Partial Fulfillment of the Requirements

for the Degree of

Doctor of Philosophy

McMaster University

DOCTOR OF PHILOSOPHY (2011) McMaster University

(Biochemistry and Biomedical Sciences) Hamilton, Ontario

TITLE: THEORETICAL STUDY OF STATE-DEPENDENT ACTION OF TOXINS AND DRUGS IN A VOLTAGE GATED SODIUM CHANNELS

AUTHOR: Daniel P. Garden, B. Sc. (McMaster University)

SUPERVISOR: Professor Boris S. Zhorov

NUMBER OF PAGES: xi, 129

ABSTRACT

Ion permeation through voltage gated sodium channels is modulated by many drugs and toxins. However, the atomistic mechanisms of action of most these ligands are poorly understood. This study focuses on three compounds: a steroidal alkaloid batrachotoxin (BTX), a pyrethroid insecticide deltamethrin, and an alkylamide insecticide BTG 502, which bind to distinct but allosterically coupled receptor sites. BTX belongs to the class of the sodium channel agonists (activators), which cause persistent channel activation by inhibiting channel inactivation. Traditionally, BTX is believed to bind at the channel-lipid interface and allosterically modulate ion permeation through the channel. However, in the last decade, amino acid residues that affect BTX action have been found in the pore-facing inner helices of all four domains, suggesting that BTX binds in the channel pore (Tikhonov and Zhorov, *FEBS Letters* 2005). An alkylamide insecticide BTG 502 reduces sodium currents and antagonizes the action of BTX on cockroach sodium channels, suggesting that it also binds inside the pore. Conversely, pyrethroids bind at the lipid-exposed cavity formed by a short intracellular linker-helix IIS4-S5 and transmembrane helices IIS5 and IIIS6.

In this study we first developed a new method of electrostatic-energy calculations, a new protocol of ligand docking, and tested this methodology on 60 ligand-protein complexes of known structure (Garden and Zhorov 2010). We then applied this methodology to rationalize effects of various mutations in the domain III inner helix of the cockroach sodium channel BgNav1.1 on the action of BTX, BTG 502 and deltamethrin. Our collaborators, Dr. Ke Dong et al. from Michigan State University, mutated all residues in the pore-lining helix of domain III (IIIS6) and found several new BTX and BTG 502 sensing residues. Using these data along with other published data on BTX- and deltamethrin-sensing residues as distance constrains, we docked BTX, BTG 502 and deltamethrin in a Kv1.2-based homology model of the open BgNav1.1 channel. We arrived at models, which are consistent with all currently available data on the action of the ligands. In the BTX-binding model, the toxin adopts a “horseshoe” conformation and binds in the channel pore with the horseshoe plane normal to the pore axis. In this binding mode BTX allows would allow ion permeation through the hydrophilic inner face of the horseshoe, and resist the activation-gate closure. Various BTX moieties interact with known BTX sensing residues. In particular, the tertiary ammonium group of BTX is engaged in cation-π interactions with the newly discovered BTX-sensing residue Phe^{3i16}. In the BTG 502-binding model, the ligand wraps around IIIS6 making direct contacts with all known BTG 502-sending residues, including buried residues on the IIIS6 helix side, which does not face the pore. Deltamethrin binds within the cavity formed by the linker-helix IIS4-S5, the outer helix IIS5, and the inner helix IIIS6 at the interface between domains II and III, similar to the pyrethroid-binding mode predicted by others (O'Reilly, Khambay et al. 2006). Our study revealed a unique mode of action of BTX in which the agonists enables the ion permeation by forming a “channel within a channel”. We also found that the BTG 502 receptor site overlaps with receptors for BTX and deltamethrin, which are located in different parts of the channel.

ACKNOWLEDGEMENTS

My time at McMaster University was a remarkable experience because of the people I had an opportunity to meet. There are far too many to name individually here, but there are a few special ones that have made profound impacts on my life.

"Truly great friends are hard to find, difficult to leave, and impossible to forget." – G. Randolf

I would like to thank the many friends who have made my time more enjoyable than I could have ever imagined. My lab mates Iva and Ricky, who made every day unique. Kevin, Jack, Joel and Yulia from neighboring labs, for making lunch breaks the best time of the day. My lifelong friends, Bridget, Peter, Anand and David, for keeping my life in balance.

"Teachers teach more by what they are than by what they say" – Anonymous

After spending the majority of my academic career working with Professor Boris Zhorov, I can say with confidence, he is by far the greatest supervisor I will ever have. From his motivational ability to his genuine, heartfelt concern for his students' careers and beyond, his leadership is unparalleled and will be missed. I have also been guided by an exceptional group of scientist, Dr. Denis Tikhonov, Dr. Daniel Yang and Dr. Giuseppe Melacini, whose knowledge and comments have helped me throughout the years.

Finally, I am most thankful to my loving parents John and Betty, for their constant, unwavering support and encouragement. My Dad's uncanny ability to learn and my Mom's foresight have helped me through all of my life's challenges. I am very thankful for my brother Benjamin, who continually challenges and inspires me. I could not have hoped for a more perfect younger brother. Lastly to Duke, whose daily routines and playful spirit have always cheered me up. Without my family, I would not have been able to accomplish what I have nor would it have been nearly as meaningful.

TABLE OF CONTENTS

LIST OF FIGURES

LIST OF TABLES

LIST OF ABBREVIATIONS

AGM	Apparent Global Minimum
BgNav1.1	A voltage gated sodium channel from cockroach
BTG 502	A Na^+ channel antagonist
BTX	Batrachotoxin, a Na^+ channel agonist
CNG	Cyclic Nucleotide Gated
DDD	Distance-Dependent Dielectric
DEKA	Asp-Glu-Lys-Ala residues forming the selectivity filter of Na^+ channels
EEEE	Four glutamate residues forming the selectivity filter of Ca^{2+} channels
KcsA	Proton-gated K+ channel (crystallized in the closed state)
Kv	Voltage gated K+ channels
Kv1.2	A mammalian voltage gated K+ channel (crystallized in the open state)
KvAP	A bacterial voltage gated K+ channel (crystallized in the open state)
MCM	Monte Carlo-energy Minimization
MthK	Bacterial calcium activated K+ channel (crystallized in the open state)
NaK	Non-selective cyclic-nucleotide gated Na^+-K^+ channel
NaChBac	Bacterial voltage gated sodium channel
Nav	Voltage gated Na+ channels
P-loop	Membrane-diving re-entrant loop between transmembrane helices S5 and S6
PD	Pore Domain
PDB	Protein Data Bank
PVP	Pro-Val-Pro motif in the inner helices of Kv channels
RMSD	Root Mean Square Deviation
SEDDD	Solvent Exposure- and Distance-Dependent Dielectric
VSD	Voltage-Sensor Domain

CHAPTER ONE

INTRODUCTION

Ion channels are integral membrane proteins that play underlying roles in many fundamental biological processes including the electrical signaling of the nervous system. They regulate the flow of specific ions through the cell membrane by opening and closing the central pore in response to an external stimulus. The movement of ions across the cell membrane has important implications ranging from immune response to sensing touch (Tombola, Pathak et al. 2006). This is made possible by the continually active homeostatic mechanisms that include ion channels and sodium-potassium pumps that maintain a potential gradient across the membrane. A higher extracellular concentration of Na^+ and a higher cellular concentration of K^+ maintains the intracellular side of the membrane at -70mV (Bezanilla 2000). With such a resting potential, rapid depolarization is possible due to the passive movement of ions through ion channels according to their electrochemical gradient. Although Ca^{2+}, Na^+ and K^+ ions differ only moderately in size, ion channels are selective for only a specific ion; an open Na^+ channel permeates Na^+ ions into the cell, increasing the intracellular potential (Catterall 2000). In contrast, an open K^+ channel allows K^+ ions to flow out of the cell, returning the cell to its resting membrane potential (Tombola, Pathak et al. 2006). It might be reasonable to think that since K^+ and Na^+ ions have the same charge, a smaller Na^+ ion would pass through a K^+ channel, however the selectivity filter is discriminating enough to allow only ions of exact size and charge to pass (Heginbotham, Lu et al. 1994). Channels have evolved so that the distances between the permeating ion and chemical groups that line the selectivity filter make binding of a smaller ion energetically unfavourable due to the desolvation cost of water molecules around the ion.

In the past, ion channels were named based on their corresponding gene product, which often caused confusing nomenclature. A unified nomenclature is currently used for mammalian K^+ (Chandy and Gutman 1993), Na^+ (Goldin, Barchi et al. 2000) and Ca^{2+} (Ertel, Campbell et al.

2000) channels. Channels are now named using the chemical symbol of the permeating ion (K, Na, Ca), followed by the principle physiological regulator (voltage or ligand) as a subscript. Finally, a numerical identifier represents the subfamily and the order of discovery within that subfamily (ie. $K_v1.2$, $Ca_v2.1$)

ARCHITECTURE OF ION CHANNELS

Ion channels represent a group of more than 400 transmembrane proteins that respond to various but specific stimuli. The main channel subunits have been identified for various channel families, including the alpha, beta and gamma subunits (Catterall 2000). The alpha subunits are the primary determinant of the channels' physiological characteristics, however, the auxiliary subunits interact directly with the alpha subunits and alter both their properties and localization (Striessnig, Grabner et al. 1998; Kaczorowski and Garcia 1999; Catterall 2000). Most potassium channels are homotetramers, consisting of four identical alpha subunits, each with six transmembrane segments numbered S1 to S6, folded around a central pore. Sodium and calcium channels are composed of a single alpha subunit, which contains four repeats numbered I-IV in a single polypeptide chain. Each repeat is composed of six transmembrane segments and is homologous to a single alpha subunit of a potassium channel (Sato, Ueno et al. 2001) (Figure 1.1).

The S1 to S4 helices together form the voltage sensor domain (VSD), responsible for channel gating (activation and deactivation). Of particular importance is the S4 helix, which contains four positively charged arginine/lysine residues and moves across the membrane and allows the VSD to "sense" the membrane potential (Tombola, Pathak et al. 2006). All members

A

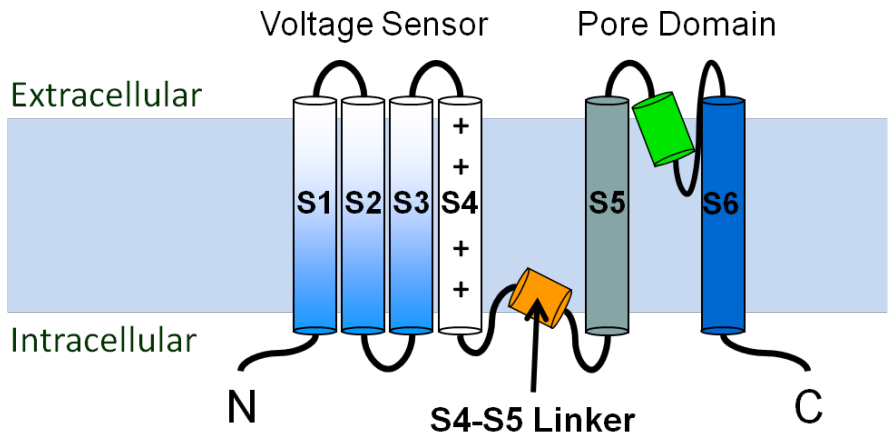

B

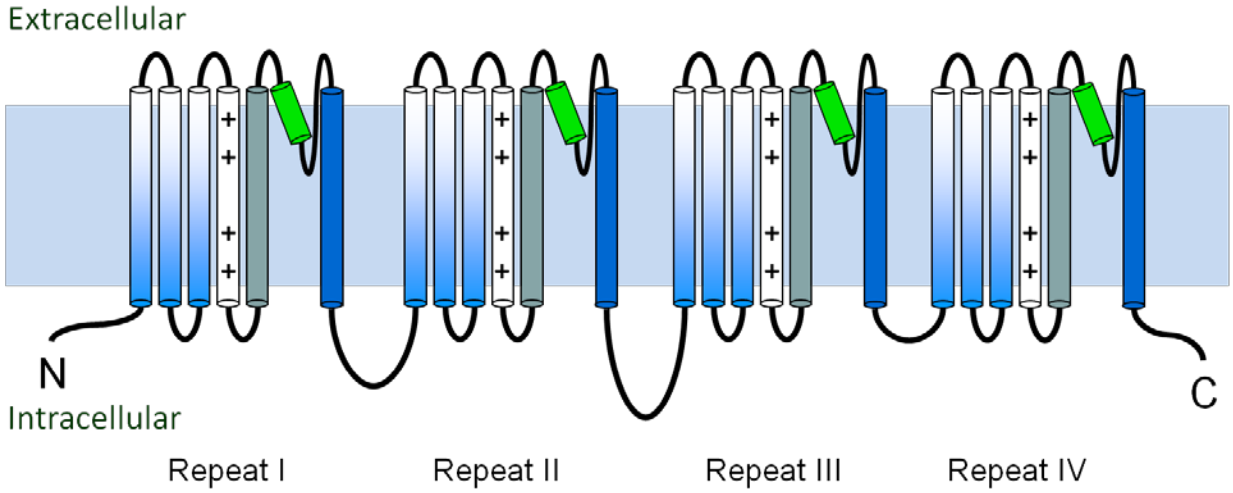

Figure 1.1. General architecture of voltage gated K^+, Na^+ and Ca^{2+} channels. (***A***) Potassium channels are formed by four identical or homologous subunits which self-assemble around the central pore. Each domain contributes to the selectivity filter and the aqueous inner cavity. (***B***) Sodium and calcium channels are heterotetramers, where the four repeats (I-IV) are connected along a single polypeptide chain. Each domain/repeat consists of six transmembrane helices, numbered S1-S6, where S1-S4 form the voltage sensing domain (VSD), S5 and S6 form the pore domain and the re-entrant loop between S5-S6 forms the selectivity filter.

of the voltage-gated superfamily have voltage-dependent gates that open in response to changing membrane potentials and shut quickly after repolarization.

Ion permeation and selectivity is determined by the pore-forming domain, which is connected to the VSD through the S4-S5 linker. The pore-forming domain is composed of four structural motifs, each consists of two transmembrane segments, an outer (S5) and inner helix (S6) (Figure 1.2). The membrane re-entrant loop between these two helices forms the P-loop and selectivity filter. Due to this conserved structural motif, the term P-loop ion channels is often used to refer to tetrameric K^+, Na^+ and Ca^{2+} channels, as well as, to glutamate- and cyclic nucleotide-gated channels.

The ability to distinguish specific ions based on size and charge is the major property of the selectivity filter, and as expected, the selectivity filters of different channel families contain unique sequences. In K^+ channels, the selectivity filter is formed by the backbone carbonyls in the highly conserved TVGYGD sequences from the four subunits (Heginbotham 1994; Doyle, Morais Cabral et al. 1998). In contrast, the selectivity filter of Na^+ channels is formed by the side chains in the ring of highly conserved residues Asp-Glu-Lys-Ala (the DEKA locus) and in Ca^{2+} channels, by four glutamates, the EEEE locus (Heinemann, Terlau et al. 1992; Yang, Ellinor et al. 1993) (Table 1.1). Linker helices between the four voltage sensor domains and the pore domain allow the channel to control the flux of ions across the cell membrane in response to voltage changes. As such, these channels may exist in several different states: closed (resting), open (activated), fast-inactivated and slow-inactivated, however, only in the open state can ions pass through the channel. Currently, most structural data comes from several crystallized K^+ channels, notably, KcsA (Doyle, Morais Cabral et al. 1998), K_vAP (Jiang, Lee et al. 2003; Lee, Lee et al. 2005), MthK (Jiang, Lee et al. 2002) and K_v1.2 (Long, Campbell et al. 2005).

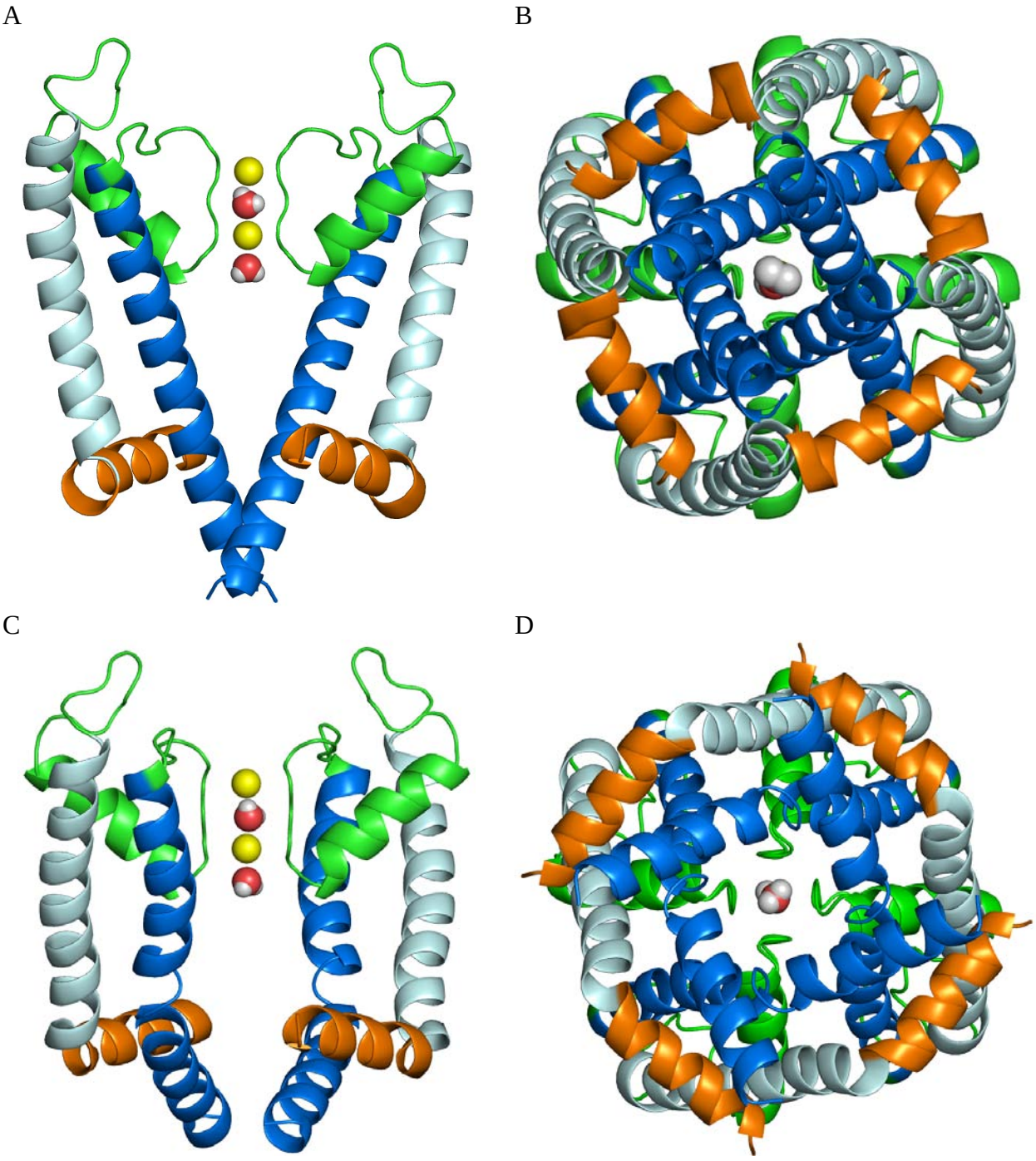

Figure 1.2. The pore domain of the eukaryotic voltage gated potassium channel Kv1.2. The closed state homology model based on the x-ray structure of KcsA shown from the side (***A***) and cytoplasm (***B***). The side (***C***) and cytoplasmic (***D***) views of the open-state x-ray structure of Kv1.2. The S4-S5 linkers are shown in orange, the outer helix (S5) in grey, the pore helices (P) in green ribbons, the selectivity filter (SF) in green strings and the inner helices (S6) in blue. K^+ ions are shown as yellow spheres along with spaced filled water.

Table 1.1. Sequence alignment of voltage gated K^+ and Na^+ channels.

Channel	Domain	Number	Relative Numbers[a] 1	11	
KcsA					
MthK					
KvAP	L45	133	RGSKFLSAIA	DA	
$K_v1.2$	L45	311	SKGLQILGQT	LK	
Shaker	L45	379	SKGLQILGRT	LK	
BgNav1-1	IL45		VPGLKTIVGA	VI	
	IIL45		WPTLNLLISI	MG	
	IIIL45		MQGMRVVVNA	LV	
	IVL45		AKGIRTLLFA	LA	
Channel	Domain	Number	1	11	21
KcsA	M1	23	LHWRAAGAAT	VLLVIVLLAG	SYLAVLAER
MthK	M1	15	VLKVPATRIL	LLVLAVIIYG	TAGFHFIEG
KvAP	S5	144	ADKIRFYHLF	GAVMLTVLYG	AFAIYIVEY
$K_v1.2$	S5	322	ASMRELGLLI	FFLFIGVILF	SSAVYFAEA
Shaker	S5	390	ASMRELGLLI	FFLFIGVVLF	SSAVYFAEG
BgNav1-1	IS5	254	ESVKNLRDVI	ILTMFSLSVF	ALMGLQIYM
	IIS5	899	RTVGALGNLT	FVLCIIIFIF	AVMGMQLFG
	IIIS5	1394	QAIPSIFNVL	LVCLIFWLIF	AIMGVQLFA
	IVS5	1712	MSLPALFNIC	LLLFLVMFIF	AIFGMSFFM
Channel	Domain	Number	33	41	51
KcsA	P	59	LITYPRAL	WWSVETATTV	GYGDLYPV
MthK	P	43	GESWTVSL	YWTFVTIATV	GYGDYSPS
KvAP	P	180	IKSVFDAL	WWAVVTATTV	GYGDVVPA
$K_v1.2$	P	358	FPSIPDAF	WWAVVSMTTV	GYGDMVPT
Shaker	P	426	FKSIPDAF	WWAVVTMTTV	GYGDMTPV
BgNav1-1	IP	289	CIKNFWAF	LSAFRLMTQD	YWENLYQL
	IIP	934	VERFPHSF	MIVFRVLCGE	WIESMWDC
	IIP	1394	STTLSKAY	LCLFQVAT**F**K	GWIQIMND
	IVP	1712	GLDDVQSM	ILLFQMSTSA	GWDGVLDG
Channel	Domain	Number	1	11	21
KcsA	M2	86	LWGRLVAVVV	MVAGITSFGL	VTAALATWFV
Mthk	M2	70	PLGMYFTVTL	IVLGIGTFAV	AVERLLEFLI
KvAP	S6	207	PIGKVIGIAV	MLTGISALTL	LIGTVSNMFQ
$K_v1.2$	S6	385	IGGKIVGSLC	AIAGVLTIAL	PVPVIVSNFN
Shaker	S6	453	VWGKIVGSLC	AIAGVLTIAL	PVPVIVSNFN
BgNav1-1	IS6	391	PWHMLFFIVI	IFLG**S**FYL**VN**	LI**L**AIVAMSY
	IIS6	978	WSCIPFFLAT	VVIG**N**LVV**L**N	LFLALLLSNF
	IIS6	1503	IYMYLYFVFF	I**I**F**GSFF**TLN	LFIGVIIDNF
	IVS6	1803	TVGLAFLLSY	LVIS**F**LIVI**N**	MYIAVILENY

[a] A universal numbering scheme is used that numbers residues according to their position in the sequence alignment.
The selectivity filter of K^+ (GYGD) and Na^+ (DEKA) are shown in red.
Underlined residues have been experimentally determined to decreases BTX activity.
Green residues have been experimentally determined to decreases BTX activity.
Yellow residues were mutated based on the BTX binding mode.

AVAILABLE CRYSTAL STRUCTURES OF ION CHANNELS

High resolution X-ray structures are critical for any molecular modeling study to ensure that the simulations and eventual models. Currently, only a limited number of x-ray structures are available, most of which are from the K^+ channel family. These crystal structures have helped explain a large body of experimental data that was previously not well understood. This includes ion selectivity and permeation, channel gating and mechanisms of channel block.

KcsA

The first channel crystallized was KcsA, a bacterial, proton-gated potassium channel (Doyle, Morais Cabral et al. 1998). Until this structure was solved, there were many uncertainties about the mechanism that discriminates K+ ions from others, yet allow them to pass rapidly though the channel. Indeed, K^+ channels are >10,000 times more permeable for K^+ ions over Na^+ ions, despite the atomic radius of Na^+ (0.95 Å) is smaller than K^+ (1.33 Å). The x-ray structure of KcsA revealed that the selectivity filter is formed by the re-entrant loops of all 4 domains. These create a passageway lined by the main chain carbonyls of four highly conserved amino acid residues (GYGD). Interestingly, the distance between opposite carbonyl oxygens exactly matches the distance between the oxygen atoms in the opposite water molecules of the first hydration shell of the K^+ ion. This match provides an energetically favourable mechanism for dehydration of K^+ ions in the selectivity filter. The probability for a Na^+ ion to pass through the channel is very low because the passageway is wider than the Na+ atomic radius and dehydrating the ion is energetically unfavourable (Doyle, Morais Cabral et al. 1998). Further work with KcsA has revealed mechanism of slow inactivation through structural rearrangements at the selectivity filter (Zhou, Morais-Cabral et al. 2001; Cordero-Morales, Jogini et al. 2007).

The crystal structure shows KcsA in its closed state with the straight inner helices, which form a helical bundle at the C-termini. The bundle crossing functions as the activation gate by closing the cytoplasmic entrance of the channel, preventing ions from entering. A water-filled cavity in the center of the channel between the selectivity filter and the gate is a site where ligands can bind in the open channel and be trapped in the closed channel (Zhou, Morais-Cabral et al. 2001). Ligand binding in the inner cavity is further described in Chapters Two and Three. While logical, the idea that the inner helices would spread apart in the open state to allow ions to enter the inner cavity wasn't known until the structures of the open K^+ channels were solved.

MthK and KvAP

Structure of the bacterial Ca^{2+} gated K+ channel MthK was published first (Jiang, Lee et al. 2002; Jiang, Lee et al. 2002), followed by the bacterial voltage gated K+ channel KvAP (Jiang, Lee et al. 2003; Jiang, Ruta et al. 2003). These studies revealed significant changes in the inner helices between the closed and open conformation. The structures also suggested that the highly conserved glycines in the inner helices play a role in gating (Jiang, Lee et al. 2002). Similarly the Pro-Val-Pro (PVP) motif C-terminal to the conserved glycine allows the helix to kink slightly permitting the cytoplasmic half of the inner helices to diverge wider with less disruption to the extracellular half of the channel. In the open state, the channel's inner pore is wide enough for a variety of channel blockers to enter from the cytoplasm and disrupt the ion permeation (Zhou, Morais-Cabral et al. 2001).

Kv1.2

The next crystallized channel was the mammalian voltage gated K^+ channel Kv1.2, solved in the open conformation (Long, Campbell et al. 2005). Like KvAP, it includes both the pore forming domain and the voltage sensing domain (VSD). It was immediately noticed that the VSD in Kv1.2 is in a more vertical orientation relative to the pore, unlike the horizontal orientation of the VSD KvAP, which also extended outside of the membrane (Long, Campbell et al. 2005). This raised questions about whether the solved structure of KvAP was in fact the native conformation, or if it had been distorted when removed from the lipid membrane, which prompted the structure of KvAP to be solved again (Lee, Lee et al. 2005). The second solved structure of KvAP (Lee, Lee et al. 2005) revealed that the VSD was indeed in a nonnative conformation, likely the result of weak interactions between the VSD and the pore domain. These studies suggested that the pore-forming and voltage-sensing domains represent separate functional units and they do not tightly adhere to each other within the membrane. This was later confirmed by making channel chimeras where pore domains of different channels could be interchanged without disrupting the channel functionality (Lu, Klem et al. 2002). Without the lipid membrane that provides external forces to hold the two domains together, they would adopt a non native conformation as seen in the first KvAP x-ray structure. However, this problem was not relevant to Kv1.2 as it was crystallized with its T1 domain intact, a large cytoplasmic bundle formed by subunits at the N-terminal end of the voltage sensor from each of the 4 domains. This T1 domain helped maintain the native orientation of the VSD domain when the channel was removed from the lipid membrane and inserted into a micelle (Long, Campbell et al. 2005).

The S4 helix of the VSD contains four positively charged arginines spaced 3 residues apart. Two of the arginines are lipid exposed, while the other two are buried in the protein and

interact through salt bridges with negatively charged residues (typically glutamic acid) in the S1 and S2 helices (Long, Campbell et al. 2005). These arginines allow the VSD to sense changes in the membrane potential and cause the S4 helix to shift, apply forces to the pore domain through the S4-S5 linker, and thus open or close the channel. Due to the diverging position of the voltage sensor in the original KvAP and Kv1.2 structures, several models have been proposed to explain the mechanism of voltage dependent channel gating; the transporter model, the helical screw model and the paddle model. According to the transporter model, the S4 in the closed state is found in a crevice contacting the cytoplasmic side of the membrane. Upon depolarization, the helix rotates in place and the surrounding helices change shape, exposing the charges to a crevice in contact with the extracellular side (Bezanilla 2002; Starace and Bezanilla 2004; Bezanilla 2005; Chanda, Asamoah et al. 2005). The paddle model was directly inspired from the first KvAP crystal structure, which showed the voltage sensor in an orientation almost parallel to the membrane. The S3, S3b (extracellular segment of S3) and S4 helices form a helical hairpin motif, which resembles a paddle, and is believed to move from the cytoplasmic side in the closed conformation, to the extracellular side of the membrane, resulting in channel opening (Jiang, Lee et al. 2003; Jiang, Ruta et al. 2003). Finally, in the helical screw model, the S4 helix rotates and translates across the membrane similar to the motion of a screw. As S4 rotates, each of the sequential arginines form salt bridges with the fixed negatively charged residues in the surrounding VSD helices. This movement across the membrane is coupled to the pore domain, opening and closing the channel. The original helical screw model (Catterall 1986; Guy and Seetharamulu 1986) has evolved over time to account for new data from FRET analysis, solvent exposure and mutational studies (Keynes and Elinder 1999; Gandhi and Isacoff 2002; Lecar, Larsson et al. 2003; Ahern and Horn 2004; Durell, Shrivastava et al. 2004). This includes a

revised translation distance, the degree of rotation and the angle of S4 relative to the pore domain. A unified model is still needed to explain the gating mechanism of voltage gated channels and without an x-ray structure of a closed Kv channel, the mechanism will likely remain controversial. Kv1.2 was chosen to build the homology model of the Na^+ channel BgNav1-1 in Chapter Three and Chapter Four.

NaK

The cyclic-nucleotide gated (CNG), prokaryotic non-selective sodium-potassium channel NaK (Shi, Ye et al. 2006; Alam and Jiang 2009; Alam and Jiang 2009) to date is the only channel that has been crystallized in both the open and closed states, however, the open state is truncated by 19 residues at the N-terminal. Although the solved structure contains a domain similar to the VSD from Kv channels, NaK behaves as a ligand gated channel. Examining of the conformation and position of the NaK VSD in open and closed conformations shows only minor displacements between the two states. Besides permeating Na^+ ions, the channel also leaks K^+, Rb^+, Cs^+, Ba^{2+} and Ca^{2+} ions, indicating a different selectivity mechanism than in Na^+ channels (Alam and Jiang 2009).

NaChBac

The voltage gated Na^+ channel family was first thought to only exist in eukaryotic organisms, until NaChBac from alkaliphilic Bacillus was identified as the first bacterial sodium channel (Catterall 2001; Ren, Navarro et al. 2001). Although this family of channels has been well characterized though electrophysiological and microbiological studies, structural data pertaining to voltage-dependence, fast inactivation and a detailed mechanism for ion permeation

remains unknown. Based on sequence alignments, mutagenesis and other analyses, NaChBac combines characteristics of K^+, Ca^{2+} and Na^+ channels, and is assumed to be the ancestor of modern eukaryotic voltage-gated channels (Ren, Navarro et al. 2001; Zhao, Yarov-Yarovoy et al. 2004). However, unlike eukaryotic Ca^{2+} and Na^+ channels, NaChBac is a homotetramer similar to Kv channels and therefore is likely to become the first Na^+ channel with a solved 3D structure.

MOLECULAR MODELING OF ION CHANNELS

Structural and electrophysiological studies of ion channels have provided abundant information about structure-function relationships of ion channels. However, due to the difficulty in crystallizing membrane proteins and in particular ion channels, there are only a limited number of solved K^+ channel structures and no x-ray structures of Na^+ and Ca^{2+} channels. Without atomic-resolution channel structures, exploring the mechanism of action of toxins and synthetic small molecules remains a challenge in development of potent and selective drugs. In the absence of these atomic-resolution experimental structures, molecular modeling provides an alternative method called homology modeling. Homology models can be used to predict the interactions of drugs and toxins with ion channels. Homology modeling is based on the assumption that channels from the same family share similar three-dimensional backbone geometry. Using the atomic coordinates of a solved crystal structure as a template and the amino acid sequence from a target channel, we can build a model of the target ion channel before its crystal structure becomes available.

There are two main classes of molecular modeling software, which employ molecular dynamics (MD) or Monte Carlo minimization (MCM) methods to sample the energy hypersurface. Each class has advantages and disadvantages. This study explores the interactions

of various drugs with ion channels. The time scale required to observe these events is beyond the capability of MD, therefore, the MCM-based ZMM software was used. The MC energy minimization method is efficient for non-local optimization (Li and Scheraga 1987). The energy components are calculated as follows. First, for van der Waals interactions we use a force field, which is a set of energy functions describing bonded and non-bonded interactions (Weiner, Kollman et al. 1984; Weiner, Kollman et al. 1986). Most modeling programs use a distant dependent dielectric function to calculate the electrostatic interactions (Abagyan and Totrov 2001; Friesner, Banks et al. 2004; Meiler and Baker 2006). We recently developed a new dielectric function that takes into account both the environment around the charge and the distance between interacting atoms (Garden and Zhorov 2010) (Chapter 2). MD simulations are usually performed with explicit water molecules. MCM simulations usually employ implicit-solvent method to calculate the dehydration energy (Lazaridis and Karplus 1999).

LIGAND DOCKING

Initial attempts of high-throughput *in silico* drug docking claimed high success rates of 60% to 75% (Goodsell, Morris et al. 1996; Ewing, Makino et al. 2001), however respective docking programs ignored protein and ligand flexibility, using an approach termed rigid-docking. In some studies, the binding pocket was approximated by a surface and the ligand was docked into the surface based on geometric criteria, followed by short energy minimizations (Ewing, Makino et al. 2001). This approach neglects interactions between flexible side chains lining the ligand-binding pocket and the ligand. It also biases the initial conformation of the protein side chains, taking their coordinates directly from the crystal structure. Without

accounting for ligand and protein flexibility, the conformation search space is dramatically decreased.

The test sets for evaluation contained a high degree of redundancy and bulky semi-rigid compounds like steroids, which do not represent many classes of drug-like compounds (Egan, Walters et al. 2002).

Subsequent generations of docking programs take into consideration the ligand flexibility. Programs such as AutoDock, DOCK, FlexX, GOLD and ICM were tested on a common set of 37 flexible ligands in 11 receptors, reporting success rates of 46%, 30%, 35%, 46% and 76%, respectively, for predicted structures under 2.0 Å root mean squared deviation (RMSD) from the crystal structure (Ferrara, Gohlke et al. 2004); reviewed by (Bursulaya, Totrov et al. 2003). The introduction of highly flexible ligands dramatically decreased the success rates (e.g. from 76 to < 50% for ICM), however the test set was still enriched with easily predictable structures and lacked diversity of the receptors. Furthermore, most of the ligands were not relevant to therapeutic drugs, over-representing peptides, sugars and nucleotide-based ligands (Perola, Walters et al. 2004). A second independent test of Glide, GOLD, and ICM, placed focus on an accurate and representative library of drug-like molecules. Two hundred ligand-protein complexes were chosen, filtered based on drug-like criteria (Egan, Walters et al. 2002), yielding a test set of 100 complexes for docking. The results showed a decrease from the previously stated success rates to 61%, 48% and 45% for Glide, GOLD and ICM respectively (Perola, Walters et al. 2004).

Another novel docking program, ROSETTALIGAND, accounts for both side chain and ligand flexibility. Over a test set of 100 ligands, ROSETTALIGAND states a success rate of 71%. However, in their calculation of RMSD, the side chains lining the binding pocket and

hydrogen atoms are also included (Meiler and Baker 2006). The authors state that accounting for deviation in side chains near the ligand increases the sensitivity of their RMSD to structure changes in the protein and ligand. However, this also decreases their RMSD due to small deviations of side chains and lowers the ligand contribution to the RMSD value, since the number of atoms in the side chains greatly outnumbers the atoms in the ligand.

OVERVIEW

The goal of this study was to explore the atomistic mechanism of action of various state-dependent toxins on ion channels. Modeling interactions between various toxins and ion channels and understanding their effects on channel kinetics encompasses a large amount of data. Therefore, this work has been divided into three sections, each contributing a critical component towards the overall goal.

Developing docking methodology – Chapter one

First, while ZMM has been previously used to predict the binding sites of different compounds (Zhorov and Lin 2000; Blanchet, Lin et al. 2005), it has not been tested on a large scale. As an examining set, we selected 60 high resolution x-ray structures of ligand-protein complexes and accounted for the ligand and protein flexibility. Using several training sets of ligand-receptor complexes, which do not overlap with the examining set, the docking protocol was designed and tuned. The resulting protocol includes three stages. 1) The ligand is removed from the protein and all the torsion angles are randomly sampled followed by energy minimization without attractive van der Waals forces. The low-energy ligand conformations form a library of ligand structures to be docked into the protein. 2) The seeding stage takes each

conformation from the library, rigidly docks it into the protein by sampling the ligand's position and orientation, and ranks all ligand-protein complexes by the energy. 3) The refinement stage takes the most favourable complexes from the seeding stage and MC-minimizes them in a longer trajectory, with completely flexible torsions in the ligand and protein. The lowest energy structure after the refinement stage represents the predicted structure. During tuning the protocol, a problem was identified with electrostatics and desolvation energy. The electrostatic energy term includes the dielectric permittivity of the medium. Most molecular modeling programs use simple distant-dependent dielectric function ($\varepsilon = kr$), where k is a constant (1, 2, or 4) and r is the distance between the charges. We found that when used for drug docking, this is an over simplification and proposed a more robust dielectric function, which accounts for both distance between the charges and the location of the charges. Using this solvent exposure- and distance-dependent dielectric function, the docking protocol was benchmarked on the examining set of 60 complexes and yielded a success rate of ~58%, on par with leading docking software.

Predicting the binding site and mode of batrachotoxin (BTX) – Chapter two

The above docking protocol was able to reproduce the binding site of various ligands within a high resolution crystal structure. A more challenging goal is to predict a binding site and binding mode of a ligand in a homology model of an ion channel, which is not expected to be as precise as high-resolution x-ray structures. The goal was to predict ligand-binding sites in sodium channels, which have yet to be crystallized. The channel of interest is a voltage gated Na^+ channel from the cockroach (BgNav1-1), a known target of the sodium channel agonists such as batrachotoxin (BTX) and pyrethroid insecticides. An open-state homology model of the channel was built using the structure of Kv1.2 as a template and the P-loop was modeled

separately (Tikhonov and Zhorov 2005). Currently, there are conflicting concepts about the binding mode of BTX. Traditionally, this classical site 2 toxin is thought to bind at the lipid-channel interface (Trainer, Brown et al. 1996). Subsequent mutational studies have identified BTX sensing residues in the pore-lining helices S6s in all four domains, which is inconsistent with a lipid-exposed binding mode. Dr. Dong and her colleagues in the Michigan State University have recently identified two new BTX sensing residues, a glycine and phenylalanine in IIIS6. We used these new data to build a BTX-bound model of the sodium channel that would rationalize all currently available data on BTX-sensing residues.

Since homology models are inherently less accurate than high-resolution x-ray structures, we employed constraint driven docking. The constraints, which are based on experimental data, can focus the docking search. A problem is that mutational and ligand-binding experiments do not specify which functional groups of the ligand interact with which functional groups of the channel residue. We constrained residues known to be critical for BTX action to various functional groups of BTX that were most likely to form favourable interactions. Testing various combinations led to many different binding modes, but only one of them was able to accommodate all the currently known BTX sensing residues and yield a low energy complex with the channel. This model is named the “horseshoe” binding mode, because of its U-shaped conformation. When bound in this mode in the center of the pore, BTX exposes its hydrophobic side towards the pore wall, while oxygen atoms and an aromatic ring are exposed towards the pore axis, thus creating a hydrophilic ring at the hydrophobic level of the channel. This model was able to explain mutational data, permeation of ions and the mechanism of BTX action. To validate the model, an anonymous reviewer of our manuscript, when it was submitted to JBC, requested us to make and test additional mutants. Seven residues were proposed for mutations

based on the BTX-channel complex. Mutational experiments demonstrated that results of five mutations were in complete agreement with the model, thus providing a strong support for the proposed binding mode.

Exploring the mechanism of a partial agonist BTG 502 – Chapter three

We further modeled the binding of other toxins to Na^+ channels. In collaboration with Dr. Dong, we investigated the mechanism of action of the Na+ channel partial antagonist BTG 502 and its interaction with a pyrethroid agonist, deltamethrin. Intriguingly, some of the BTG 502-binding residues contribute to the receptor site of BTX and deltamethrin, but the latter toxins are known to bind in different locations within the channel. Furthermore, when BTG 502 is applied to the channel alone, it behaves as a partial agonist, decreasing the flow of ions through the channel but resists channel closure, however in channels pre-treated with deltamethrin, BTG 502 behaves as an antagonist. A similar constraints-driven docking approach was used to predict the binding sites of BTG 502 and deltamethrin. We docked BTX 502 alone and then in combination with deltamethrin to explore the dual nature of BTG 502 action. We reproduced a binding mode for deltamethrin that was similar to the earlier propose binding model of several pyrethroids (O'Reilly, Khambay et al. 2006), which bind in the triangle formed by IIL45-IIS5-IIIS6, exposing one side towards the voltage sensor and the other towards the inner cavity. We proposed a novel binding mode for BTG 502, where the flexible ligand wraps around the IIIS6 helix, placing one end into the II/III interface and the other in the III/IV interface. This binding model explains how BTG 502 can interact with both pore facing and buried side chains.

I hope that through this study, we have integrated experimental data, which previously were considered as controversial, and provided new insight into the mechanism of action of various toxins on Na^+ channels

CHAPTER TWO

DOCKING FLEXIBLE LIGANDS IN PROTEINS WITH A SOLVENT EXPOSURE- AND DISTANCE-DEPENDENT DIELECTRIC FUNCTION

CHAPTER 2 – PREFACE

The work presented in this chapter has been published in:

Garden, D. P. and B. S. Zhorov (2010). "Docking flexible ligands in proteins with a solvent exposure- and distance-dependent dielectric function." J. Comput. Aided Mol. Des. **24**(2):91-105.

Permission has been granted from the publisher to reproduce the material here.

I preformed all the experiments, calculations and analyses for this study.

ABSTRACT

Physics-based force fields for ligand-protein docking usually determine electrostatic energy with distance-dependent dielectric (DDD) functions, which do not fully account for the dielectric permittivity variance between ~ 2 in the protein core and ~ 80 in bulk water. Here we propose an atom-atom solvent exposure- and distance-dependent dielectric (SEDDD) function, which accounts for both electrostatic and dehydration energy components. Docking was performed using the ZMM program, the AMBER force field, and precomputed libraries of ligand conformers. At the seeding stage, hundreds of thousands of positions and orientations of conformers from the libraries were sampled within the rigid protein. At the refinement stage, the ten lowest-energy structures from the seeding stage were Monte Carlo-minimized with the flexible ligand and flexible protein. A search was considered a success if the root mean square deviation (RMSD) of the ligand atoms in the apparent global minimum from the x-ray structure was < 2 Å. Calculations on an examining set of 60 ligand-protein complexes with different DDD functions and a solvent-exclusion energy term revealed outliers in most of which the ligand-binding site was located at the protein surface. Using a training set of 16 ligand-protein complexes, which did not overlap with the examining set, we parameterized the SEDDD function to minimize the RMSD of the apparent global minima from the x-ray structures. Recalculation of the examining set with the SEDDD function demonstrated a 20% increase in the success rate versus the best-performing DDD function.

INTRODUCTION

In the past decade, growth of high-resolution structures in the Protein databank (Berman, Westbrook et al. 2000), increase of computational power, and new software have boosted

applications of *in-silico* docking of ligands into proteins of known 3D structure and their homology models. Among the aims of these studies are the discovery of new drugs, understanding atomic mechanisms of ligand-receptor interactions, designing new experiments, and improvement of ligand-docking methodology. *In-silico* docking can predict ligand-binding poses, rank ligands by their interaction energy with the protein, and ideally, predict the ligand affinity. According to a recent assessment, ten popular ligand-docking programs were able to generate ligand-binding poses similar to the crystallographic complexes for some targets, however were less successful at distinguishing the x-ray structure from the set of docked poses, and were unable to predict ligand affinities (Warren, Andrews et al. 2006). Most drug candidates are still discovered via experimental high-throughput screening methods, but computational docking is becoming a major source of lead molecules in drug discovery (McInnes 2007).

Scoring functions used in ligand-docking programs can be categorized as knowledge-based (Gohlke and Klebe 2002) and physics-based (Gilson and Zhou 2007). Programs GLIDE (Friesner, Banks et al. 2004), GOLD (Jones, Willett et al. 1997), and FlexX (Rarey, Kramer et al. 1996) employ knowledge-based scoring functions developed with training sets of high-resolution structures and search for ligand-protein complexes with the optimal score. Programs AutoDock (Goodsell, Morris et al. 1996), ICM (Totrov and Abagyan 1997), RosettaLigand (Meiler and Baker 2006), and ZMM (Zhorov 1981), use physics-based force fields that present the energy as the sum of van der Waals, electrostatic, and solvation components as well as the valence-geometry strain energy of the ligand and protein. The latter three programs search for the apparent global minimum (AGM) and local minima in the space of generalized coordinates using the Monte Carlo-minimization (MCM) method (Li and Scheraga 1987). The local minima may be a few kcal/mol or less from the AGM. A challenge is to tune the force field to ensure that the

root mean square deviation (RMSD) of the AGM from the x-ray structure is below 2 Å. Imprecise calculation of electrostatic energy (Gilson and Zhou 2007) seems to be a major obstacle in meeting this challenge.

The most advanced approach to calculate electrostatic energy treats the protein interior as a low-dielectric medium, the solvent as the high-dielectric medium and numerically solves the Poisson-Boltzmann equation (Gilson 1995; Honig and Nicholls 1995; Fogolari, Zuccato et al. 1999; Mallik, Masunov et al. 2002). The high computational cost of this method currently prevents its application for high-throughput ligand docking. Besides, available implementations of the method involve inaccuracies that currently are difficult to eliminate (Gilson and Zhou 2007). The Generalized Born model (Still, Tempczyk et al. 1990), which is an approximation of the Poisson-Boltzmann equation, is used e.g. in the CHARMM program for molecular dynamic simulations (Dominy and Brooks 1999).

A traditional approach to calculate electrostatic energy is based on Coulomb's law, but uncertain dielectric permittivity, unknown location of counterions, and unknown protonation of titrable groups may have a big impact on the electrostatic energy. As an empirical solution, titrable residues can be considered neutral (Momany, McGuire et al. 1975; Lazaridis and Karplus 1999) and the linear distance-dependent dielectric (DDD) function $\varepsilon = kr$ is used (McCammon, Wolynes et al. 1979; Weiner, Kollman et al. 1984). In most programs, coefficient k equals 1, 2, or 4 (Morris, Goodsell et al. 1996; Rarey, Kramer et al. 1996; Jones, Willett et al. 1997; Totrov and Abagyan 1997; Wang, Kollman et al. 1999; Ewing, Makino et al. 2001; Friesner, Banks et al. 2004; Meiler and Baker 2006). However, it is well known that the dielectric permittivity varies from to ~ 2 in the hydrophobic interior of a protein to ~ 80 in bulk water around the protein (Finkelstein and Ptitsyn 2002; Gohlke and Klebe 2002). Dielectric permittivity at the

surface is an order of magnitude smaller than that of the bulk water (Bockris and Reddy 1977; Teschke, Ceotto et al. 2001; Rubinstein and Sherman 2007) and the permittivity inside the protein may be greater than 2. Besides the linear DDD functions, sigmoidal-shaped DDD functions are used to screen electrostatic interactions at solvent-exposed areas (Mehler and Solmajer 1991; Garrett M. Morris, Goodsell et al. 1998; Gelpi, Kalko et al. 2001; Morreale, Gil-Redondo et al. 2007). The DDD functions *per se* do not completely account for large variations of the dielectric permittivity and usually overestimate electrostatic interactions at the protein surface. Computationally efficient solutions for this problem are solvent-exclusion models, which account for solvent screening of electrostatic interactions as well as for hydrophobic interactions between nonpolar groups inside the protein (Augspurger and Scheraga 1996; Lazaridis and Karplus 1999).

Here we propose a solvent exposure- and distance-dependent dielectric (SEDDD) function that depends on the distance between a pair of atoms, the degree of their exposure to the aqueous environment, and parameters ε_0 and ε_1 ($\varepsilon_0 \leq \varepsilon_1$). For a water-exposed pair of atoms, a high-range dielectric function $\varepsilon_{ij} = r_{ij}\varepsilon_1$ is used. For a pair of atoms buried inside the protein, a low-range dielectric function $\varepsilon_{ij} = r_{ij}\varepsilon_0$ is used. For a pair of partially exposed atoms, the dielectric function varies between $r_{ij}\varepsilon_0$ and $r_{ij}\varepsilon_1$. Since theoretical derivation of parameters ε_0 and ε_1 is hardly possible, we used an empirical approach. We selected a training set of sixteen ligand-protein complexes for which high-resolution x-ray structures are available and systematically varied ε_0 and ε_1 from 1 to 10 with the step of 1. For each combination of ε_0 and ε_1, ligand-protein energy for 500,000 poses of the rigid ligand in the rigid protein was calculated (the seeding stage). The ten lowest-energy poses were refined by MCM with the flexible ligand and flexible protein, and RMSD of the AGM was plotted against ε_0 and ε_1. Considering the ligand flexibility at the

seeding stage would have increased the already large computational cost of parameterization by 100 fold. We found that for most of the complexes, the combination $\varepsilon_0 = 2$ and $\varepsilon_1 = 8$ minimizes the RMSD of the AGM from the x-ray structure. Calculations with an examining set of 60 high-resolution ligand-protein complexes were performed with considering the ligands flexibility at the seeding stage. This was achieved by using precomputed libraries of ligand conformers. For each ligand, a library was generated by randomly sampling the ligand torsions, minimizing the repulsive energy, and merging similar conformers. Flexible docking with the SEDDD function demonstrated a 20% increase of the success rate versus the best-performing DDD function.

METHODS

Energy components. We use the ZMM program, which is partially described in various applications (Zhorov and Bregestovski 2000; Blanchet, Lin et al. 2005; Bruhova and Zhorov 2007; Tikhonov and Zhorov 2007). The website www.zmmsoft.com provides a detailed description of the program, controlling parameters, and tests. Briefly, ZMM minimizes the energy in the space of generalized coordinates (Zhorov 1981; Zhorov 1983) and employs the MCM method (Li and Scheraga 1987) for a non-local search of energetically optimal structures. In this study, the van der Waals energy was calculated using the AMBER force field (Weiner, Kollman et al. 1984; Weiner, Kollman et al. 1986). Computations with the DDD function were performed with a dehydration energy component, which is based on the Gaussian solvent-exclusion model (Lazaridis and Karplus 1999). Henceforth we refer to the energy component as the solvent-exclusion term. Ionizable residues were considered in both their neutral states (Momany, McGuire et al. 1975; Lazaridis and Karplus 1999) as well as in ionized states. Electrostatic interactions involving metal ions and/or ionized groups of the ligands were

calculated at all distances. Other interactions were truncated at a cutoff distance of 10 Å with a 1 Å switching function (Brooks, Pettitt et al. 1985). The ligands were imported from the PDB files using the ZMM module, which automatically assigns hybridizations of heavy atoms, adds hydrogens, and corrects bond lengths and bond angles that deviate significantly from the standard values. The module then submits ligand coordinates to the MOPAC program and imports atomic charges calculated by the AM1 method (Dewar, Zoebisch et al. 1985). The ZMM-generated chemical structures of the ligands were compared with those at PDBSum website (Laskowski, Hutchinson et al. 1997). Upon importing the x-ray structure of a protein to ZMM, tautomers of histidines and starting orientations of OH and $CONH_2$ groups in amino acid were chosen to minimize steric clashes and maximize H-bonds. The electrostatic energy was calculated with either the DDD or SEDDD function described in section 3.2.

Training and examining sets. We optimized our docking protocol (see below) with the DDD function using the first training set of 10 structures (Table 2.1) and parameterized the SEDDD function using the second training set of the following 16 structures: 1bk0, 1cbx, 1cc8, 1cmd, 1ctq, 1dmp, 1dry, 1ds1, 1g5a, 1g67, 1hb2, 1ky3, 1yds, 2gbp, 2ypi, and 8atc. The SEDDD function accounts for variation in the dielectric permittivity through screening the electrostatic interactions for water-exposed charges and strengthening interactions in buried regions of the protein and ligand-binding pockets. The function is described in section 3.2.

The DDD and SEDDD functions were tested with the examining set of 60 high-resolution structures (Fig. 2.1) chosen to represent diverse ligand-receptor complexes. Fifty of these complexes were used earlier to test ICM, GLIDE, and RosettaLigand (Friesner, Banks et al. 2004; Perola, Walters et al. 2004; Meiler and Baker 2006). The examining set contains charged

Table 2.1: Training set of ligand-protein complexes

PDB code	Ligand			Ligand binding site		
	Atoms	Torsions	Heteroatoms	Residues [a]	Ionizable residues [a]	Depth [b]
1b6n	36	17	7	21	6	1.4
1bl7	25	4	7	14	3	1.7
1byg	35	2	7	16	3	1.3
1c2t	35	12	11	18	1	1.3
1dy9	35	19	14	13	5	2.9
1elc	36	15	10	8	3	4.5
1ett	30	8	8	8	4	2.5
1ivc	19	3	6	10	7	1.8
1srh	22	6	7	17	1	2.2
1tnh	12	1	2	13	1	3.0

[a] Within 4 Å from the ligand

[b] Determined as the ratio of the number of flexible residues in the protein double-shell model to the number of the ligand's heavy atoms.

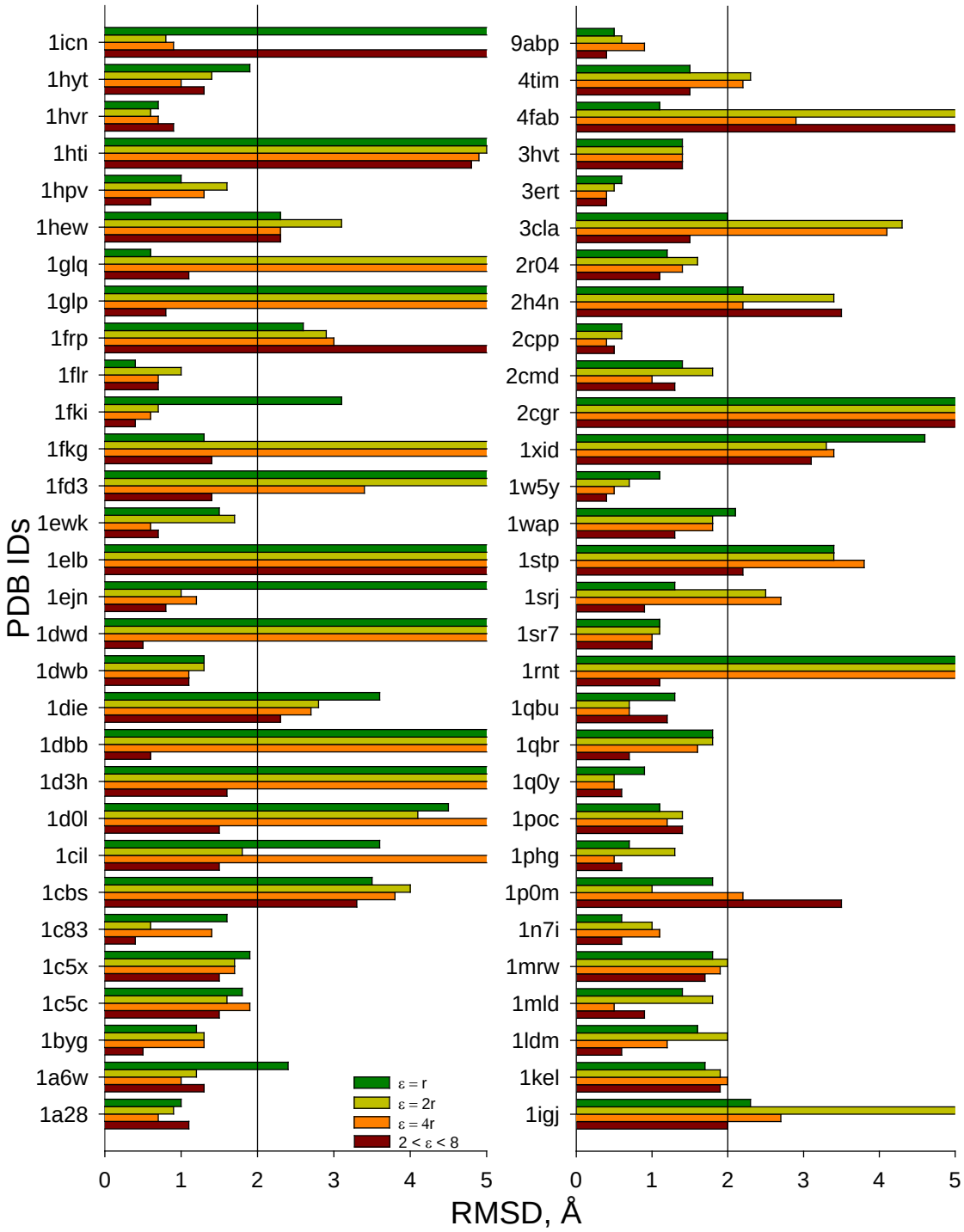

Figure 2.1. RMSD of the AGM of the examining-set structures from the corresponding x-ray structures computed with the solvent-exclusion term and DDD functions $\varepsilon = r$ (light green), $\varepsilon = 2r$ (dark green), and $\varepsilon = 4r$ (orange), as well as the SEDDD function without solvent-exclusion term (brown). Flexible-ligand dockings have been performed with the enriched libraries of ligand conformers. The black vertical line shows the 2.0 Å RMSD cutoff. Bars crossing the line correspond to false-positive predictions. The best-performing protocol with the DDD function $\varepsilon = 2r$ and solvent-exclusion term yields 24 (40.0 %) false-positives, while the protocol with the SEDDD function and without solvent yields only 13 (21.7 %) false-positives.

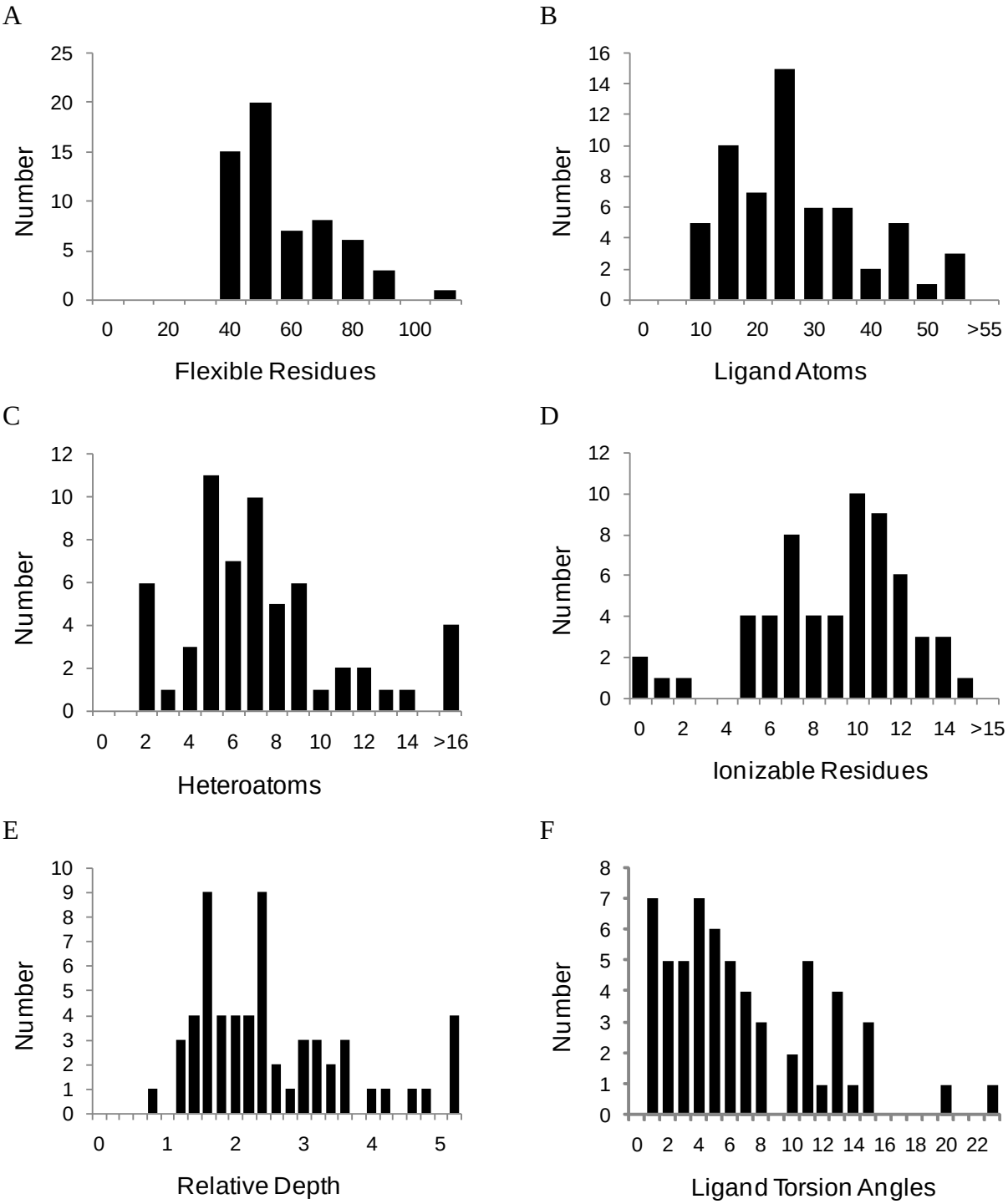

Figure 2.2. Characteristics of the examining-set complexes. ***A,*** The number of flexible residues in the double shells whose torsions have been sampled at the refinement stage. ***B,*** The number of heavy atoms in the ligands. ***C,*** The number of heteroatoms in the ligands. ***D,*** The number of ionizable residues in the flexible shells of the proteins. ***E,*** The relative depth of the ligand-binding pockets calculates as the ratio of the number of flexible residues in the double shell to the number of heavy atoms in the ligands. ***F,*** The number of torsion angles in the ligands.

and neutral ligands of varying size, shape and number of rotatable bonds (Fig. 2.2). Structures with resolutions > 2.5 Å and complexes involving multi-residue ligands were discarded. Structures with metal ions other than K^+, Na^+, Ca^{2+}, and Zn^{2+} were not considered. Not a single x-ray structure used in this work belongs to more than one set (training or examining).

Libraries of ligand conformers. ZMM docking with flexible ligands and flexible proteins has reproduced various x-ray structures (Zhorov and Lin 2000; Blanchet, Lin et al. 2005), but at a large computational cost. In this study, ligand flexibility was accounted for by generating libraries of ligand conformers (Fig. 2.3), rigid docking hundreds of thousands of binding poses for each conformer in the protein, and refining low-energy poses by MC minimizing flexible conformers in flexible proteins. First, we sampled a thousand random starting conformers for each ligand and minimized the ligand energy in vacuum. Due to nonbonded attractions, flexible ligands usually adopted compact low-energy conformations that largely differ from the extended conformations seen in the x-ray structures of the ligand-protein complexes. To resolve the problem, we have used an *ad hoc* force field, which is referred henceforth as AMBERL, to increase the chances of accepting extended conformations of flexible ligands into the libraries. In AMBERL, parameters for nonbonded interactions, torsional energy, and bond-angle deformation energy are the same as in AMBER (Weiner, Kollman et al. 1986), except for the nonbonded-potential well depth ε, which is assigned a value of 0.001 for all atom types. Electrostatic interactions were not included in AMBERL. Most ligands were calculated in vacuum with the exception of highly lipophilic flexible ligands (PDB codes 1icn and 1qbu) that were calculated using the implicit-octanol method (Hopfinger and Battershell 1976) and highly hydrophilic ligands (1glp and 1n7i) that were calculated in water. Each unbiased library of ligand conformers

1cbs

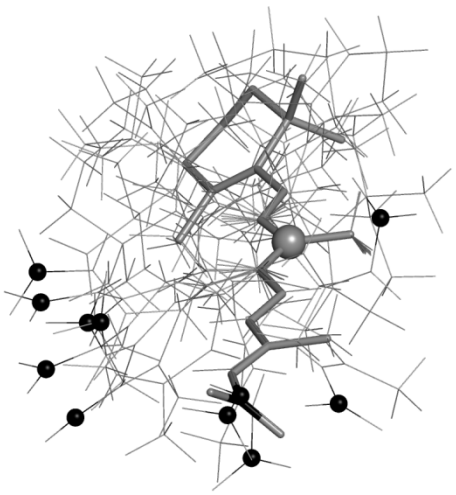

1rnt

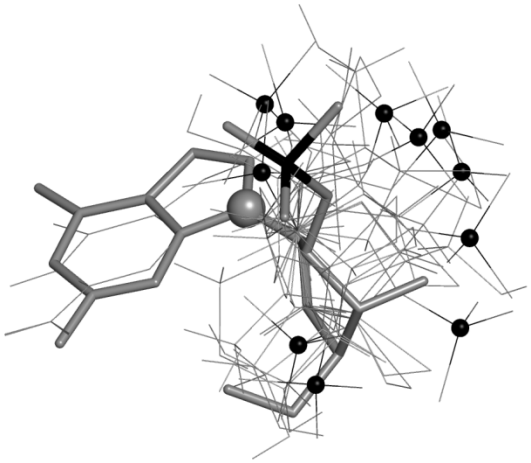

1hpv

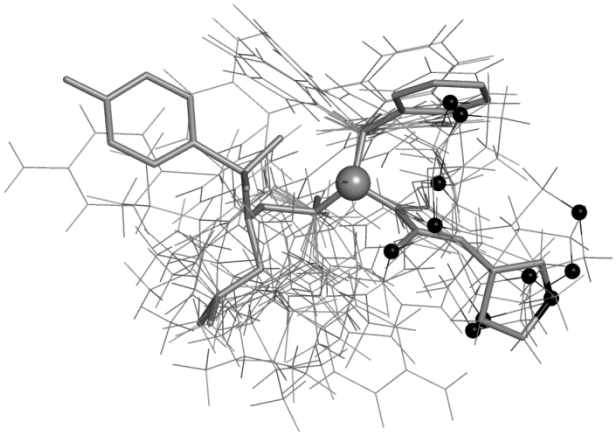

1qbr

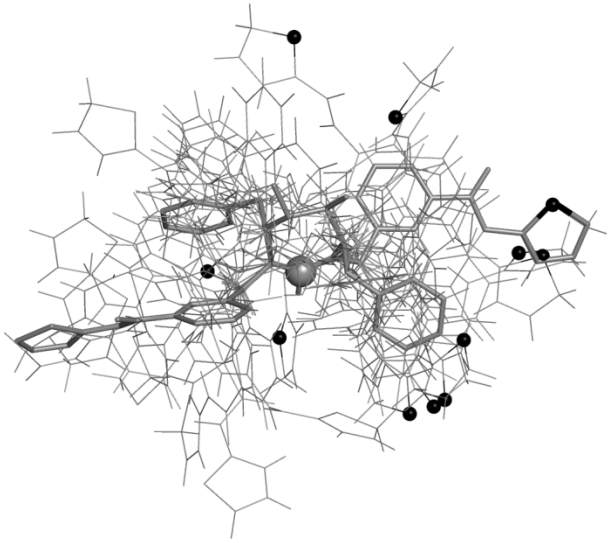

Figure 2.3. Four libraries of ligand conformers. The 10 lowest-energy conformers in each library are shown by thin lines. The x-ray conformation is represented by thick lines. The atom in the origin of the ligand local system of coordinates is shown as a large gray sphere, and a reference atom is marked by a dot.

was built by sampling a thousand random starting points and minimizing the AMBERL energy during 100 steps. Conformers with energy < 10 kcal/mol from the AGM were accumulated in a stack (see below) whose size was limited to 100 conformers. Among the 60 examining-set ligands, for 56 ligands at least one conformer in the stack had RMSD < 2 Å from the x-ray conformation in the respective ligand-protein complex and for 4 ligands the RMSDs was > 2 Å (Fig. 2.4). The latter are highly flexible molecules with > 9 "essential" torsions whose variations result in big conformational changes. (Non-essential torsions specify rotations of terminal groups such as $–CH_3$, $-NH_3$, -OH, and -Ph, as well as torsions in 3- to 6-membered rings.) All libraries included conformers with RMSDs up to 7 Å, which served as decoys for flexible ligand docking. In some calculations we used enriched libraries, which were created from the unbiased libraries by replacing the highest-energy conformer with the conformer from the x-ray structure of ligand-protein complex. To tune the docking protocols and parameterize the SEDDD function, we used single-conformer "libraries", which contained just the ligand conformers from the x-ray structures.

Docking protocol. To reduce computational cost, ligands were docked in double-shell models (Zhorov and Lin 2000). A double shell contains flexible residues having at least one atom within 8.0 Å from the ligand as seen in the x-ray structure and fixed residues that do not belong to the flexible shell and contain at least one atom within 16.0 Å from the ligand. A protein can adopt different conformations in the presence of different ligands (Teague 2003), but high throughput docking with flexible ligand and flexible protein remains a challenging problem. Here we employed a two-stage docking protocol. At the first, the seeding stage, each structure from a library of ligand conformers was placed at 500,000 random positions and orientations within the

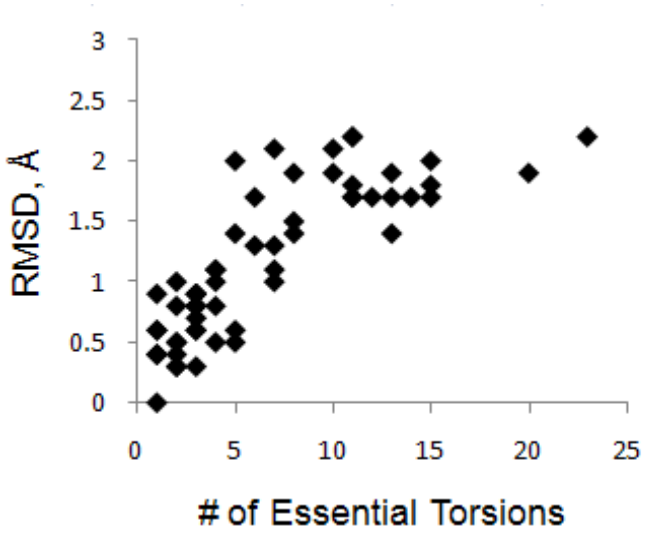

Figure 2.4. RMSD of ligand conformers vs. # of essential torsions. In the libraries of ligand conformers, RMSD of the best match to the x-ray conformation increases with the number of essential torsions.

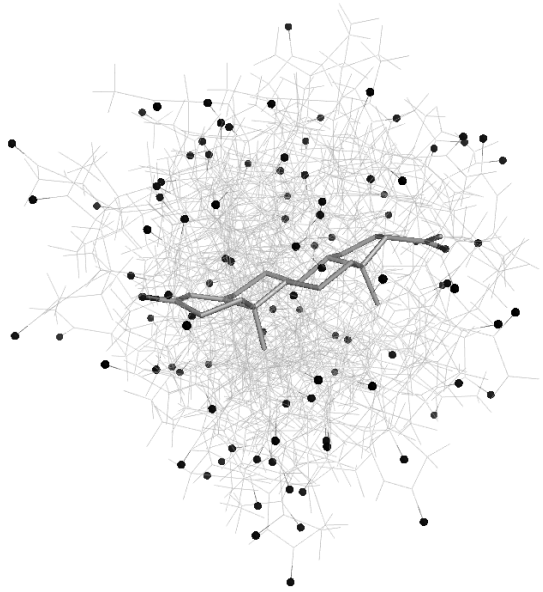

Figure 2.5. Sampling progesterone binding poses. The first 100 of 500,000 progesterone poses generated at the seeding stage are shown by thin lines with black oxygens. Thick lines show the protein-bound progesterone in the x-ray structure (1a28).

rigid protein (Fig. 2.5). At the second, the refinement stage, both the ligand and protein were flexible. The sampling space for the ligand center was a cube with 8 Å edges approximately matching the flexible-shell size. (Other programs use comparable dimensions of the seeding box. In ICM, the ligand mass center is displaced randomly within a sphere of 3 Å radius (Cavasotto and Abagyan 2004). GLIDE (Friesner, Banks et al. 2004) and RosettaLigand (Meiler and Baker 2006) place the ligand center in a cube with edge of 12 and 10 Å, respectively.) Low-energy structures collected at the seeding stage were MC-minimized at the refinement stage, in which position/orientation of the ligand and torsion angles of the ligand and protein were sampled. After each sampling, the energy was minimized in the space of above generalized coordinates as well as bond angles of the ligand. To prevent large deformations of the protein backbones at the refinement stage, α-carbon atoms were constrained (pinned) to their crystallographic position with allowing a penalty-free deviation of up to 1.0 Å from the x-ray position. This two-stage protocol decreased computational cost by rejecting numerous ligand-binding poses that overlapped with the protein at the seeding stage. Parameterization of the SEDDD function was performed with neutral titrable residues; examining-set calculations were performed twice: with all the titrable residues being either neutral or ionized.

Stack control. Multiple predicted 3D structures of a system were collected in a stack and ordered by increasing energy. Each structure in a stack was represented by a record that included its energy and generalized coordinates. During sampling a stack was updated as follows. Initially, a large positive value was assigned to the AGM energy E_g. If the energy E_i of a newly generated structure was $< E_g$, the new structure was placed at the top of the stack, E_g was assigned the E_i value, and all structures with $E > E_g + \Delta E$ were removed from the stack. Here ΔE is the threshold to keep a structure in the stack. We used ΔE = 10 kcal/mol to generate libraries

of ligand conformers. For docking calculations, we used ΔE = 5,000 kcal/mol at the seeding stage and ΔE = 100 kcal/mol at the refinement stage. The high thresholds were necessary to collect at least ten structures at both the seeding and refinement stages. If for a newly-generated structure $E_i < E_g + \Delta E$, the structure was compared with all other structures in the stack. When generating a library of ligand conformers, two conformers were considered similar if none of their matching essential torsions differed by > 1 radian. When docking a ligand in a protein, two ligand-binding poses were considered similar if the RMSD of all the matching atoms were < 1 Å. If the new structure was dissimilar from any structure in the stack, it was added to the stack. Otherwise, the new structure and its closest match in the stack were compared by energy. If the energy of the new structure was lower than that of the match, the former replaced the latter in the stack. Otherwise the new structure was rejected. Thus, a record in a ligand-conformers stack represented a family of conformers. A record in the seeding-stage stack represented a family of binding poses with similar positions and orientations of the ligand. A record in the refinement-stage stack represented a family of complexes with similar positions, orientations, and conformations of the ligand and similar conformations of side chains in the protein flexible shell.

Success rate estimation. The RMS deviations of the ligand binding poses from the x-ray structure were calculated by comparing Cartesian coordinates of heavy atoms in the predicted and experimental structures. No attempts were made to decrease the RMS deviations by superimposing the structures by the least-squares method. An approximate match to the x-ray structure almost always can be found among the many thousands of ligand poses seeded in the protein. A challenge is to ensure that the refinement stage yields the AGM, which has an RMSD from the x-ray structure below 2.0 Å, the standard success criterion in literature (Cavasotto, Orry et al. 2003; Ferrara, Gohlke et al. 2004; Friesner, Banks et al. 2004; Meiler and Baker 2006). In

some flexible-docking studies the success is measured by calculating RMSD values over both ligand and binding-site atoms. We calculated RMSD only for heavy atoms of the ligand.

Optimizing docking protocol. Various ligand-docking programs use a two-stage protocol in which many structures are generated at the seeding stage and low-energy structures are refined in the second stage (Wang, Kollman et al. 1999; Cavasotto and Abagyan 2004; Friesner, Banks et al. 2004). Computational cost of the global minimization depends, in particular, on the number of starting structures in the seeding stage (N_s), length of the MCM trajectory optimizing each seed (L_s), number of energy-minimizing iterations in each MCM step (N_{im}), number of low-energy seeds submitted for the refinement (N_r), and length of the MCM trajectory refining each seed (L_r). Systematically exploring how the success rate depends on these parameters is hardly possible. Therefore we used a heuristic approach to optimize the docking protocol with the DDD function and the solvent-exclusion term in the first training set of 10 ligand-protein complexes (Table 2.1). Earlier N_{im} = 200 was found optimal (Zhorov, *unpublished*). To explore how the success rate depends on L_s, we generated 50,000 seeds for each complex and MC-minimized each seed. Brief MC-minimizations decreased the success rate (Fig. 2.6A) by yielding false-positives. Since optimizing all the seeds in long MCM trajectories is computationally prohibitive, we further ranked the seeds basing on the starting energy. Next we MC-minimized the 100 lowest-energy structures collected for each complex at the seeding stage. The success rate of these calculations increased up to 200 MCM steps then has a plateau at 40% (Fig. 2.6B). Further increasing the number of MCM steps only increased the computational time without increasing the success rate. Therefore we used L_r = 200 for docking experiments.

Next we explored how the success rate of the two-stage protocol depends on the number of low-energy seeds submitted for the refinement and found N_r = 10 to be optimal (Fig. 2.6C). The

fact that N_r > 10 decreased the success rate indicates that high-energy seeds deviated significantly from the x-ray structures and their MC-minimizations created false-positives. Finally, we explored how the success rate of the two-stage protocol depends on the number of seeds N_s. The success rate fluctuated with N_s < 50,000, indicating an incomplete sampling and reached a plateau of 60% with N_s ~ 500,000 (Fig. 2.6D). The above parameters were used in further calculations.

For a protein-ligand complex, building a library of 100 ligand conformers, generating 500,000 seeds per conformer, determining energies of 50,000,000 seeds and clustering the low-energy seeds requires ~5 hours on a 2.2 GHz CPU (AMD Opteron). Refining the top 10 seeds involves a total of 1,000 energy minimizations and takes ~2 hours on the same-type CPU. All calculations were performed using a parallel version of ZMM.

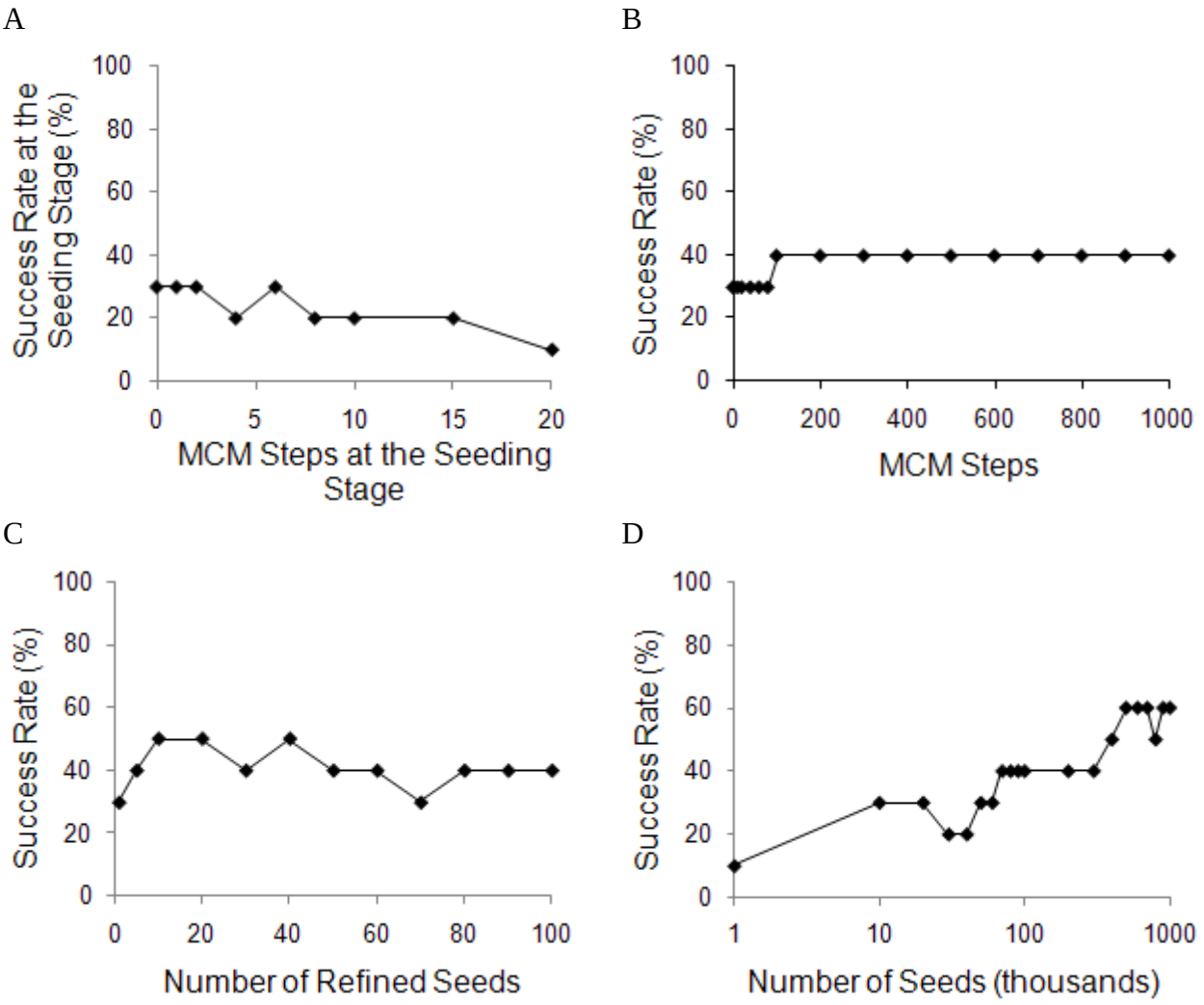

Figure 2.6. Optimizing the docking protocol using a training set of ten complexes (Table 2.1) with the DDD function. ***A***, Success rate of correct predictions *vs.* length of the seeding-stage MCM trajectories optimizing 50,000 sampled poses of each ligand. The rate decreases with the trajectory length. See text for further explanation. ***B***, Success rate *vs.* length of the refinement-stage MCM trajectories optimizing 100 lowest-energy poses found at the seeding stage without energy minimizations. The rate plateaus to 40% at 100 to 200 MCM steps. ***C***, Success rate of the two-stage docking *vs*. the number of structures taken from the seeding stage to the refinement stage. Note that a better success rate is obtained with small number of seeds. ***D***, Success rate of the two-stage protocol *vs.* number of sampled seeds.

RESULTS

Examining set with the DDD function and the solvent-exclusion term. Using the enriched libraries of ligand conformers and the DDD function $\varepsilon = kr$ with the solvent-exclusion term (Lazaridis and Karplus 1999) we obtained success rates of 60.0, 60.0 and 58.3, respectively, for $k = 1$, 2, and 4 (Table 2.2). Most false-positives in these experiments corresponded to ligand-binding sites at the protein surface (Fig. 2.7). Comparison of the energies of the false-positives with the MC-minimized energies of the corresponding x-ray structures demonstrated large differences in both the desolvation and electrostatic components. The solvent-exclusion term benefits hydrophobic ligand-protein interactions, which usually occur in deep ligand-binding pockets. Since ligand-protein contacts in such pockets are rather tight, they are accounted for by van der Waals interactions. The solvent-exclusion term also benefits location of the ligand hydrophilic groups at the protein surface where the dielectric permittivity is high and electrostatic interactions are weak. The DDD function does not completely account for this effect. For example, when calculated with the DDD function $\varepsilon = 2r$, the electrostatic energy $E_{ij} = 332q_iq_j / \varepsilon r$ between atoms i and j bearing equal charges q_i and q_j of 0.5 proton charge units and separated by 6 Å equals 1.15 kcal/mol. This value is an overestimate at the protein surface where electrostatic interactions are very week (Finkelstein and Ptitsyn 2002).

SEDDD function. We attempted to resolve the above problem by using a new dielectric function

$$\varepsilon_{ij} = r_{ij} \cdot \left[\varepsilon_0 + \left(1 - s_{kl}\right) \cdot \left(\varepsilon_1 - \varepsilon_0\right)\right], \quad (1)$$

where r_{ij} is the distance between interacting atoms i and j, s_{kl} is the overlap of volumes of solute groups k and l that include atoms i and j, respectively, with the protein and/or ligand, and ε_0 and

Table 2.2: Success rate (SR) and average RMSD[a] (Å) for examining-set docking experiments

Pro-tocol	Solvent-exclusion term	Titrable residues	Dielectric Function	Match to the x-ray structure			
				AGM		One of top 10 local minima [b]	
				SR, %	RMSD	SR, %	RMSD
Enriched libraries of ligand conformers							
1	Yes	Neutral	$\varepsilon = r$	58.3	2.65	75.0	1.66
2	Yes	Ionized	$\varepsilon = r$	60.0	2.46	72.7	1.83
3	Yes	Neutral	$\varepsilon = 2r$	58.3	2.94	71.6	1.86
4	Yes	Ionized	$\varepsilon = 2r$	60.0	2.84	75.0	1.71
5	Yes	Neutral	$\varepsilon = 4r$	56.7	2.70	66.7	2.00
6	Yes	Ionized	$\varepsilon = 4r$	58.3	2.64	71.6	1.90
7	No	Neutral	$2r \leq \varepsilon \leq 8r$	71.6	1.82	81.6	1.23
8	No	Ionized	$2r \leq \varepsilon \leq 8r$	**78.3**	**1.70**	85.0	1.18
Unbiased libraries of ligand conformers							
9	Yes	Ionized	$\varepsilon = 2r$	45.0	3.24	55.0	2.62
10	No	Ionized	$2r \leq \varepsilon \leq 8r$	**58.3**	**2.51**	71.3	2.23

Bolded values are the final success rates used to compare with other programs

[a] RMSD of the apparent global minima from corresponding x-ray structures averaged over the 60 examining-set complexes.

[b] Best-RMSD structure from the 10 lowest energy structures including the AGM.

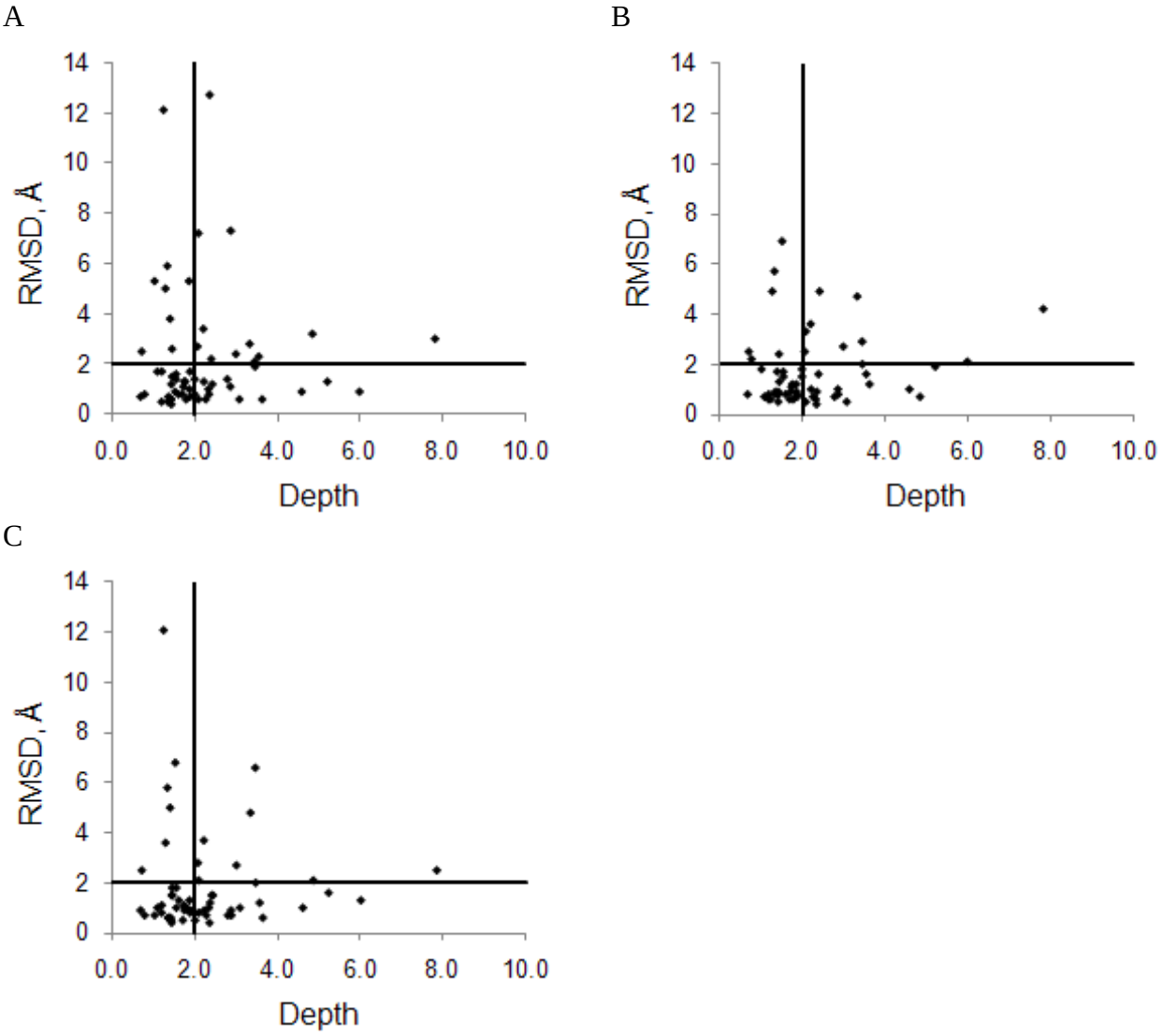

Figure 2.7. **RMSDs from the x-ray structures of the AGM structures predicted with the DDD function plotted against the depths of the ligand-binding pockets.** Each point represents an examining-set ligand-receptor complex. The ligand-binding pocket depth was determined as the ratio of the number of flexible residues in the protein double-shell model to the number of the ligand's heavy atoms. ***A***, ***B***, and ***C*** show, respectively, data obtained with the DDD functions $\varepsilon = r$, $\varepsilon = 2r$, and $\varepsilon = 4r$. Note high-RMSD points at shallow binding sites.

ε_1 ($\varepsilon_1 > \varepsilon_0$) are parameters. For a buried pair of solute groups that overlap with the protein and/or ligand, $s = 1$ and a low-range dielectric $\varepsilon_{ij} = r_{ij}\varepsilon_0$ is used. For a pair of water-exposed atoms, $s_{kl} = 0$ and a high-range dielectric function $\varepsilon_{ij} = r_{ij}\varepsilon_1$ is used. For a pair of partially exposed atoms, $0 < s_{kl} < 1$ and the dielectric function is an intermediate between $r_{ij}\varepsilon_0$ and $r_{ij}\varepsilon_1$. The sigmoid character of the function was chosen to enable smooth transitions between the low- and high-dielectric values. Overlap of the hydration-shell volumes of two solute groups with the protein and/or ligand is given by

$$s_{kl} = c(v_k + v_l), \tag{2}$$

where v_k and v_l are fractions of the hydration-shell volumes of solute groups k and l, respectively, which overlap with the protein and/or ligand. For every solute group in the system, values v are computed upon each update of the interaction list by using equations (6) and (21) derived by Lazaridis and Karplus for their Gaussian solvent-exclusion model (Lazaridis and Karplus 1999):

$$v_m = \sum_{n \neq m} \frac{2V_n}{4\pi\sqrt{\pi}\lambda_m r_{mn}^{\ 2}} \exp\left[-\frac{(r_{mn} - R_m)}{\lambda_m} \right]^2. \tag{3}$$

Here, λ is the hydration-shell thickness, which equals 6 Å for neutral titrable groups and 3.5 Å for other groups, R is the van der Waals radius of a solute group (Brooks, Bruccoleri et al. 1983). V is the hydration-shell volume of a solute group taken from Table 1 of (Lazaridis and Karplus 1999).

Summation in (3) is over solute groups, while electrostatic interactions are summed over all pairs of nonbonded atoms including hydrogens. Thus, (3) cannot be used to estimate values v_H

for hydrogen atoms. We tested $v_H = 0$ and $v_H = v_s$, where *s* stands for the hydrogen-containing solute group. Better results were obtained for $v_H = v_s$. Coefficient $c = 0.625$ was empirically calibrated to ensure that $0 < s_{kl} < 1$ for any pair of solute groups at any distance. The SEDDD function is not differentiable, but since the hydration-shell volumes are constant between updates of the interaction list, the electrostatic energy term involving the SEDDD function is differentiable between the updates. Derivatives of energy in the space of generalized coordinates were calculated analytically (Zhorov 1981; Zhorov 1983).

Optimizing parameters ε_0 and ε_1. Expressions (1-3) provide a physically meaningful model, but the challenge is to determine the combination of ε_0 and ε_1, which minimizes the RMSD between the predicted and experimental structures. The dielectric permittivity varies from ~ 2 inside a protein to ~ 80 in bulk water around the protein (Finkelstein and Ptitsyn 2002; Gohlke and Klebe 2002). For a pair of solvent-exposed nonbonded atoms at distance of 3 Å, $r_{ij}\varepsilon_1 = 80$ when $\varepsilon_1 \sim 27$. The dielectric permitivity at the protein surface is intermediate between the protein core and bulk water (Bockris and Reddy 1977; Teschke, Ceotto et al. 2001; Rubinstein and Sherman 2007). Therefore, we varied ε_0 and ε_1 from 1 to 10 with a step of 1, which gives 55 combinations of ε_0 and ε_1. For each combination, the AGM was searched using the two-stage docking protocol and the single-conformer ligand library. The RMSD of the ligand's heavy atoms between the AGM and the x-ray structure was plotted as the function of ε_0 and ε_1. Trial maps computed with and without the solvent-exclusion term demonstrated that omitting the solvent-exclusion term improves RMSD (not shown). This result indicates that calculations with the SEDDD function implicitly account for variable hydration of solute groups at different

degrees of exposure to the solvent. We further computed RMSD plots against ε_0 and ε_1 without the solvent-exclusion term for 16 ligand-protein complexes in the second training set.

Most of the plots have several RMSD minima (Fig. 2.8). The diagonal corresponds to calculations with the DDD function $\varepsilon = kr$ without the solvent-exclusion term. For commonly used DDD functions $\varepsilon = r$ to $\varepsilon = 4r$ the RMSD on the maps is usually above 2 Å. The majority of areas with RMSD < 1.0 Å occurred at regions where $\varepsilon_0 \neq \varepsilon_1$ indicating that when the solvent-exclusion term was omitted, calculations with the SEDDD function produced superior results as compared to calculations with the DDD function. The maps depend, in particular, on the number of the ligand polar groups. In the case of polar ligands, results depend dramatically on the dielectric function as exemplified by complex of chloramphenicol acetyltransferase with the ligand, which has a nitro group and two chlorine atoms (Fig. 2.8*B*). Maps for hydrophobic ligands, such as progesterone (1A28) have wide low-RMSD regions indicating the rather low effect of electrostatics (Fig. 2.9).

Examining set with the SEDDD function. Parameters $\varepsilon_0 = 2$ and $\varepsilon_1 = 8$ minimize RMSD in maps computed for the second training-set complexes (Fig. 2.8). We used these parameters to test the ability of the two-stage docking protocol to reproduce the examining-set complexes with the unbiased and enriched libraries of ligand conformers. Calculations were performed using titrable residues considered in both ionized and neutral forms (Table 2.2). In calculations with the enriched libraries and the DDD function, the highest success rate of 60% was obtained with ionized residues and $\varepsilon = r$ or $\varepsilon = 2r$, while calculations with neutral titrable residues yielded slightly lower success rates. Docking using the SEDDD function with ionized residues and enriched libraries resulted in a success rate as high as 78.3%. Besides an increase in the success

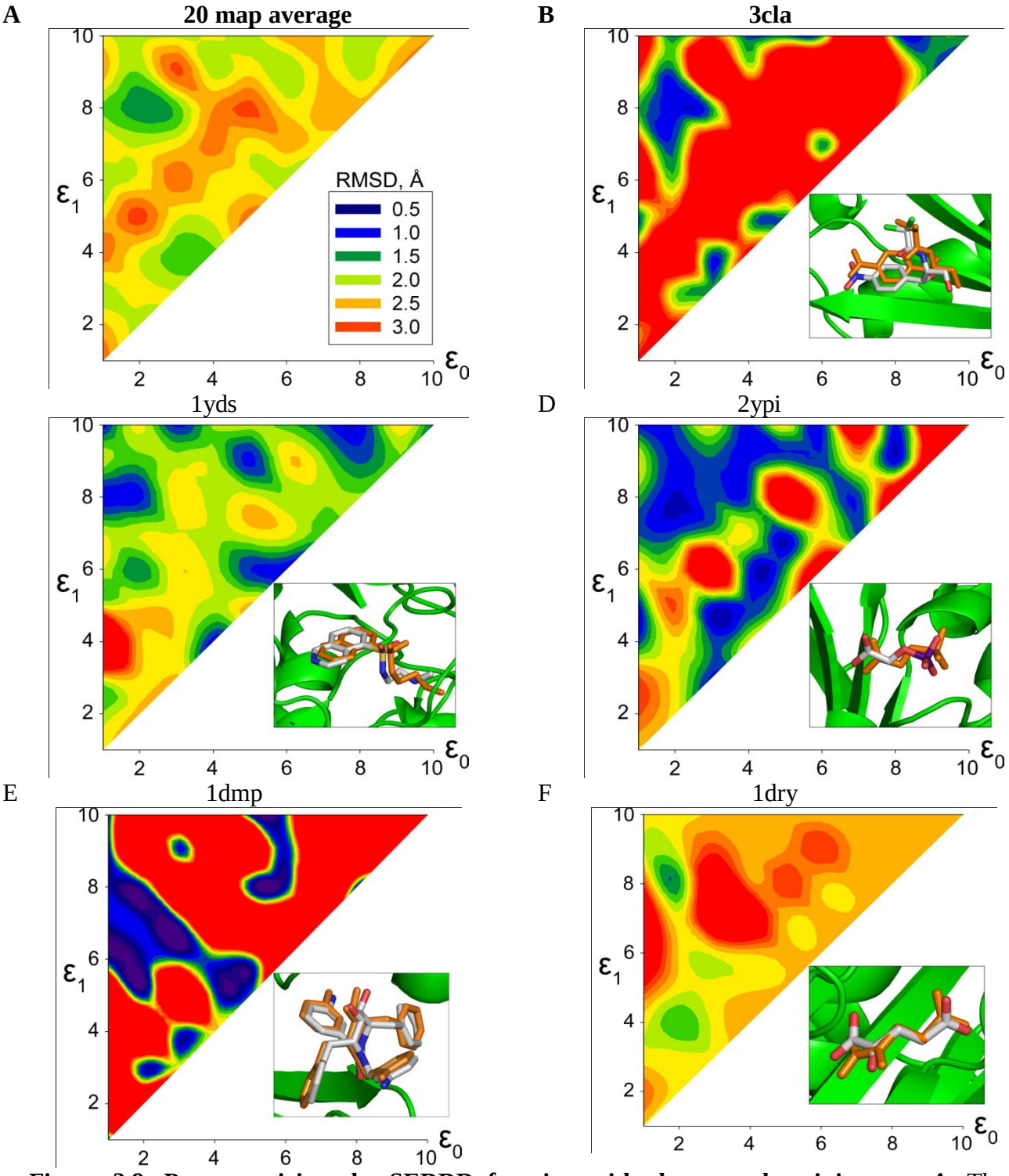

Figure 2.8. Parameterizing the SEDDD function with the second training set. ***A***, The RMSDs of the apparent global minima from the corresponding x-ray structures are averaged over the 20 training-set complexes and plotted against parameters ε_0 and ε_1. Note the global minimum of RMSD at $\varepsilon_0 = 2$ and $\varepsilon_1 = 8$. ***B–F***, RMSD maps for individual complexes identified by PDB codes. Inlets show the x-ray structures with CPK-colored ligands superimposed with the orange-colored ligands in AGM structures found with $\varepsilon_0 = 2$ and $\varepsilon_1 = 8$.

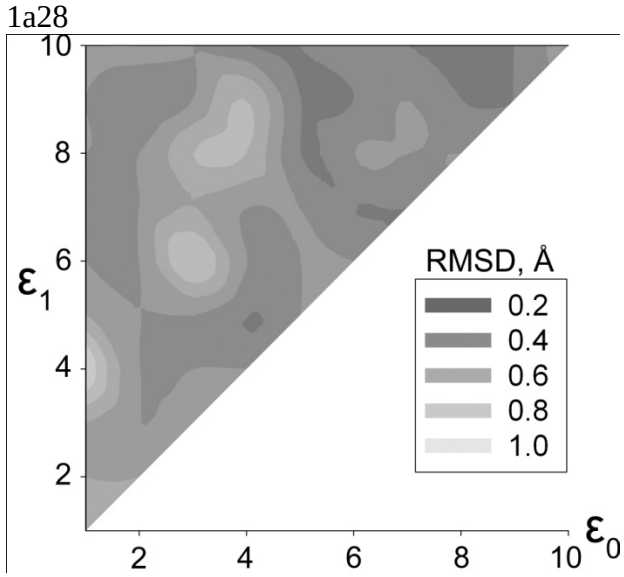

Figure 2.9. RMSD map for a complex 1A28 between a progesterone receptor and progesterone, a hydrophobic ligand. Low RMSDs are obtained at all tested combinations of ε_0 and ε_1, indicating a small impact of electrostatic interactions on the results.

rate, the SEEDD function also decreased the average RMSD of the AGMs from the x-ray structures from 2.46 to 1.7Å. Ionization of titrable residues had little effect with the DDD functions, but noticeably improved the success rate with the SEDDD function. These results show the potential of the SEDDD function when the libraries of ligand conformers contain structures close to those in protein-bound complexes.

The final comparison of the DDD and SEDDD functions was performed with ionized residues and unbiased libraries of ligand conformers. The SEDDD function yielded a success rate of 58.3, which is 13.3 % better than the best performing DDD function $\varepsilon = 2r$. Thus, flexible liganddocking with both unbiased and enriched libraries of ligand conformers demonstrated that the SEDDD function consistently yields higher success rates than the DDD functions.

DISCUSSION

Electrostatic and solvent-dependent interactions. Various sophisticated, physically rigorous methods have been proposed for calculations of electrostatic interactions between molecules in solvents, e.g. (Hassan 2007) and references therein. Such methods usually involve large computational cost and we are not aware of their systematic testing on large examining sets of ligand-protein complexes of various structures. Commonly used ligand-docking programs typically calculate electrostatic interactions with the DDD functions (Morris, Goodsell et al. 1996; Rarey, Kramer et al. 1996; Jones, Willett et al. 1997; Totrov and Abagyan 1997; Wang, Kollman et al. 1999; Ewing, Makino et al. 2001; Friesner, Banks et al. 2004; Meiler and Baker 2006). In this study we proposed the SEDDD function that accounts for both electrostatic interactions and dehydration effect and increases the success rate of ligand docking.

To parameterize the function, we computed 16 RMSD maps and at each map found a minimum at ε_0 = 2 and ε_1 = 8 (Fig. 2.8). Other low-RMSD regions at higher values of ε_0 and ε_1 are also seen (Fig. 2.8) indicating that sometimes underestimation of electrostatic interactions is better than their overestimation. Comprehensive analysis of this observation is hardly possible given an approximate character of classical force fields. However, we found that local minima of RMSD at high values of ε_0 and ε_1 usually appear for complexes with ligand-protein H-bonds. Since H-bonding potential is included in the AMBER force field, the H-bonds were predicted even with underestimated electrostatic energy.

Electrostatic and solvation energy components are interrelated and in many programs the DDD function is used along with the solvent-exclusion term or other stand-alone terms for the solvation energy. In this study, the highest success rate was obtained in calculations with the SEDDD function without the solvent-exclusion term. A likely cause of the lower success rate of calculations with the SEDDD function and the solvent-exclusion term is double counting of some charge-screening effects. Another cause may be overestimation of electrostatic attractions at solvent-exposed regions where beneficial hydration may overweight electrostatic repulsions. A disadvantage of omitting the solvent-exclusion term is that exposure of hydrophobic groups to the solvent is not penalized, but this is partially compensated by favorable van der Waals ligand-protein interactions in the protein buried regions.

Mallik and coauthors proposed a method to calculate electrostatic energy with taking into account exposure of interacting atoms in the aqueous environment (Mallik, Masunov et al. 2002). The method solves the Poisson-Boltzmann equation to predict the electrostatic-potential field and calculates the effective dielectric permittivity as function of distance from the surface. For atoms close to the surface, their exposure to the aqueous environments is also taken into

consideration. The method was parameterized using subtilisin, a rather spherical protein. When tested on three small proteins of various shape, the method produced better results as compared with the DDD function and Generalized Born model. However, the method was not tested on a wide variety of ligand-protein complexes. The computational cost of this method seems too high for high throughput ligand docking.

Combining the AMBER force field with the hydration shell model yielded correlation of the experimental and predicted binding energy in a series of 23 glucose analogue inhibitors of glycogen phosphorylase (Venkatarangan and Hopfinger 1999). In our approach, the solvent exposure-dependent component of the SEDDD function weakens interactions at the protein surface thus accounting for the dehydration energy. Indeed, the examining-set calculations with the SEDDD function in vacuum increased the success rate *vs.* analogous calculations with the solvent-exclusion term (Table 2.2).

In this study we optimized the ligand-docking protocol and parameterized the SEDDD function using two training sets of 26 ligand-protein complexes, which represent diverse types of ligand-protein interactions. The SEDDD function enables smooth variations of the dielectric permittivity between $2r_{ij}$ and $8r_{ij}$. The lower limit is often used in molecular simulations. The upper limit allows weakening of the electrostatic interactions at the water-exposed surface. All of the 16 RMSD maps, which were computed with the second training set, have a RMSD minimum at $\varepsilon_0 = 2r$ and $\varepsilon_1 = 8r$ and this combination was chosen to parameterize the SEDDD function. Thus the latter apparently does not involve a “knowledge-based“ component specific for the training sets and remains as “physics-based” as the DDD functions used with classical force fields including AMBER and CHARMM.

Flexible ligand docking is commonly performed by two-stage protocols in which precomputed libraries of ligand conformers are used at the seeding stage. Such libraries are easy to build for semirigid ligands and ligands containing a small number of rotatable bonds. However, flexible ligands with six or more rotatable bonds often adopt extended conformations in proteins, which are energetically unfavorable in lone ligands and may be unfavorable in water or lipid environments. An extended ligand conformation in complex with a protein maximizes ligand-protein contacts at the expense of the intra-ligand attractions. The fact that such conformations are observed in experimental structures suggests that the binding of corresponding ligands is an entropy driven process in which water molecules expelled from the ligand-binding site gain entropy. A similar mechanism explains, for example, the binding of antifreeze proteins to ice (Jorov, Zhorov et al. 2004). Energy-minimized extended conformations of lone ligands calculated with standard force fields have much higher energy than energy-minimized folded conformations. Therefore a flexible-ligand library including both folded and extended energy-minimized conformers accepted with only energy as the criteria (without any bias towards the experimental structure in complex with the protein) may contain many thousands of conformers. We are not aware of published algorithms for generating small libraries of ligand conformers without the protein context that would contain with a high probability a close match to the x-ray conformation. Here we generated libraries of ligand conformers using an *ad hoc* force field that ignores intra-ligand attractions. To reduce the number of conformers we used a clustering method in which structures were compared by torsion angles. Matching torsions in a pair of conformers were considered similar if they differed by less than 1 radian. Using this approach, we were able to generate 93% of the examining-set libraries in which at least 1% of conformers had an RMSD < 2.0 Å from the x-ray structures. A disadvantage of this hands-free approach is

the size of the 100-conformers libraries compared to libraries of 10 conformers per ligand (Meiler and Baker 2006). Our large libraries contain many decoys. This may explain why ZMM-based flexible docking with the DDD function performed worse than analogous approaches by others with smaller libraries. However, docking with the SEDDD function and large unbiased libraries yielded a success rate comparable with those reported by other groups. The SEDDD function would have performed better with smaller libraries. Indeed, our calculations with the enriched 100-conformers libraries yielded a success rate as high as 78.3% in spite the fact that most of the conformers in the libraries are decoys. Automatic generation of small libraries of ligand conformers having a close match to the protein-bound conformation should involve analysis of the binding-site structure. This challenging problem was not addressed in the current study.

As mentioned above, docking a ligand in the current version of the ZMM program involves hours of CPU time per ligand, whereas programs like GLIDE, GOLD, ICM, and FlexX, which are optimized for high-throughput ligand docking, involve minutes. The high docking speed of such programs is due to several features, which are not implemented in ZMM. These include (*i*) replacing explicit receptor atoms with grid potentials (Totrov and Abagyan 1997; Friesner, Banks et al. 2004), (*ii*) filtering-out at the screening stage unpromising binding modes that mismatch the binding-pocket shape (Rarey, Kramer et al. 1996) or lack chemical complementarity between the ligand and its receptor (Jones, Willett et al. 1997) and (*iii*) using libraries of ligand conformers that are much smaller than those described here (Meiler and Baker 2006). ZMM calculations with the SEDDD function not only achieved a higher success rate *vs.* those with the DDD function and solvent-exclusion term, but they were also about two times faster. Furthermore, application of the SEDDD function to simulations of large scale

conformational transitions in ion channels has demonstrated a higher accuracy than those with the standard ZMM approach (Garden, Bruhova et al. 2010).

CONCLUSION

In this work we proposed a new dielectric function SEDDD that depends on the distance between interacting atoms and their exposure to the aqueous environment. The SEDDD function allows quantifying large variations of the dielectric permittivity between the buried and water-exposed areas in the protein. These variations have long been well recognized and different computational approached are proposed to consider them in molecular simulations. A classical example is a combination of the distance-dependent dielectric (DDD) function and the solvent-exclusion term. However, the DDD function contains a heuristic coefficient whose choice is difficult and may require preliminary computations for a system under consideration. In our test calculations, the SEDDD function with the AMBER force field significantly improved the success rate of correct predictions of ligand-protein complexes versus results achieved with the DDD function and the solvent-exclusion term. Thus, the simple and physically meaningful SEDDD function may be a method of choice to substitute both the DDD function and the solvent-exclusion term. The function does not contain parameters specific for particular ligands or proteins and may be adapted to various programs for molecular simulations.

CHAPTER THREE

PREDICTING THE BINDING MODE OF BATRACHOTOXIN IN SODIUM CHANNELS USING CONSTRAINT DRIVEN DRUG DOCKING

CHAPTER 3 – PREFACE

The work presented in this chapter has been published in:

Du, Y.*, Garden, D. P.*, Wang. L, Zhorov, B. S., Dong. K. (2011) "Identification of new batrachotoxin-sensing residues in segment IIIS6 of sodium channel." J. Biol. Chem. 286(15): 13151-60.

*These authors contributed to the work equally

Permission has been granted from the publisher to reproduce the material here.

I built the models, preformed all the simulations and wrote the manuscript for this study.

ABSTRACT

Ion permeation through voltage gated sodium channels is modulated by various drugs and toxins. The atomistic mechanisms of action of many toxins are poorly understood. A steroidal alkaloid batrachotoxin (BTX) causes persistent channel activation by inhibiting channel inactivation and shifting the voltage-dependence of activation to more negative potentials. Traditionally, BTX is considered to bind at the channel-lipid interface and allosterically modulate the ion permeation. However, in the past decade amino acid residues critical for BTX action are found in the inner helices of all four repeats of the alpha-subunit suggesting that BTX binds in the channel pore. In the octapeptide segment IFGSFFTL in IIIS6 of a cockroach sodium channel $BgNa_V$, besides Ser_3i15 and Leu_3i19, which correspond to known BTX-sensing residues in mammalian sodium channels, we found that a putative gating-hinge Gly_3i14 and Phe_3i16 are critical for the BTX action. Using these data along with published data as distance constrains, we docked BTX in the Kv1.2-based homology model of the open $BgNa_V$ channel. We arrived at a model in which BTX adopts a horseshoe conformation with the horseshoe plane normal to the pore axis. The BTX ammonium group is engaged in cation-pi interactions with Phe_3i16 and BTX moieties interact with known BTX-sensing residues in all four repeats. Oxygen atoms at the horseshoe inner surface constitute a transient binding site for permeation cations, while the bulky BTX molecule would resist the pore closure thus causing persistent channel activation. Our study reinforces the concept that steroidal sodium channel agonists bind in the inner pore of sodium channels and elaborates the atomistic mechanism of BTX action.

INTRODUCTION

Voltage gated sodium channels (Na_V) are responsible for the rapid rising phase of the action potential in nerve and muscle cells. The pore-forming α-subunit of Na_V channels contains four repeats, each repeat having six transmembrane helices (S1-S6). The S1-S4 helices form the voltage sensor domain. Positively charged S4 helices move outward in response to membrane depolarization. The S5 and S6 helices contribute to the pore-forming domain. The extracellular linkers connecting S5 and S6 helices form the four reentrant P-loops, which contain the selectivity-filter residues. In the absence of x-ray structures of Na_V channels, their homology models, which are based on x-ray structures of potassium channels, are used to explain structure-activity relationships of various sodium-channel ligands including local anesthetics (Lipkind and Fozzard 2005; Tikhonov, Bruhova et al. 2006; Tikhonov and Zhorov 2007; Bruhova, Tikhonov et al. 2008), steroidal activators (Tikhonov and Zhorov 2005; Wang, Mitchell et al. 2006; Wang, Tikhonov et al. 2007; Wang, Tikhonov et al. 2007), and pyrethroid insecticides (O'Reilly, Khambay et al. 2006; Du, Lee et al. 2009). Recent reinterpretation of data on substituted cysteine accessibility of $Ca_V2.1$ channel (Zhen, Xie et al. 2005) in view of a the channel homology model, which is based on the x-ray structure of the open voltage-gated potassium channel Kv1.2 (Long, Campbell et al. 2005), further supports general similarity of the inner-pore architecture in different voltage-gated cationic channels (Bruhova and Zhorov 2010).

Sodium channels are targets for numerous drugs and naturally occurring toxins. Batrachotoxin (BTX) is a steroidal sodium-channel agonist, which was first isolated from the skin of the Colombian frog *Phyllobates bicolr* (Daly, Witkop et al. 1965). BTX binds preferentially to the open Na_V channels (Khodorov and Revenko 1979; Hille 2001; Wang and Wang 2003) and alters several channel properties. First, it shifts the voltage-dependence of

activation in the hyperpolarizing direction thus causing the channel to open at more negative membrane potentials. Second, BTX inhibits inactivation. Third, BTX-modified channels demonstrate reduced selectivity to sodium ions and reduced conductance (Ulbricht 1969; Quandt and Narahashi 1982; Zlotkin 1999; Narahashi 2000). Due to their high affinity and specificity to Na_V channels, BTX and other steroidal agonists are useful tools to probe the channel functions, including the gating mechanisms.

Earlier studies demonstrated that point mutations in the inner helices IS6 and IVS6 ($I^{1i19}K$, $N^{1i20}K$, $L^{1i23}K$, $F^{4i15}K$, and $N^{4i20}K$)[1] make the $Na_V1.4$ channel BTX-resistant (Wang and Wang 1998; Wang and Wang 1999), leading to the idea that BTX binds in the interface between repeats I and IV (Linford, Cantrell et al. 1998). Subsequent mutational studies identified BTX-sensing residues in the inner helices of all four repeats including residues S^{3i15} and L^{3i19} in repeat III (Wang, Barile et al. 2001; Wang, Tikhonov et al. 2007; Du, Lee et al. 2009). Architecture of voltage-gated potassium channels is inconsistent with a scenario that a lipid-exposed ligand simultaneously binds to more than two inner helices. A unitary Hill coefficient of BTX action (Khodorov and Revenko 1979) and largely different amino acid sequences of the four repeats rule out a possibility that the channel contains more than one BTX receptor. (Khodorov and Revenko 1979; Huang, Moran et al. 1984; Garber and Miller 1987; Behrens, Oberhauser et al. 1989). Although allosteric effects could explain the modifications of channel conductance, ion selectivity and gating by BTX (Catterall 1977), another possibility is that BTX is directly exposed to the permeation pathway (Zhorov, Folkman et al. 2001; Tikhonov and Zhorov 2005).

[1] We designate residues using labels that are universal for P-loop channels (Table 1). A residue label includes the repeat number (1 to 4), segment type (*p*, P-loop; *i*, the inner helix; *o*, the outer helix), and relative number of the residue in the segment.

In a structural model of sodium channel with BTX exposed to the permeation pathway, the pore should accommodate a large BTX molecule. Furthermore, the model should suggest how ions permeate through the pore in which a bulky steroidal agonist is bound. Homology models of sodium channels, which are based on x-ray structures of distantly related potassium channel templates, are not expected to be precise enough to unambiguously predict ligand-binding model based solely on the computed toxin-channel binding energy. Additional experimental constraints are desirable to elaborate details of BTX binding inside the pore. Systematic mutations of residues around known BTX-sensing residues may reveal additional amino acids involved in BTX binding and thus provide further experimental constraints to dock BTX in the sodium channel model.

In this study, we first mutated six residues flanking the BTX-sensing S^{3i15} in the octapeptide segment IFGSFFTL (S^{3i15} and L^{3i19} are underlined) of a cockroach sodium channel $BgNa_v1$-1a (Song, Liu et al. 2004) and explored effects of mutations on the channel gating in the presence and absence of BTX. We identified F^{3i16} and a putative gating-hinge glycine G^{3i14} as new BTX-sensing residues. Using these and published data as distance constraints, we explored different possible binding models of BTX in the $K_v1.2$-based model of the open $BgNa_v$ channel and arrived to a new model, which is consistent with most of the available experimental data on BTX actions on sodium channels. We further tested the new model by generating seven additional mutations in the four pore-forming repeats and found that most of the mutations exhibited the BTX sensitivity in agreement with the model.

EXPERIMENTAL PROCEDURES

Expression of BgNav Sodium Channels in Xenopus Oocytes. The procedures for oocyte preparation and cRNA injection are identical to those described previously (Tan, Liu et al. 2002). For robust expression of the $BgNa_v$ sodium channels, cRNA was coinjected into oocytes with *Drosophila melanogaster* tipE cRNA (1:1 ratio), which enhances the expression of insect sodium channels in oocytes (Warmke, Reenan et al. 1997; Feng, Deák et al. 1995).

Electrophysiological Recording and Analysis. The voltage-dependence of activation and inactivation was measured using the two-electrode voltage clamp technique. Methods for two-electrode recording and data analysis were similar to those described previously (Tan, Liu et al. 2005). Sodium currents were measured with a Warner OC725C oocyte clamp (Warner Instrument, Hamden, CT) and processed with a Digidata 1322A interface (Axon Instruments Inc., Foster City, CA). Data were sampled at 50 kHz and filtered at 2 kHz. Leak currents were corrected by p/4 subtraction. pClamp 8.2 software (Axon Instruments Inc., CA) was used for data acquisition and analysis. The maximal peak sodium current was limited to < 2.0 μA to achieve optimal voltage control by adjusting the amount of cRNA and the incubation time after injection.

The voltage dependence of sodium channel conductance (G) was calculated by measuring the peak current at test potentials ranging from -80 mV to +65 mV in 5-mV increments and divided by (V - Vrev), where V is the test potential and Vrev is the reversal potential for sodium ion. Peak conductance values were normalized to the maximal peak conductance (G_{max}) and fitted with a two-state Boltzmann equation of the form $G/G_{max} = [1 + \exp(V - V_{1/2})/k]^{-1}$, or with the sum of two such expressions, in which V is the potential of the voltage pulse, $V_{1/2}$ is the voltage for half maximal activation, and k is the slope factor.

The voltage dependence of sodium channel inactivation was determined by using 100-ms inactivating pre-pulses ranging from -120 mV to 0 mV in 5 mV increments from a holding potential of -120 mV, followed by test pulses to -10 mV for 20 ms. The peak current amplitude during the test depolarization was normalized to the maximum current amplitude and plotted as a function of the pre-pulse potential. Data were fitted with a two-state Boltzmann equation of the form $I/I\text{max} = [1 + (\exp(V - V_{1/2})/k)]^{-1}$, in which I is the peak sodium current, I_{max} is the maximal current evoked, V is the potential of the voltage prepulse, $V_{1/2}$ is the half maximal voltage for inactivation, and k is the slope factor.

BTX was a generous gift from John Daly (National Institutes of Health, Bethesda, MD). Stock solution of BTX (1 mM), was dissolved in dimethyl sulfoxide (DMSO). The working concentration was prepared in ND96 recording solution just prior to the experiments. The concentration of DMSO in the final solution was < 0.5%, which had no effect on the function of sodium channels in the experiments. The method for application of chemicals in the recording system was identical to that described by Tan et al.(Tan, Liu et al. 2005). The effects of BTX were measured 10 min after toxin application.

Homology Model. We have built a homology model of the open $BgNa_v1$-1a channel based on the crystal structure of the open potassium channel Kv1.2 (Long, Campbell et al. 2005). A model of the closed $BgNa_v1$-1a channel, have been built based on the crystal structure of the closed potassium channel KcsA (Doyle, Morais Cabral et al. 1998). The ZMM molecular modeling program (www.zmmsoft.com) has been used in all calculations. The $BgNa_v1$-1a, Kv1.2, and KcsA sequences were aligned (Table 3.1) as before (Zhorov and Tikhonov 2004; Bruhova, Tikhonov et al. 2008). The extracellular loops, which are far from BTX-sensing residues, were not included in the model. The P-loops were modeled as in

Table 3.1. Sequence alignment

Channel	Helix	First residue #	1	11	21	
KcsA	M1	23	LHWRAAGAAT	VLLVIVLLAG	SYLAVLAER	
K_v1.2	S5	322	ASMRELGLLI	FFLFIGVILF	SSAVYFAEA	
$BgNa_v$1-1	IS5	254	ESVKNLRDVI	ILTMFSLSVF	ALMGLQIYM	
	IIS5	899	RTVGALGNLT	FVLCIIIFIF	AVMGMQLFG	
	IIIS5	1394	QAIPSIFNVL	LVCLIFWLIF	AIMGVQLFA	
	IVS5	1712	MSLPALFNIC	LLLFLVMFIF	AIFGMSFFM	
			33	41	51	
KcsA	P	59	LITYPRAL	WWSVETATTV	GYGDLYPV	
K_v1.2	P	358	FPSIPDAF	WWAVVSMTTV	GYGDMVPT	
$BgNa_v$1-1	IP	289	CIKNFWAF	LSAFRLMTQD	YWENLYQL	
	IIP	934	VERFPHSF	MIVFRVLCGE	WIESMWDC	
	IIIP	1433	STTLSKAY	LCLFQVAT**F**K	GWIQIMND	
	IVP	1747	GLDDVQSM	ILLFQMSTSA	GWDGVLDG	
			1	11	21	31
KcsA	M2	86	LWGRLVAVVV	MVAGITSFGL	VTAALATWFV	GREQERR
K_v1.2	S6	385	IGGKIVGSLC	AIAGVLTIAL	PVPVIVSNFN	YFYHRET
$BgNa_v$1-1	IS6	391	PWHMLFFIVI	IFLG**S**FYL**VN**	LI**L**AIVAMSY	DELQKKA
	IIS6	978	WSCIPFFLAT	VVIG**N**LVV**L**N	LFLALLLSNF	GSSNLSA
	IIIS6	1503	IYMYLYFVFF	IIF**GSF**FT**L**N	LFIGVIIDNF	NEQKKKA
	IVS6	1803	TVGLAFLLSY	LVIS**F**LIV**IN**	MYIAVILENY	SQATEDV

Experimentally determined BTX sensing residues are underlined. **Repeat I.** rNav1.4 point mutants $I^{1i19}K$, $N^{1i20}K$, and $L^{1i23}K$ are BTX-resistant (Wang and Wang 1998). Mutations $S^{1i15}K$ and $S^{1i15}R$ make hNav1.5 channel completely insensitive to 5 μM BTX (Wang, Tikhonov et al. 2007). **Repeat II.** Point mutations $N^{2i15}K$ and $L^{2i19}K$ render rNav1.4 completely insensitive to 5 μM BTX (Wang, Barile et al. 2001). **Repeat III.** Point mutations $S^{3i15}K$ and $L^{3i19}K$ render rNav1.4 completely insensitive to 5 μM BTX (Wang, Nau et al. 2000). Mutations $F^{3p49}K$ and $F^{3p49}R$ make hNav1.5 severely resistant to BTX (Wang, Mitchell et al. 2006). Effects of BTX on $BgNa_v$ mutants $G^{3i14}A$ and $F^{3i16}A$ are described in the current study. **Repeat IV.** Point mutations $F^{4i15}K$ and $N^{4i20}K$ render rNav1.4 completely insensitive to 5 μM BTX (Wang and Wang 1999). Mutation $V^{4i19}C$ protects rNav1.4 from modification by BTX (Vedantham and Cannon 2000).

(Tikhonov and Zhorov 2005). The Monte Carlo-energy minimization (MCM) method (Li and Scheraga 1987) was used to optimize the channel model and dock BTX. The energy was calculated using the AMBER force field (Weiner, Kollman et al. 1984; Weiner, Kollman et al. 1986) and solvent exposure- and distance dependent dielectric function (Garden and Zhorov 2010). Atomic charges at BTX molecule were calculated using the AM1 method (Dewar, Zoebisch et al. 1985) realized in MOPAC. The energy was minimized in the space of generalized coordinates (Zhorov 1981; Zhorov 1983). Bond angles were varied in BTX, but not in the protein. Program SCWRL3 (Canutescu, Shelenkov et al. 2003) was used to assign starting conformations of the channel side chains.

BTX Docking. BTX binding modes, which are consistent with mutational data, were imposed by distance constraints (Table S3.1). A constraint is a flat-bottom parabolic penalty function added to the energy expression. When a distance between a given BTX atom and a given atom in the BTX-sensing residue exceeds the upper limit of the constraint (5 Å in this study), the penalty contribution to the energy increases sharply, with the force constant of 100 $kcal \cdot mol^{-1} \cdot Å^{-1}$. A flat-bottom constraint ensures proximity between two atoms but does not impose specific contacts between them (e.g., an H-bond or a cation-π contact). To search for low-energy binding modes of BTX, we employed our three-stage flexible docking protocol (Garden and Zhorov 2010). In the first stage, a library of BTX conformers was generated by randomly sampling BTX torsions, followed by energy minimizations to ensure that all the rings were closed. Ten thousand BTX conformations were generated and the ten lowest-energy conformations were collected for docking. The lowest-energy conformer in the library corresponds to the x-ray structure of BTX. In the second stage, the position and orientation of each BTX conformer in the library were sampled 200,000 times by assigning random values to

six rigid-body degrees of freedom of the ligand. The energy of the BTX-receptor complexes (including the distance-constraint penalties) was calculated without energy minimization and the ten lowest energy complexes were collected. In the third stage, the ten collected complexes were refined by a 1,000 step MC-minimization and the lowest energy structure was used as a BTX binding model consistent with the given combination of distance constraints. At this stage, the torsion angles in the protein side chains and in BTX were sampled. Finally, all distance constraints were removed and the model was MC-minimized to check its intrinsic stability. If during the final MC-minimization BTX moved away from the constraints-imposed binding mode, the latter was excluded from further analysis.

RESULTS

G3i14A and F3i16A/K substitutions reduce the action of BTX on the BgNav1-1a channel. Previously we reported that two amino acid residues, S^{3i15} and L^{3i19} are critical for the action of BTX on the cockroach sodium channel (Du, Lee et al. 2009). To determine whether other residues flanking these two BTX-sensing residues in the IFGSFFTL segment (S^{3i15} and L^{3i19} are underlined) are also involved in the action of BTX, we examined the effect of BTX on six mutant $BgNa_v1$-1a channels, $I^{3i12}A$, $F^{3i13}A$, $G^{3i14}A$, $F^{3i16}A$, $F^{3i17}A$ and $T^{3i19}A$, that were made previously for another study (Du, Lee et al. 2009). None of the substitutions alter channel gating except for $G^{3i14}A$ which shifted the voltage-dependence of activation in the depolarizing direction by ca. 12 mV (Du, Lee et al. 2009).

In agreement with results reported for mammalian sodium channels, e.g. (Linford, Cantrell et al. 1998; Wang and Wang 2003), BTX inhibited inactivation inducing a noninactivating current and a tail current upon repolarization, and shifted the voltage-dependence of activation to more

negative membrane potentials (Fig. 3.1A and 3.1B). The BTX effects on $BgNa_v1$-1a channels were incomplete because two voltage dependent components of activation were observed: one with the voltage-dependence similar to unmodified channels and the other with the negatively shifted voltage dependence of BTX-modified channels (Fig. 3.1B). At 500 nM, 44% of $BgNa_v1$-1a channels were modified by BTX, and BTX did not alter the amplitude of peak current. The BTX effect on inactivation is also evident in the voltage dependence of steady-state inactivation where the foot of the inactivation curve at the depolarizing potentials was lifted in the presence of BTX (Fig. 3.1C).

Alanine substitutions of G^{3i14} and F^{3i16} significantly reduced the percentage of the BTX-induced tail current and noninactivating current (Fig. 3.1D and 3.1E). In contrast, $I^{3i12}A$, $F^{3i13}A$, $F^{3i17}A$ and $T^{3i19}A$ did not (Fig. 3.1D and 3.1E). Furthermore, a lysine substitution of F^{3i16} almost completely abolished the action of BTX (Fig. 3.1D and 3.1E). Similarly, the BTX effect was not observed in the voltage-dependence of inactivation of $G^{3i14}A$ and $F^{3i16}A/K$ channels (Fig. 3.1F-3.1H) (note a slightly lifted foot of the inactivation curve in the $G^{3i14}A$ and $F^{3i16}A$ channels). Consistent with these results, substitutions $G^{3i14}A$ and $F^{3i16}A$, but not $I^{3i12}A$, $F^{3i13}A$, $F^{3i17}A$ and $T^{3i19}A$, significantly reduced the percentage of BTX-modified channels (Fig. 3.1B and 3.1I). No $F^{3i16}K$ channels were modified by BTX (500 nM) (Fig. 3.1I). These results collectively demonstrated that $G^{3i14}A$ and $F^{3i16}A/K$ substitutions significantly reduced the effects of BTX on the $BgNa_v1$-1a channel.

BTX-bound Model of Sodium Channel. The BTX molecule has a hydrophobic and hydrophilic faces (Fig. 3.2) (Tikhonov and Zhorov 2005). Previously published data on BTX-sensing residues were rationalized in a model in which BTX extends along the pore axis, its

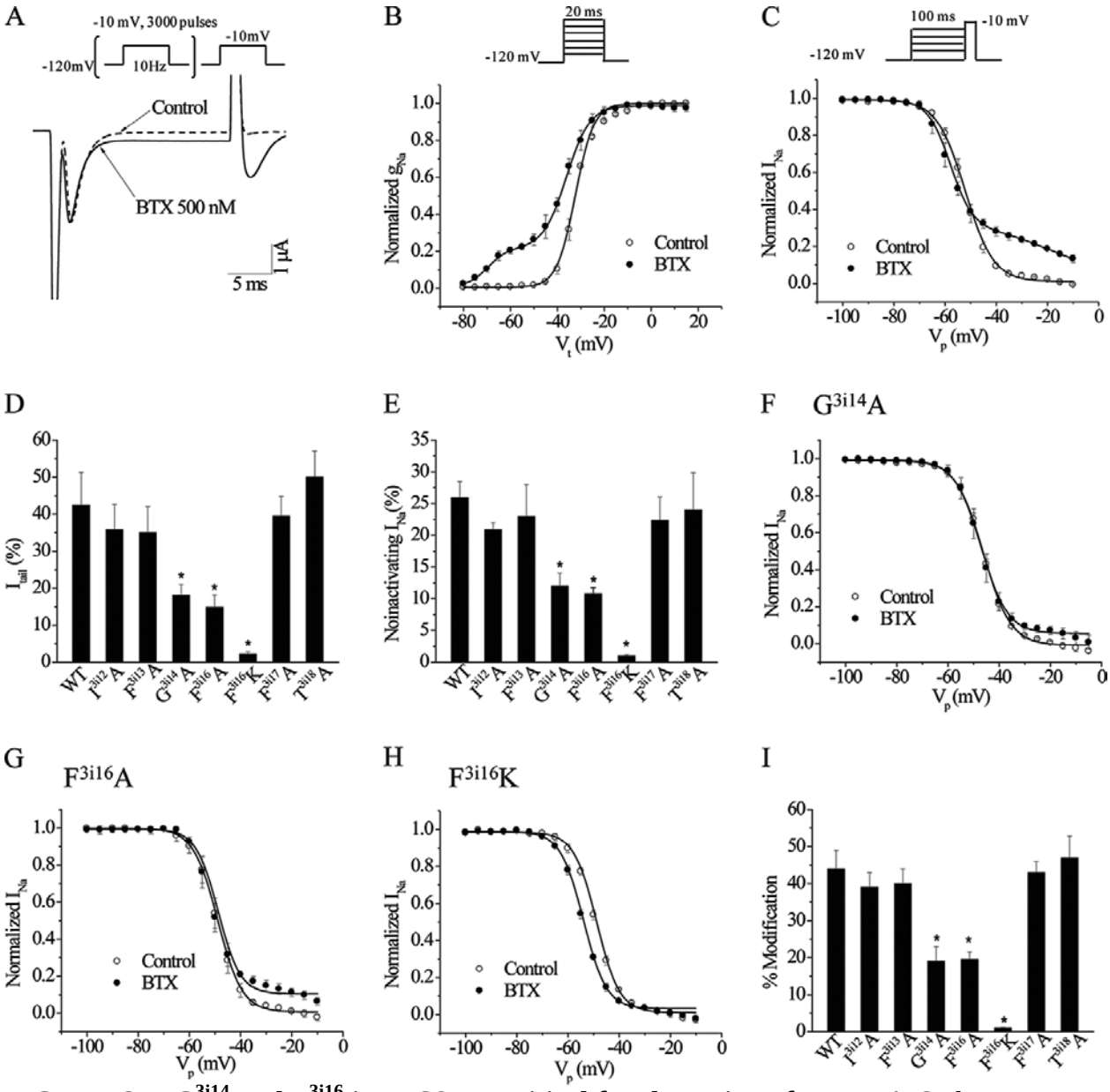

FIGURE 3.1. G^{3i14} and F^{3i16} in IIIS6 are critical for the action of BTX. *A.* Sodium currents before and after the application of 500 nM BTX. BTX-induced noninactivating current and tail current were elicited by a 20-ms test pulse to -10 mV from a holding potential of -120 mV after 3000 repetitive pulses to -10 mV at a frequency of 10 Hz in the presence of 500 nM BTX. *B* and *C*. Voltage-dependence of activation (B) and inactivation (C). *D* and *E*. Effects of amino acid substitutions on BTX-induced tail current (D) and noninactivating current (E). The amplitude of tail current and noninactivating current induced by BTX was normalized to the peak current after toxin application. *F* and *H*. Voltage dependence of inactivation of $G^{3i14}A$, $F^{3i16}A$ and $F^{3i16}K$ channels before and after the application of BTX. *I.* Percentage of channels modified by BTX for $BgNa_v1$-1a and mutants. The voltage-dependence of activation (conductance curves) in the presence of BTX was fitted with the sum of two Boltzmann relationships to determine the percentage of channels that were modified by BTX. The asterisks indicate significant differences from the wild-type channel as determined by t-test ($p<0.05$).

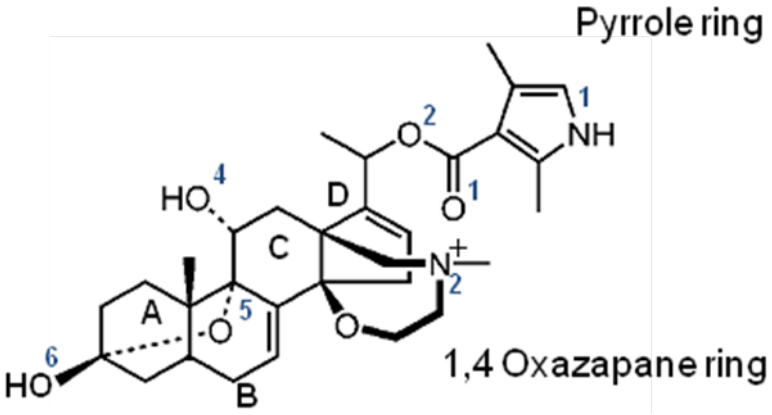

FIGURE 3.2. Structural formulae of BTX.

hydrophobic face interacts with hydrophobic residues that line the inner pore, and the hydrophilic face contributes in the ion permeation pathway along with the channel hydrophilic residues (Tikhonov and Zhorov 2005; Wang, Mitchell et al. 2006). Our present finding that phenylalanine F^{3i16} is essential for BTX binding is inconsistent with the previously proposed orientation of BTX. This motivated elaboration of an updated model, which would be consistent with all currently available experimental data on BTX action.

Hands-free docking of semi-flexible BTX in the channel with flexible sidechains is possible (Garden and Zhorov 2010), but lowest-energy binding mode may or may not correspond to the native ligand-channel conformation. Indeed, even when high-resolution x-ray structures of proteins are used to dock flexible ligands, the probability that the ligand conformation and orientation in the apparent global minimum would match those in the x-ray structure does not exceed 70% (Totrov and Abagyan 1997; Friesner, Banks et al. 2004; Meiler and Baker 2006). The homology model of the sodium channel is obviously less precise than high-resolution x-ray structures. Therefore, we sought various low-energy binding modes of BTX, which are consistent with mutational data on BTX-channel interactions, by applying various combinations of distance constraints that bring different BTX moieties to BTX-sensing residues of the channel (see *Methods*). Among many possibilities we focused on those that satisfy the following criteria. First, the model should be stable after all distance constraints are removed and refining unconstrained MC-minimization is performed. Second, the energy of the specific BTX binding mode should not exceed the energy of the apparent global minimum by more than 7 kcal/mol. Third, as many as possible experimentally known BTX-sensing residues should directly interact with the ligand. Fourth, BTX in the model should not block the pore, but allow the ion permeation through the BTX-bound channel. Fifth, the model should explain why BTX-bound

channel resists the activation-gate closure (Hille 2001). For each binding mode, which was initially imposed by the distance constraints, ten lowest complexes were collected and then refined without any constraints. Several constraint-imposed BTX binding modes, in which only part of the known BTX-sensing residues directly interact with BTX, are described in Supplementary Data.

The binding mode in which many of the currently known BTX-sensing residues are in direct contacts with BTX is shown in Fig. 3.3. This lowest-energy BTX-channel complex was obtained by flipping BTX in the constraints-imposed model (Fig. S3.1*F*) by 180^{o} around the vertical axis and MC-minimizing the complex. In this binding mode, BTX adopts a horseshoe conformation with the horseshoe plane normal to the pore axis. The ligand ammonium group is engaged in cation-π interactions with the BTX-sensing residue F^{3i16}, which was identified in the current study. We tested the axial and equatorial orientations of the ammonium hydrogen. In both orientations, the cation-π interactions are possible. The advantage of the axial orientation is that BTX ammonium group donates an H-bond to S^{3i15}, a known BTX-sensing residue (Wang, Nau et al. 2000). The carbonyl oxygen and pyrrole nitrogen of BTX accept H-bonds from N^{2i15} and S^{1i15}, respectively, in agreement with the data that mutations of these amino acids affect BTX action (Wang, Tikhonov et al. 2007; Wang, Tikhonov et al. 2007). Hydrophobic groups in the outer surface of the horseshoe interacts with the hydrophobic BTX-sensing residues L^{2i19} (Wang, Barile et al. 2001), L^{3i19} (Wang, Nau et al. 2000) and F^{4i15} (Wang and Wang 1999). Besides binding to BTX-sensing residues in the inner helices, BTX strongly interacts with F^{3p49} by its oxazepane ring. The latter BTX-sensing residue was initially predicted in the modeling study (Tikhonov and Zhorov 2005) and later lysine and arginine substitutions of F^{3p49} were demonstrated to dramatically decrease BTX action (Wang, Mitchell et al. 2006). Most

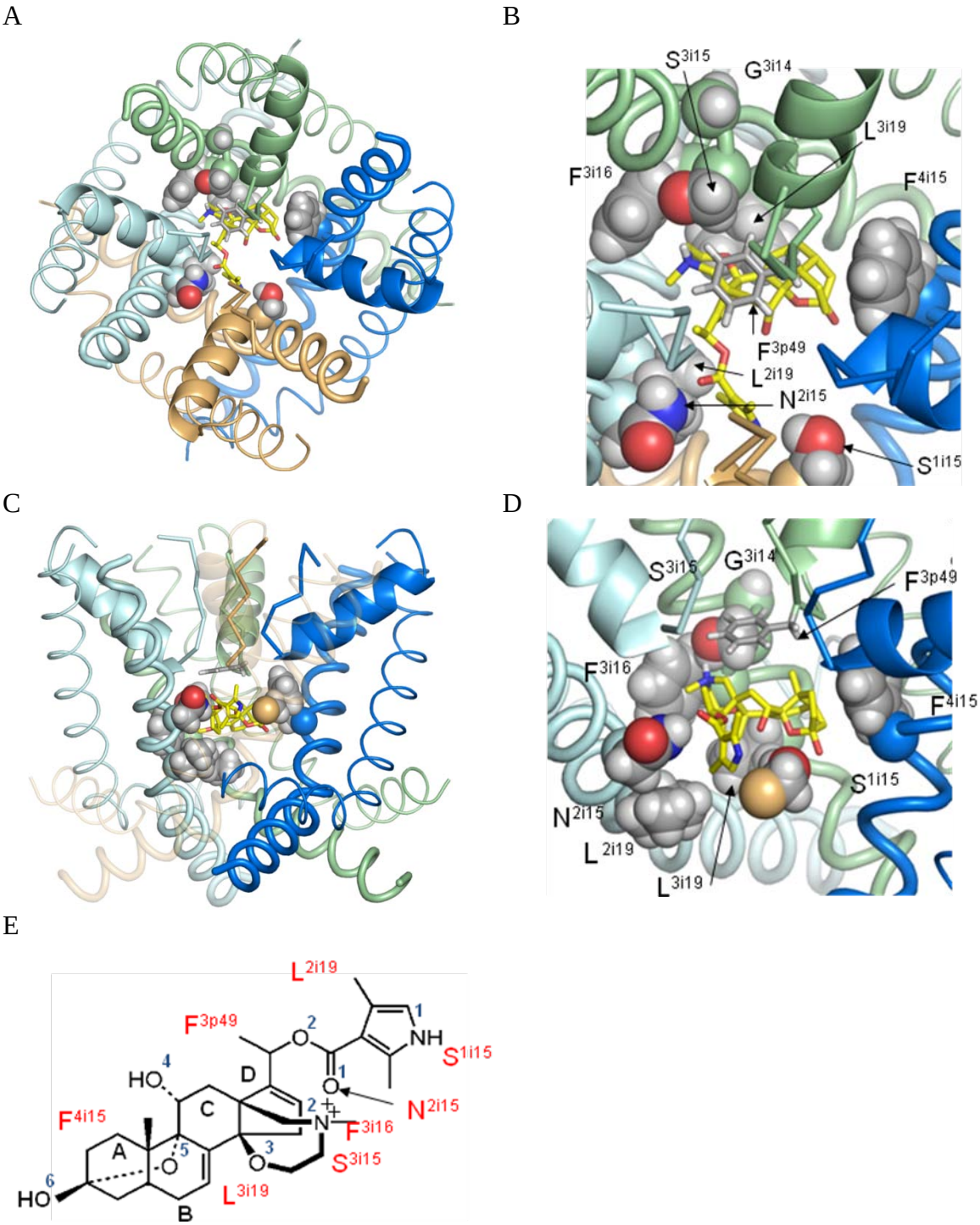

FIGURE 3.3. Predicted binding mode of BTX in BgNa$_v$1-1. The pore-forming domain of the channels is shown with the inner helices (thick rods), outer helices (thin rods), P-helices (ribbons) and ascending limbs (thin rods). Repeats I, II, III, and IV are colored orange, cyan, green and blue respectively. Known BTX sensing residues are spaced filled. BTX is shown by sticks with yellow carbons. BTX adopts a horseshoe conformation with its hydrophobic side interacting with the inner helices and its hydrophilic side forming a binding site for permeating cations. *A* and *B.* Top views. *C* and *D***,** Side views with the front repeat removed for clarity. *E*. Schematic view of BTX-channel interactions.

importantly, four oxygen atoms of BTX as well as pyrrole nitrogen atom and π-electrons of carbon atoms in the pyrrole ring line the inner surface of the horseshoe, which bends over the pore axis. In other words, the inner surface of the BTX horseshoe forms a hydrophilic arch inside the inner pore of the channel. Na^+ ions would permeate through this arch and thus through the BTX-bound channel (Fig. 3.4 *A*,*B*).

In our model BTX adopts the horseshoe conformation, which is about 2 kcal/mol less preferable than the global minimum found by MC-minimization of BTX in vacuum (the global minimum corresponds to the BTX conformation in the crystal). The cause of the intramolecular BTX strain is electrostatic repulsion between BTX ether oxygen in the linker between the pyrrole ring and steroidal core and the oxygen atom of the hydroxy substituent in the steroidal ring C. The BTX strain is compensated by strong attraction of BTX to BTX-sensing residues (Table 3.2) so that the BTX-channel complex shown in Figures 3.3 and 3.4 remains stable upon MC-minimization in the absence of distance constraints. This result suggests that the strained BTX may slightly widen the pore. Our homology model is not expected to be precise enough to simulate possible conformational rearrangements of the open channel upon BTX binding. But in view of these data the slow onset of BTX effect may be due to BTX binding to low-populated states of the channel in which the inner pore is wider than in the most populated open states.

To explore whether BTX would resist the inner-pore closing, we have built a KcsA-based model of the closed BgNav1.1a and imposed distance constrains between BTX and BTX-sensing residues to maintain the horseshoe-like conformation of the agonist at the same level of the pore as in the open channel. After intensive MC-minimization in the presence of the constraints numerous clashes were found between BTX and the channel, including BTX sensing residues (not shown). The channel closure substantially narrowed the pore lumen at the level of BTX and

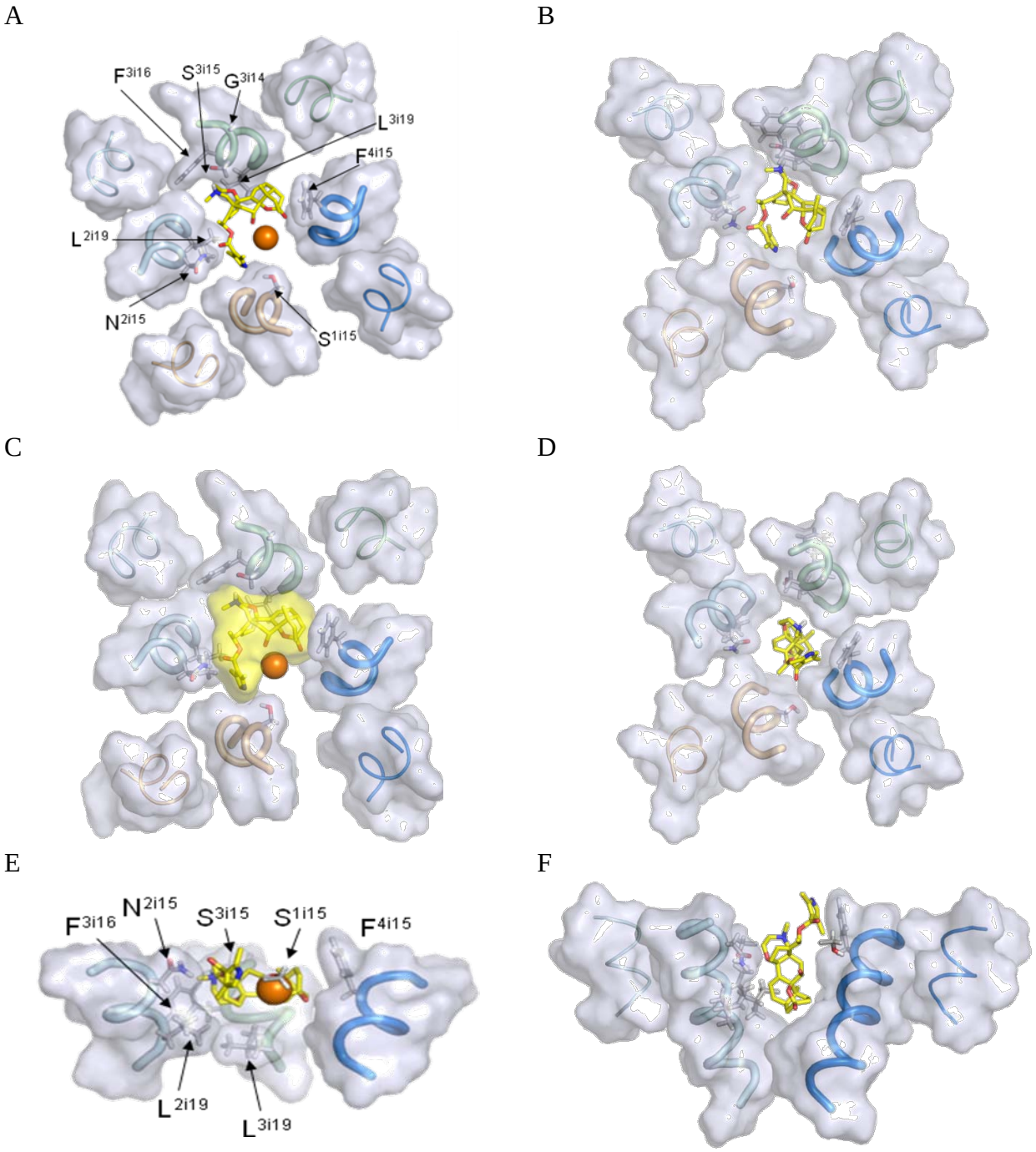

FIGURE 3.4. BTX in the open (*A,C,E*) and closed (*B,D,F*) states of the sodium channel. For clarity, only parts of the outer and inner helices around level *i15* are shown at the top (*A* - *D*) and side (*E, F*) views. The front helix IS6 is removed at *E* (except BTX-sensing residue S^{1i15}) and repeats I and IV are removed at *F*. In the open state, the inner cavity at the level *i15* is wide enough to accommodate BTX in the horseshoe conformation. The BTX van der Waals shape of the BTX horseshoe conformation approximately fits the inner cavity (*C*). A Na^+ ion (orange sphere) binds to the inner surface of the BTX horseshoe (*A, C, E*). *B*, KcsA-based model of the closed channel $BgNa_v1.1$ with BTX constrained in the same position as in *A*. Due to a small diameter of the closed pore, this orientation of BTX is unstable. *D, F*. Upon removal of the BTX-channel distance constraints. BTX adopts a vertical extended orientation in the closed pore. This may explain the fact that BTX is trapped in the closed channel.

also decreased the "diameter" of the BTX horseshoe (cf. Figs. 3.4A and 3.4B). In the constrained complex (Fig. 3.4B) the BTX-channel interaction energy was 18.7 kcal/mol higher than in the unconstrained complex (Fig. 3.4A). When we removed the BTX-channel constraints and further MC-minimized the complex, BTX shifted from level *i15* towards the selectivity filter, changed its conformation, and fit in the central cavity of the closed channels (Fig. 3.4D, F). These results are consistent with the data that BTX can be trapped in the closed channel (Li, Hadid et al. 2002).

Testing the BTX binding model. An anonymous reviewer has suggested testing our BTX binding model by mutating residues that do not contribute to the BTX-channel energy, yet are in close proximity to the residues participating in BTX binding. Following up this suggestion, we have generated four mutants: $L^{2i16}A$, $L^{2i16}F$, $L^{4i16}A$, and $I^{4i19}A$. In agreement with the model, none of these mutants demonstrated a decreased BTX sensitivity (Fig. 3.5, Table 3.2). The lack of effect of mutations $L^{2i16}A$, $L^{2i16}F$, and $L^{4i16}A$ on BTX action is of special interest because positions *2i16* and *4i16* are symmetric to position *3i16*, which contains phenylalanine residue involved in π-cation interactions with BTX. The presumed BTX contact with F^{3i16} served as a critical constraint to build our model in which the positively charged ammonium group of BTX binds in the repeat interface, rather far from the pore lumen where Na^+ ions move through BTX. If mutation $F^{3i16}A$ were affecting the BTX binding indirectly (e.g. by changing inter-repeat contacts) one could expect analogous effects of mutations in symmetric positions *2i16* and *4i16*. The fact that these mutants occurred as BTX sensitive as the WT channel reinforces our conclusion on cation-π interactions of BTX with F^{3i16} and thus supports our model.

Table 3.2. Residue that provide the largest contributions to the BTX-channel energy, selected residues that do not contribute significant energy, and effects of mutations of respective residues on the sodium channel BTX sensitivity

Residue	Energy contribution, kcal/mol [a,b]	Point mutation	BTX sensitivity of the mutant	Agreement with the model	Reference
F^{3p49}	-3.6	K	Decrease	Yes	(Tikhonov and Zhorov 2005; Wang, Mitchell et al. 2006)
F^{4i15}	-2.8	K	Decrease	Yes	(Wang and Wang 1999)
F^{3i16}	-2.5	A	Decrease	Yes	This study
N^{2i15}	-1.9	K	Decrease	Yes	(Wang, Barile et al. 2001)
L^{3i19}	-1.7	K	Decrease	Yes	(Wang, Nau et al. 2000)
S^{3i15}	-1.7	K	Decrease	Yes	(Wang, Nau et al. 2000)
L^{1i18}	-1.7	A	No change [c]	No	This study
S^{1i15}	-1.6	K	Decrease	Yes	(Wang, Tikhonov et al. 2007)
Q^{1p49}	-1.4	A	No change	No	This study
T^{3p48}	-1.0	A	Decrease	Yes	This study
L^{2i19}	-0.8	K	Decrease	Yes	(Wang, Barile et al. 2001)
G^{3i14}	> 0.1	A	Decrease	N.A.[d]	This study
I^{4i19}	> 0.1	A	No change	Yes	This study
L^{2i16}	> 0.1	F	No change	Yes	This study
L^{2i16}	> 0.1	A	No change	Yes	This study
L^{4i16}	> 0.1	A	No change	Yes	This study

[a] Side chain contribution

[b] For the horseshoe binding model proposed in this work

[c] L^{1i18}K of rNav1.4 did not express (Wang and Wang 1998).

[d] The gating-hinge mutation can modify the activation gating but structural interpretation of this effect on BTX action is hardly possible in view of our "static" model of the open channel

We further generated alanine substitutions of three residues, which contribute energy to BTX binding in our model, and evaluated their BTX sensitivity (Table 3.2; Fig. 3.5). In agreement with the model, mutant $T^{3p48}A$ has demonstrated a substantially decreased BTX sensitivity. However, point mutations $Q^{1p49}A$ and $L^{1i18}A$ in repeat I did not change the BTX sensitivity. It should be noted that repeat I is diagonally opposed to repeat III. The latter contains five BTX-sensing residues, more than any other repeat (Table 3.2), suggesting that BTX binds tightly to repeat III. The BTX sensitivity of mutants $Q^{1p49}A$ and $L^{1i18}A$ may indicate that the distance between repeats I and III in the BgNav1.1a sodium channel is somehow larger than in its Kv1.2-based model and thus repeat III-bound BTX is farther from repeat I than in our model. (Reduced BTX sensitivity of the $S^{1i15}K$ mutant does not rule out this possibility because the long, pore-facing sidechain of lysine can repel the positively charged BTX without contacting it, whereas an alanine substitution is expected to weaken BTX attraction to the channel.) The possibility that the sodium channel pore is wider than that of the Kv1.2-based model does not affect conclusions of our study due to two reasons. First, the proposed BTX-channel model remains consistent with most of the mutational data shown in Table 3.2, including BTX sensitivity of five of the seven mutants, which have been designed and generated to test the model. Second, ligand-channel contacts may maintain upon some shift of the backbone due to the ligand and side chain flexibility. Indeed, ligand docking to homology models of the L-type calcium channel demonstrated that contacts between specific ligand moieties and channel residues are much less sensitive to the choice of the x-ray template than to the alignment between K^+ and Ca^{2+} channels (Cheng, Tikhonov et al. 2009).

DISCUSSION

Increasing evidence suggest that BTX binds in the inner pore of voltage-gated sodium channels. However, atomistic details of BTX binding are poorly understood. In this study, we found that mutations of the putative gating hinge glycine G^{3i14} and phenylalanine F^{3i16} in the inner helix IIIS6 significantly decreased the BTX action. These newly discovered BTX-sensing residues do not face the inner pore. This finding motivated us to revise the previously proposed binding model in which BTX contacted only the pore-facing residues and the agonist ammonium group was rather close to the permeation pathway (Tikhonov and Zhorov 2005; Wang, Mitchell et al. 2006). We used F^{3i16} as a new distance constraint to dock BTX. In combination with the distance constraints implied from previous experimental studies by Ging-Kuo Wang and coauthors on BTX-sensing residues in mammalian channels, the new distance constraint have driven our computations to predict the horseshoe binding model described under *Results*.

In our model, BTX binds to BTX sensing residues in all four repeats. These residues are top contributors to BTX binding energy (Table 3.2). F^{3i16} plays a significant role by stabilizing the ammonium group of BTX via cation-π interactions. Mutation $G^{3i14}A$ affects BTX action (Fig. 3.1), but G^{3i14} does not interact directly with BTX in our model. We suggest that the alanine substitution of this gating-hinge glycine affects the channel gating and therefore has an allosteric effect on BTX action. Most of the currently known BTX-sensing residues directly interact with BTX in our model (Figs. 3.3, 3.4 and Table 3.2). Besides G^{3i14}, exceptions are N^{1i20} and N^{4i20} whose lysine substitutions affect BTX action (Wang and Wang 1998; Wang and Wang 1999). These asparagines do not face the pore in our models of sodium channels. In a homology model of $Ca_V2.1$ channel, respective asparagines are engaged in strong inter-repeat interactions (Bruhova and Zhorov 2010). Mutations of analogous asparagines in the sodium channels may

affect the open-pore stability and/or geometry and therefore allosterically effect the BTX action. Mutation $L^{1i23}K$ makes the channel BTX-resistant (Wang and Wang 1998). L^{1i23} does not interact with BTX in our model, but it is exposed to the pore lumen at the cytoplasmic entry to the pore; the lysine substitution can repel the charged BTX approaching its binding site from the cytoplasm.

A permanently charged BTX derivative activates the sodium channel albeit in much higher concentration (Brown 1988). An advantage of the horseshoe model of BTX binding is the location of the ligand ammonium group in the repeat interface where it interacts with F^{3i16} and S^{3i15} (Fig. 3.4*A*). In this location, the BTX cationic group would not strongly repel permeating ions. The low potency of the permanently charged BTX derivative may be due to its inability to donate an H-bond to S^{3i15}. The BTX ammonium group would facilitate the BTX approach to the open cationophilic pore and then establish favorable interactions with the aromatic and H-bonding residues in the repeat interface.

The pyrrole ring is essential for BTX activity (Warnick, Albuquerque et al. 1975; Khodorov, Yelin et al. 1992). In the horseshoe binding model, the pyrrole ring approaches S^{1i15} and the BTX carbonyl oxygen is within H-bonding distance from the amide group of N^{2i15}. Mutations $N^{2i15}K$ and $N^{2i15}R$ cause BTX to block rather than activate $hNa_v1.5$ (Wang, Tikhonov et al. 2007). In the latter mutants, the lysine or arginine residues are too long to donate an H-bond to the carbonyl oxygen of BTX and may repel the pyrrole group towards the pore axis, where it would block the ion permeation.

The reduced conductance of BTX-modified channels (Correa, Latorre et al. 1991) is readily explained by our model in which the binding site for a Na^+ ion within the BTX horseshoe is much narrower than the channel cross-section at the level *i15*. This level contains highly

conserved serine, asparagine and phenylalanine residues which are likely to form a binding site for a hydrated Na^+ ion in the inner pore.

Altered ionic selectivity of BTX-modified sodium channels was described in 70s (Revenko and Khodorov 1977; Huang, Catterall et al. 1979). More recent studies show that BTX reduces selectivity of Na^+ over K^+, Rb^+ and Cs^+ by less than 3 fold, but does not change selectivity for Na^+ over Li^+ (Garber and Miller 1987; Behrens, Oberhauser et al. 1989) or NH_4^+ (Correa, Latorre et al. 1991). The authors of the latter study suggest that the ion selectivity measured through the reversal potential for different ions is highly sensitive to experimental conditions. The selectivity filter in the BTX-modified channels is estimated to be wider than in the native channels (Revenko and Khodorov 1977; Huang, Catterall et al. 1979). Why a wider pore would show a reduced conductance? In our model BTX does not directly interact with the DEKA locus, but may widen the pore (see *Results*). Furthermore, the binding site for permeating ions within BTX, besides decreasing the channel permeability (and thus attenuating the ion selectivity of the DEKA locus), may poorly discriminate the permeating ions. In particular BTX-modified channels show increased permeability for methylammonium. This organic cation would readily permeate through the BTX horseshoe, which in our model partially embraces an ion and leaves unobstructed the ion side, which is exposed to the hydrophobic interface between IS6 and IVS6 (Fig. 3.4C). The altered ion selectivity of BTX-modified channels may be also related to the reduced sensitivity of these channels to proton block (Mozhaeva, Naumov et al. 1983). In our model, BTX would displace water molecules from hydrophilic residues at level *i15*, the most proximal to the outer pore ring of the pore-facing S6 residues. The deficiency of water molecules in the inner pore of BTX-modified channels may shift pKa values of titrable residues in the

DEKA locus, in particular pKa of K^{3p49}, a critical determinant of the sodium channel selectivity (Heinemann, Terlau et al. 1992).

Our study reinforces the concept that BTX binds in the inner pore (Tikhonov and Zhorov 2005) rather than at the protein-lipid interfaces as was thought before. A common feature of the previous and current structural models is that BTX binds in the inner pore and permeating ions bind between oxygen atom(s) in the BTX molecule and a pore-facing polar residue. The major peculiarity of the new model is that the BTX ammonium group is engaged in cation-π interactions with F^{3i16} in the repeat interface, rather far from the ion permeation pathway and thus only weakly repels the permeating ions by electrostatic interactions. Another peculiarity of the new model is that BTX adopts the horseshoe conformation and permeating ions bind between four atoms, which include three BTX atoms in the horseshoe inner surface and the sidechain hydroxyl of S^{1i15}. (The previous model suggested that permeating ions bind the sidechain oxygen of N^{2i15} and an oxygen atom of BTX.)

Limitations of our model should be spelled out. Building homology models and docking ligands require energy optimizations. However, a homology model, which includes only a part of a large transmembrane protein and lacks explicit water molecules and membrane lipids, is not expected to correspond to the global energy minimum. The touchstone of a model is its consistency with experimental observations and ability to direct experimentally testable predictions. Although we described in Table 3.2 some characteristics of the ligand-channel energetic, the concrete numbers should be treated with caution. On the other hand the fact that 13 out of 16 sodium channel mutants (Table 3.2) exhibit changes of the BTX sensitivity *vs.* the WT channel in agreement with the predicted BTX-channel contacts (or lack of such contacts) strongly supports the current model.

Supplementary Data

New Batrachotoxin-Sensing Residues in Segment IIIS6 of Sodium Channel

Yuzhe Du[1*], Daniel Garden[2*], Boris S Zhorov[2†] and Ke Dong[1†]

BTX binding modes imposed by distance constraints. We first tested the vertical binding mode (Tikhonov and Zhorov 2005) in which the steroidal group is oriented towards the cytoplasm, the pyrrole extends towards the selectivity filter, and the ester group approaches K^{3p50} (not shown). However, an attempt to constrain BTX to the new BTX-sensing residue F^{3i16} shifted BTX towards IIIS6 placing the steroidal group in the pore center where it would block the ion permeation. Constraining the pyrrole nitrogen to the side chain oxygen of N^{2i15} resulted in the binding mode in which the chain between pyrrole ring and the steroidal moiety crossed the pore axis thus blocking the ion permeation (not shown). We further imposed distance constraints between various BTX moieties and BTX-sensing residues identified in our current and previous mutational studies. Nineteen constraint combinations (Table 3.2) lead to fifteen binding modes, six of which are shown in Figure 3.3. Constraining the pyrrole nitrogen to the *para*-carbon of F^{3i16} placed the steroidal ring D at F^{4i15}, the ester oxygen within H-bonding distance from S^{3i15}, and the steroidal ring C at L^{3i19} (Fig. S3.1***A***). In this binding mode, BTX oxygens are exposed to the pore axis, but BTX-sensing residues S^{1i15}, N^{2i15}, and L^{2i19} are too far from the ligand. Model in Figure S3.1*B* was obtained by constraining steroidal ring A to F^{3i16}. In this energetically less favorable model the BTX ammonium group faces L^{3i19}, the hydrophilic side of the steroidal moiety is partially buried in the II/III domain interface, and the ester group faces the pore axis. Since only two BTX oxygens face the pore, this binding does not explain the ion permeation through BTX-bound channel or roles of S^{1i15}, N^{2i15}, and L^{2i19}. Constraining the pyrrole ring in the

II/III domain interface resulted in a binding mode that was primarily stabilized by a strong H-bond between the oxazapane nitrogen and S^{3i15} and steroidal rings A and C approaching, F^{4i15} and L^{2i19}, respectively (Fig. S3.1***C***). However, this model does not explain ion permeation, since the BTX hydrophilic groups face the channel walls while hydrophobic groups are exposed to the pore axis. Directing the steroidal group towards the selectivity filter and constraining the ammonium group to F^{3i16} resulted in the model (Fig. S3.1***D***) in which F^{3i16} interacts with ring C and the pyrrole ring interacts with F^{3p49} and F^{4i15}. The hydrophilic side of BTX does face the pore in this model. In the models shown in Figures S3.1***E,F*** BTX adopts the horseshoe conformations exposing its hydrophilic groups towards the pore axis. Thus, constraining the BTX ammonium group to S^{3i15} at the H-bonding distance (Fig S3.1***E***) resulted in the binding mode in which the pyrrole ring interacts with F^{4i15}, while hydrophobic groups in the flexible BTX chain approach L^{3i19}. In this model, steroidal ring B interacts with BTX-sensing residues L^{2i19} and the hydroxy group in ring A approaches N^{2i15}, but does not form an H-bond with it. In this model, BTX interacts with the inner helices in all for domains and BTX hydrophilic groups are exposed to the pore axis to allow ion permeation. The major disadvantage of this model is that S^{1i15} does not interact with BTX. We attempted to impose BTX interactions with S^{1i15} by rotating BTX around the pore axis to bring the pyrrole ring within hydrogen bonding distance with S^{1i15} (Fig. S3.1***F***). This binding mode is stabilized by several ligand-channel contacts including cation-π interactions between the BTX ammonium group and F^{4i15}, a hydrogen bond between the oxazapane ether oxygen and S^{3i15}, and interactions of the steroidal rings C and A and with BTX-sensing residues L^{3i19} and L^{2i19}, respectively. The hydroxyl group in ring A approaches the oxygen of N^{1i15}, but not within H-bond distance. In this binding mode F^{3i16} is not involved. Finally, we modified the binding mode shown in Fig. S3.1***F*** by flipping BTX by

around the vertical axis and arrived to the horseshoe binding mode shown in Figures 3.3 and 3.4 on the major text. This rearrangement placed the ammonium group next to S^{3i15} and F^{3i16}, but preserved interactions with other BTX sensing residues.

Table S3.1. Distance constraints used for BTX docking. The constraints were used to impose proximity of experimentally determined BTX sensing residues with indicated BTX moieties. See Figure 3.2 for designation of rings and oxygen and nitrogen atoms.

Binding Mode	BTX Sensing Residue							
	S^{1i15}	N^{2i15}	L^{2i19}	F^{3p49}	S^{3i15}	F^{3i16}	L^{3i19}	F^{4i15}
1 (A)						N1		
2 (B)						Ring A		
3 (C)					N2	N1		
4 (D)						N2		
5 (E)		O6						N1
6 (F)					N1			N2
7					O1	Ring D		
8					O2	Ring D		
9					O1			N2
10				Ring A				
11				N1				Ring D
12		N2						
13	N1							
14	O6							N1
15						Ring A		N1
16						N1		Ring A
17						Ring D		N1
18		O1						Ring D
19		O2						Ring D

Binding modes 1 to 6 are shown in panels A to F of the Supplementary Figure.

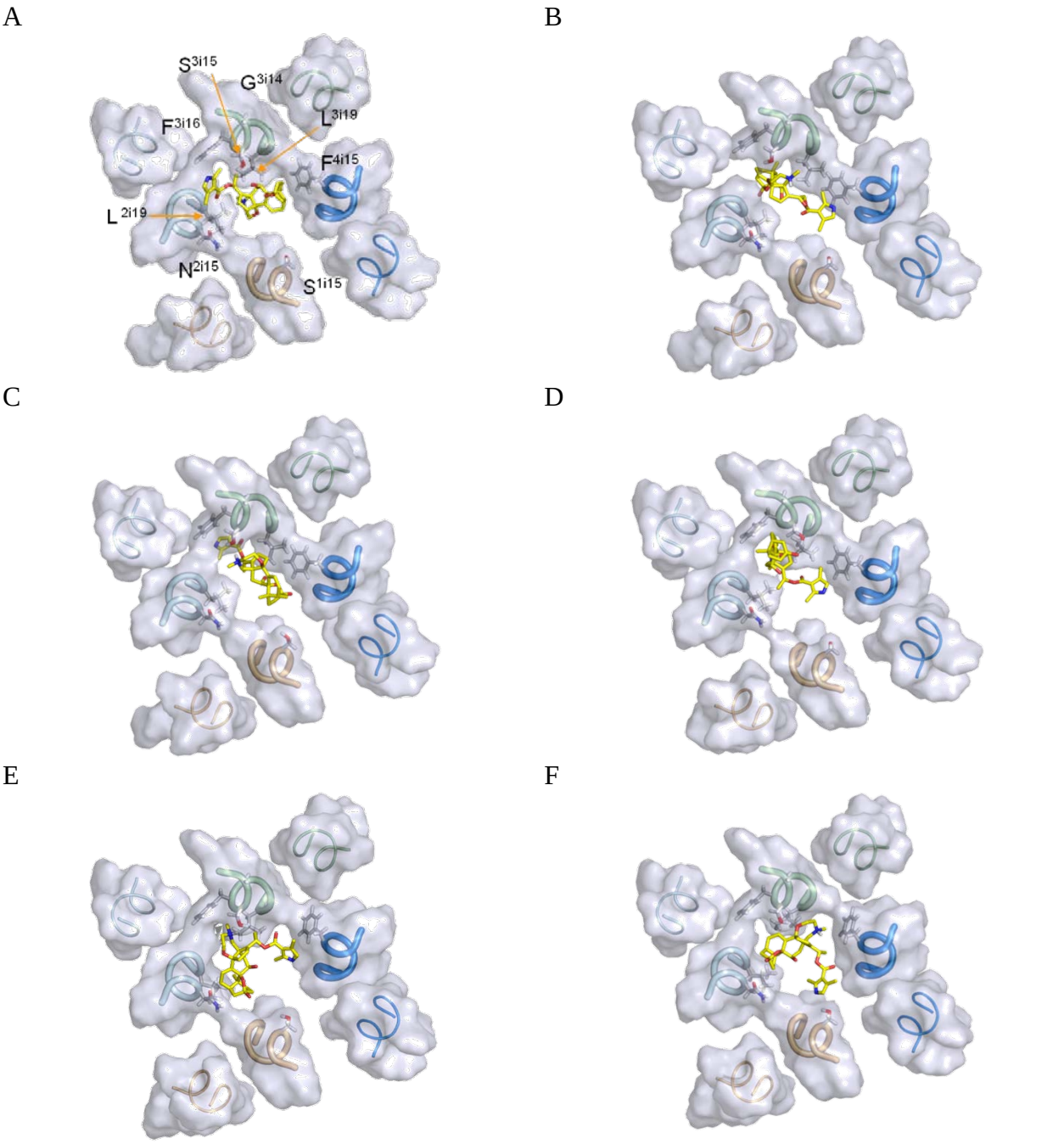

FIGURE S3.1. BTX binding modes imposed by different combinations of experimental constraints. Each panel represents the lowest energy structure predicted with specific combination of the constraints (Table S3.1). (***A***) Atom N1 was constrained to the center of aromatic ring of F^{3i16}. (***B***) Carbons of the steroidal ring A were constrained to the aromatic ring of F^{3i16}. (***C***) Noticing that the ammonium group was in close proximity to the hydroxyl group of S^{3i15}, we biased this hydrogen bond by a second constraint between the nitrogen from the oxazapane ring to the hydroxyl oxygen of S^{3i15}. (***D***) We attempted to explore a vertical binding mode where the steroidal group extended towards the selectivity filter. The tertiary ammonium group was constrained to the center of F^{3i16} to form cation-π interactions. (***E***) A single constraint

between the tertiary ammonium group and the hydroxyl oxygen of S^{3i15} yielded a horseshoe-shaped binding mode. (***F***) We explored cation-π interactions between the tertiary ammonium group and F^{4i15}. This constraint also yielded a horseshoe-like binding mode. Although in binding modes ***E*** and ***F*** BTX does form contacts with all the known BTX sensing residues, these models show that BTX could interact with all four domains simultaneously, while allowing ions to permeate. This idea was used to generate the BTX binding mode shown in Figures 3.3 and 3.4 of the manuscript.

CHAPTER FOUR

BATRACHOTOXIN, PYRETHROIDS AND BTG 502 SHARE OVERLAPPING BINDING SITES ON INSECT SODIUM CHANNELS

CHAPTER 4 – PREFACE

The work presented in this chapter has been submitted to:

Du, Y.*, Garden, D. P.*, Khambay, B., Zhorov, B. S., Dong. K. “Batrachotoxin, Deltamethrin and BTG 502 share overlapping binding sites on insect sodium channels.” Accepted to Mol. Pharmacol. June 16, 2011.

*These authors contributed to the work equally

I built the models, preformed all the simulations and wrote the manuscript for this study.

ABSTRACT

A steroidal alkaloid, batrachotoxin (BTX), and pyrethroid insecticides, bind to distinct but allosterically coupled receptor sites on voltage-gated sodium channels and cause persistent channel activation. BTX presumably binds in the inner pore, whereas pyrethroids are predicted to bind at the lipid-exposed cavity formed by the short intracellular linker-helix IIS4-S5 and transmembrane helices IIS5 and IIIS6. An alkylamide insecticide BTG 502 reduces sodium currents and antagonizes the action of BTX on cockroach sodium channels, suggesting that it also binds inside the pore. However, a pyrethroid-sensing residue, Phe_3i17 in IIIS6, which does not face the pore, is essential for the activity of BTG 502, but not for BTX. In this study, we found that three additional deltamethrin-sensing residues in IIIS6, Ile_3i12, Gly_3i14, and Phe_3i16 (the latter two are also BTX-sensing) and three BTX-sensing residues Ser_3i15 and Leu_3i19 in IIIS6 and Phe_4i15 in IVS6 are all critical for BTG 502 action on cockroach sodium channels. Using these data as constraints, we constructed a BTG 502 binding model in which BTG 502 wraps around IIIS6 likely making direct contacts with all of the above residues on the opposite faces of the IIIS6 helix except for the putative gating hinge Gly_3i14. BTG 502 and its inactive analog DAP 1855 antagonize the action of deltamethrin. The antagonism was eliminated by mutations of Ser_3i15, Phe_3i17, Leu_3i19 and Phe_4i15, but not by mutations of Ile_3i12, Gly_3i14, and Phe_3i16. Our analysis revealed a unique mode of action of BTG 502 with its receptor site overlapping with those of both BTX and deltamethrin.

INTRODUCTION

Voltage-gated sodium channels (Na_V) are responsible for the rapid rising phase of action potentials in electrically excitable cells. The pore-forming subunits of Na_V channels contain four

homologous repeats, each having six transmembrane helices (S1-S6). Helices S1-S4 form the voltage-sensing domain and transmembrane helices S5 (outer helix) and S6 (inner helix) contribute to the pore-forming domain. The residues connecting the S5 and S6 transmembrane helices form the four reentrant loops, called P-loops. These P-loops contain the amino acid residues which confer the ion selectivity in Na_V. The voltage sensor is linked to the outer helix, S5, by a short extracellular linker helix, S4-S5.

Na_V are targets of a diverse array of natural and synthetic toxins, including therapeutic drugs, insecticides (such as pyrethroids), and naturally occurring toxins (batrachotoxin; BTX). These toxin groups each bind to distinct receptor sites on sodium channels and affect channel function (Wang and Wang 2003). BTX (Fig. 4.1), isolated from the skin of a Colombian frog (Daly, Witkop et al. 1965) reduces ion selectivity and causes persistent channel activation by inhibiting inactivation and shifting the voltage-dependence of activation in the hyperpolarizing direction. Pyrethroids, such as deltamethrin (Fig. 4.1) are synthetic derivatives of the naturally occurring pyrethrum insecticides extracted from *Chrysanthemum* species (Elliott 1977). Pyrethroids bind to a unique receptor site and inhibit deactivation and inactivation resulting in prolonged opening of sodium channels (Vijverberg and van den Bercken 1990; Bloomquist 1996; Narahashi 2000).

Traditionally, BTX was believed to bind at the lipid-channel interface and alter channel selectivity and gating by an allosteric mechanism (Linford, Cantrell et al. 1998). However, mutational studies identified BTX-sensing residues in the inner helices of all four domains suggesting that BTX is directly exposed to the permeation pathway (Tikhonov and Zhorov 2005). More recent mutational and modeling studies have confirmed this

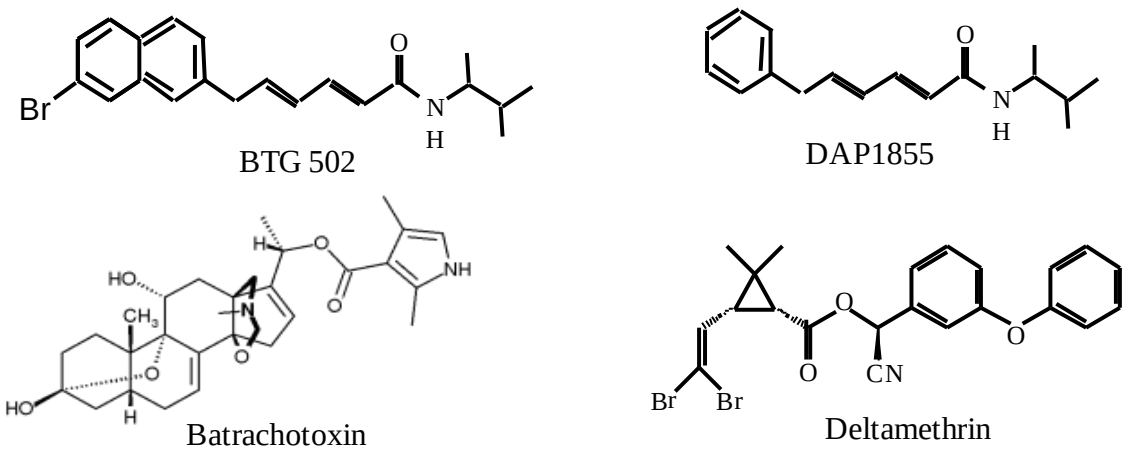

FIGURE 4.1. Chemical structures of BTG 502, DAP 1855, BTX, and deltamethrin.

prediction (Wang, Mitchell et al. 2006; Wang, Tikhonov et al. 2007; Wang, Tikhonov et al. 2007; Du, Lee et al. 2009). Studies of the mechanisms of insect resistance to pyrethroids led to the identification of pyrethroid-sensing residues in diverse regions of insect sodium channels (Soderlund 2005; Davies, Field et al. 2007; Dong 2007). These data have been used to construct a model of the sodium channel where pyrethroids bind to a cavity formed by the linker-helix IIS4-S5, the outer helix IIS5, and the inner helix IIIS6 at the interface between domains II and III (O'Reilly, Khambay et al. 2006). Systematic site-directed mutagenesis of residues in IIIS6 revealed additional four residues that are important for the action of deltamethrin (Du, Lee et al. 2009) and two of them are also critical for the action of BTX (Du, Garden et al. 2011). Despite this apparent overlap, the binding sites for BTX and pyrethroids in IIIS6 are distinct, involving opposite faces of the IIIS6 transmembrane helix (Du, Lee et al. 2009).

An alkylamide insecticide BTG 502 (Fig. 4.1) has been shown to antagonize the binding and action of BTX in ligand-binding and $^{22}Na^{+}$ influx assays using mouse brain synaptoneurosomes (Ottea et al., 1989; 1990). These results suggest that BTG 502 and BTX compete for a common receptor site on sodium channels (Ottea, Payne et al. 1989). However, unlike BTX, recent data indicate that BTG 502 acts as a partial channel blocker reducing the peak current of insect sodium channels expressed in *Xenopus* oocytes (Du, Khambay et al. 2011). Additionally, a residue important for pyrethroid activity, F^{3i17}, in IIIS6 is also critical for the action of BTG 502 (Du, Khambay et al. 2011), but not for BTX (Tan, Liu et al. 2005). These results suggest that BTG 502 and BTX must have somewhat distinct binding and/or action properties that translate into distinct electrophysiological effects.

Here we conducted mutational analysis and molecular modeling to map the binding site of BTG 502. We found that all five BTX-sensing residues (two of which are also pyrethroid-

sensing) and two deltamethrin-sensing residues are critical for BTG 502 action. Our model incorporates available experimental data on the action of BTG 502 on the cockroach sodium channel $BgNa_v$ and suggests that BTG 502 makes contact with residues on opposite faces of the IIIS6 helix. Therefore, the receptor site for BTG 502 on sodium channels is a unique receptor site that overlaps those of BTX and pyrethroids.

MATERIALS AND METHODS

Expression of BgNav Sodium Channels in Xenopus Oocytes. The procedures for oocyte preparation and cRNA injection are identical to those described previously (Tan, Liu et al. 2002). For robust expression of the $BgNa_v$ sodium channels, cRNA was coinjected into oocytes with *Drosophila melanogaster* tipE cRNA (1:1 ratio), which enhances the expression of insect sodium channels in oocytes (Warmke, Reenan et al. 1997; Feng, Deák et al. 1995).

Electrophysiological Recording and Data Analysis. Sodium currents were recorded using standard two-electrode voltage clamping. The borosilicate glass electrodes were filled with filtered 3 M KCl in 0.5% agarose and had a resistance of 0.5 to 1.0 MΩ. The recording solution was ND-96, consisting of 96 mM NaCl, 2.0 mM KCl, 1.0 mM $MgCl_2$, 1.8 mM $CaCl_2$, and 10 mM HEPES, pH adjusted to 7.5 with NaOH. Sodium currents were measured with a Warner OC725C oocyte clamp (Warner Instrument, Hamden, CT) and processed with a Digidata 1322A interface (Axon Instruments Inc., Foster City, CA). Data were sampled at 50 kHz and filtered at 2 kHz. Leak currents were corrected by p/4 subtraction. pClamp 9.2 software (Molecular Devices, Sunnyvale, CA) was used for data acquisition and analysis. The maximal peak sodium current was limited to <2.0 μA to achieve optimal voltage control by adjusting the amount of cRNA and the incubation time after injection.

To measure the effect of BTG 502 on the sodium channel, sodium currents were elicited by a 20-ms test pulse to -10 mV from a holding potential of -120 mV after 100 repetitive depolarizing pulses to -10 mV at 10 Hz (Du, Khambay et al. 2011). The pyrethroid-induced tail current was recorded during a 100-pulse train of 5-ms depolarization from –120 to 0 mV with a 5-ms interpulse interval. The percentage of channels modified by pyrethroids was calculated using the equation $M = [I_{tail}/(E_h - E_{Na})]/[I_{Na}/(E_t - E_{Na})] \times 100$ (Tatebayashi and Narahashi 1994), where I_{tail} is the maximal tail current amplitude, E_h is the potential to which the membrane is repolarized, E_{Na} is the reversal potential for sodium current determined from the current-voltage curve, I_{Na} is the amplitude of the peak current during depolarization before pyrethroid exposure, and E_t is the potential of step depolarization.

Data analyses were performed using pClamp 9 (Molecular Devices, Sunnyvale, CA), Origin 8.1(OriginLab Corp, Northampton, MA) and Adobe Illustrator (Adobe, San Jose, CA) software. Results are reported as mean ± SD. Statistical significance was determined by using one-way ANOVA with Scheffe's post hoc analysis, and significant values were set at $p < 0.05$ as indicated in the figure legend.

Chemicals. BTG 502 and an inactive analog, DAP 1855 (Fig. 4.1) were provided by Rothamsted Research Ltd, Harpenden, UK. BTX and deltamethrin were generous gifts from John Daly (National Institutes of Health, Bethesda, MD), and Klaus Naumann and Ralf Nauen (Bayer CropScience AG, Monheim, Germany), respectively. Stock solutions of BTX (1 mM), BTG 502 (50 mM) and deltamethrin (100 mM) were made in dimethyl sulfoxide (DMSO). The working concentration was prepared in ND96 recording solution immediately prior to the experiments. The concentration of DMSO in the final solution was < 0.5%, which had no effect on the function of sodium channels in the experiments. The method for application of chemicals

in the recording system was identical to that described previously (Tan, Liu et al. 2002) The effects of deltamethrin, BTX, and BTG 502 were measured 10 min after toxin application.

Homology Model of $BgNa_v1.1$. A homology model of the open cockroach sodium channel variant $BgNa_v1$-1a was constructed based on the crystal structure of $K_v1.2$ (Long, Campbell et al. 2005). Amino acid sequences of $BgNa_v1$-1a (Fig. 4.2A) and $K_v1.2$ were aligned as before (Zhorov and Tikhonov 2004; Bruhova, Tikhonov et al. 2008) and positions of residues are labeled using a universal scheme (Zhorov and Tikhonov 2004), see Table 4.1. The extracellular loops, which are too far from residues important for BTX- and deltamethrin activity, were not included in the model. The P-loops were modeled as in (Tikhonov and Zhorov 2005). Energy was calculated using the AMBER force field (Weiner, Kollman et al. 1984; Weiner, Kollman et al. 1986) and the solvent exposure- and distance dependant dielectric function (Garden and Zhorov 2010). The atomic charges of the toxin molecules were calculated using the AM1 method (Dewar, Zoebisch et al. 1985) through MOPAC. Bond angles were varied in the toxins, but not in the protein. Energy was minimized in the space of generalized coordinates (Zhorov 1981; Zhorov 1983). The Monte Carlo-energy minimization (MCM) method (Li and Scheraga 1987) was used to optimize the channel homology model and to dock the ligands. The SCWRL3 program (Canutescu, Shelenkov et al. 2003) was used to assign starting conformations of the channel side chains. The ZMM program (www.zmmsoft.com) was used to perform all calculations.

Docking BTG 502. Various binding modes of BTG 502 were explored using distance constraints implied by our experimental data (Supplementary Table S4.1). A constraint is a flat-bottom parabolic penalty function added to the energy expression. When the distance between a given toxin atom and a given atom in the toxin-sensing residue exceeds the upper limit of the

TABLE 4.1. Sequence alignment

Channel	Domain	First residue #	k1 | k11 |			
KcsA						
K_v1.2	L45	311	SKGLQILGQT	L		
$BgNa_v$1-1	I L45	253	VPGLKTIVGA	V		
	II L45	890	WPTLNLLISI	M		
	III L45	1385	MQGMRVVVNA	L		
	IV L45	1703	AKGIRTLLFA	L		
			o1 |	o11 |	o21 |	
KcsA	M1	23	LHWRAAGAAT	VLLVIVLLAG	SYLAVLAER	
K_v1.2	S5	323	ASMRELGLLI	FFLFIGVILF	SSAVYFAEA	
$BgNa_v$1-1	IS5	265	ESVKNLRDVI	ILTMFSLSVF	ALMGLQIYM	
	IIS5	902	RTVGALGNLT	FVLCIIIFIF	AVMGMQLFG	
	IIIS5	1397	QAIPSIFNVL	LVCLIFWLIF	AIMGVQLFA	
	IVS5	1715	MSLPALFNIC	LLLFLVMFIF	AIFGMSFFM	
			p33 |	p41 |	p51 |	
KcsA	P	59	LITYPRAL	WWSVETATTV	GYGDLYPV	
K_v1.2	P	358	FPSIPDAF	WWAVVSMTTV	GYGDMVPT	
$BgNa_v$1-1	IP	300	CIKNFWAF	LSAFRLMTQD	YWENLYQL	
	IIP	937	VERFPHSF	MIVFRVLCGE	WIESMWDC	
	IIIP	1436	STTLSKAY	LCLFQVATFK	GWIQIMND	
	IVP	1750	GLDDVQSM	ILLFQMSTSA	GWDGVLDG	
			i1 |	i11 |	i21 |	i31 |
KcsA	M2	86	LWGRLVAVVV	MVAGITSFGL	VTAALATWFV	GREQERR
K_v1.2	S6	385	IGGKIVGSLC	AIAGVLTIAL	PVPVIVSNFN	YFYHRET
$BgNa_v$1-1	IS6	402	PWHMLFFIVI	IFLGSFYLVN	LILAIVAMSY	DELQKKA
	IIS6	981	WSCIPFFLAT	VVIGNLVVLN	LFLALLLSNF	GSSNLSA
	IIIS6	1506	IYMYLYFVFF	I**I**F**GSF**F**F**T**L**N	LFIGVIIDNF	NEQKKKA
	IVS6	1806	TVGLAFLLSY	LVIS**F**LIVIN	MYIAVILENY	SQATEDV

Bold-typed and underlined are experimentally determined residues that, when mutated, affect action of BTG 502 and deltamethrin, respectively.

A residue designation includes a segment identifier and position in the segment. Symbols “k”, “o”, “p” and “i”, represent, respectively, the L45 lin**k**er between S4 and S5, the outer helix, the P-loop, and the inner helix.

A

```
D3S6   rNav1.4    MYLYF VIFII FGSFF TLNLF IGVII DNF
       BgNav1-1   MYLYF VFFII FGSFF TLNLF IGVII DNF
                             3i14  3i19
D4S6   rNav1.4    GICFF CSYII ISFLI VVNMY IAIIL ENF
       BgNav1-1   GIAFL LSYLV ISFLI VINMY IAVIL ENY
                             4i15
```

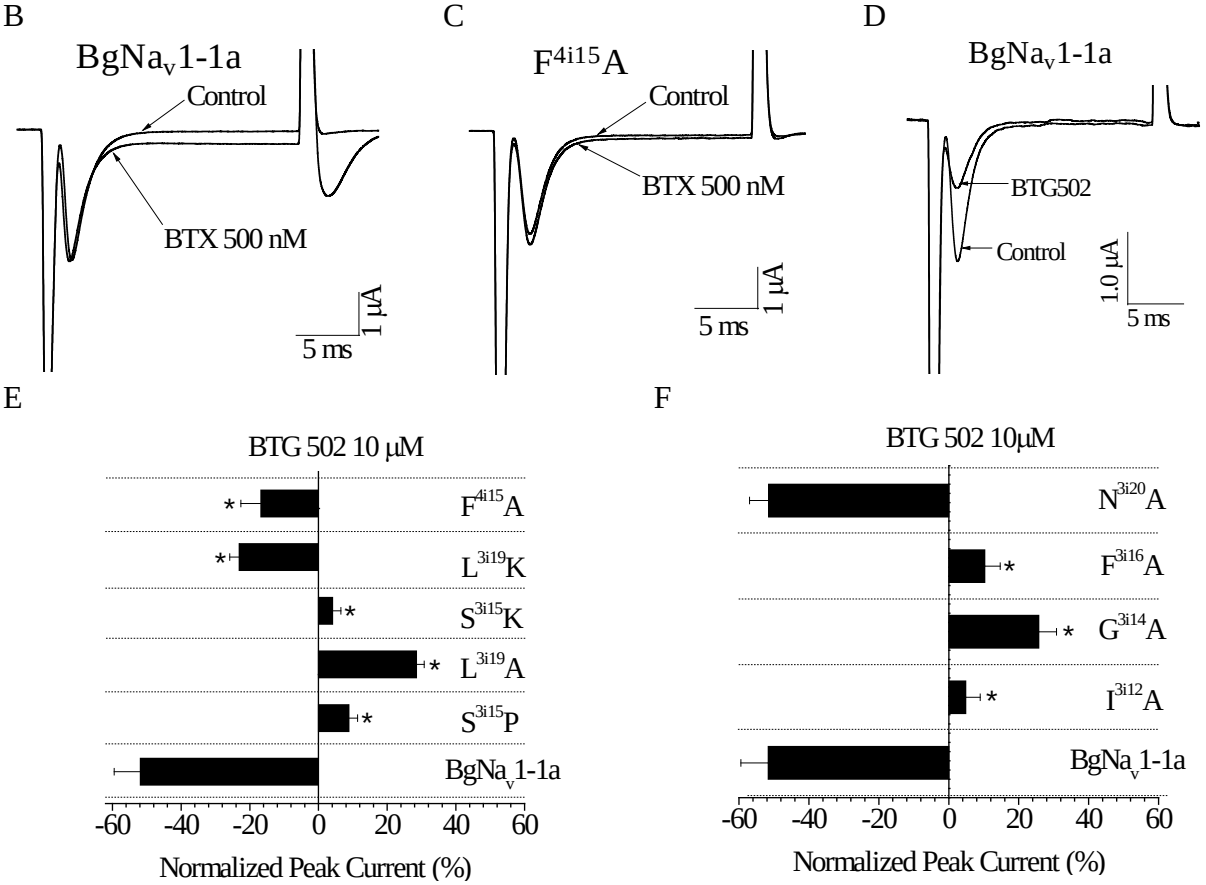

FIGURE 4.2. Both BTX- and pyrethroid-sensing residues are critical for the action of BTG 502. A, Amino acid sequences of segments IIIS6 and IVS6 in rNa$_v$1.4 and BgNa$_v$ proteins. BTX-sensing residues S^{3i15}, L^{3i19} and F^{4i15} are underlined. Pyrethroid-sensing residues I^{3i12}, G^{3i14}, F^{3i16}, F^{3i17}and N^{3i20} are in bold. B, Effects of BTX (500 nM) on BgNa$_v$1-1a channels. C, Substitution F^{4i15}A reduced the action of BTX on BgNa$_v$1-1a channels. D, Effects of BTG 502 (10 µM) on BgNa$_v$1-1a channels. E, Effects of amino acid substitutions for BTX-sensing residues on peak current inhibition by BTG 502. F, Effects of substitutions of pyrethroid-sensing residues on the peak current inhibition by BTG 502 at 10 µM. The peak current reduction by BTG 502 was measured by a 20-ms test pulse to -10 mV from a holding potential of -120 mV following 100 repetitive prepulses to -10 mV at a frequency of 10 Hz before and after the application of 10 µM BTG 502. The asterisks indicate significant differences from the BgNa$_v$1-1a channel as determined by ANOVA ($p<0.05$).

constraint (5 Å in this study), the penalty contribution to the total energy increases sharply, with a force constant of 100 kcal·mol^{-1}·Å^{-1}. The flat-bottom constraint ensures proximity between two atoms but does not impose specific disposition orientation of chemical groups the atoms belong to, for instance an H-bond or π-stacking.

To search for the lowest-energy binding modes of BTG 502, we employed our three-stage flexible docking protocol (Garden and Zhorov 2010). In the first stage, a library of toxin conformers was generated by randomly sampling the toxins torsion angles, followed by energy minimizations to ensure that all the rings were closed. Ten thousand toxin conformations were generated and the ten lowest-energy conformations were collected for docking. In the second stage, the position and orientation of each toxin conformer in the library was sampled 200,000 times by assigning random values to six rigid-body degrees of freedom of the toxin. The energy of the toxin-receptor complexes (including the distance-constraint penalties) was calculated without energy minimization and the ten lowest energy complexes were collected. In the third stage, the ten collected complexes were refined by a 1,000 step MC-minimization and the lowest energy structure was used as the toxin binding model consistent with the given combination of distance constraints. At this stage, the torsion angles in the protein side chains and in the toxin were sampled. Finally, all the distance constraints were removed and the model was MC-minimized to check its intrinsic stability. If during the final MC-minimization the toxin drifted from the constraints-imposed binding mode, the latter was excluded from further analysis.

RESULTS

Three BTX-sensing residues are critical for the action of BTG 502. We have previously shown that lysine substitutions of two amino acid residues in IIIS6, S^{3i15} and L^{3i19} (Fig. 4.2A), dramatically reduce the action of BTX on $BgNa_v1$-1a channels (Du, Lee et al. 2009). Residue F^{4i15} in IVS6 (Fig. 4.2A) is important for the binding and action of BTX on mammalian sodium channels (Linford, Cantrell et al. 1998). Here we show that F^{4i15} is also a BTX-sensing residue for $BgNa_v1$-1a channels. BTX (500 nM) inhibited channel inactivation resulting in a noninactivating current and a tail current associated with repolarization of $BgNa_v1$-1a channels (Fig. 4.2B). The $F^{4i15}A$ substitution, which was available from another study (Silver, Nomura et al. 2009), significantly reduced the action of BTX on $BgNa_v1$-1a channels (Fig. 4.2C).

As reported previously (Du, Khambay et al. 2011), the effect of BTG 502 on $BgNa_v1$-1a channels was quite different from those of BTX. In response to 100 repetitive pre-pulses at a frequency of 10 Hz, BTG 502 reduced the amplitude of peak current of the $BgNa_v1$-1a channel and no tail current was detected upon repolarization (Fig. 4.2D). To determine whether S^{3i15}, L^{3i19} and F^{4i15} are also critical for the action of BTG 502, we examined the effect of BTG 502 on $S^{3i15}P$, $S^{3i15}K$, $L^{3i19}A$, and $L^{3i19}K$ mutant channels that were previously made from $BgNa_v1$-1a channels, as well as the $F^{4i15}A$ mutant channel. While BTG 502 (10 μM) inhibited 50% of the peak current of the $BgNa_v1$-1a channel, it only inhibited 23% and 17% for $L^{3i19}K$ and $F^{4i15}A$ mutant channels, respectively (Fig. 4.2E). Surprisingly, BTG 502 increased the amplitude of peak current of $S^{3i15}P$ and $S^{3i15}K$ channels by 5-10%, and 30% for $L^{3i19}A$ channels (Fig. 4.2E).

Four pyrethroid-sensing residues are critical for the action of BTG 502. Our laboratory recently identified four additional residues in IIIS6 (I^{3i12}, G^{3i14}, F^{3i16}, and N^{3i20}), besides F^{3i16}, (Fig. 4.2A) that are critical for the action of pyrethroids (Du, Lee et al. 2009).

Additionally, we showed that G^{3i14} and F^{3i16} are also critical for the action of BTX (Du, Garden et al. 2011). To determine whether these residues are also critical for the action of BTG 502, we examined the effect of BTG 502 on these four mutant channels. Substitutions $I^{3i12}A$, $G^{3i14}A$ and $F^{3i16}A$ completely abolished the action of BTG 502, while substitution $N^{3i20}A$ did not (Fig. 4.2F). In fact, BTG 502 increased the amplitudes of peak current of $I^{3i12}A$, $G^{3i14}A$ and $F^{3i16}A$ channels (Fig. 4.2F).

BTG 502 and its inactive analog DAP 1855 antagonize the action of deltamethrin. To explore possible interactions between BTG 502 and pyrethroids, we examined the response of the $BgNa_v1$-1a channel to deltamethrin in the presence of varying concentrations of BTG 502 or DAP 1855. DAP 1855 is an analog of BTG 502 that has no insecticidal activities, but inhibits the binding of BTX to sodium channels in mouse brain synaptoneurosomes (Ottea, Payne et al. 1989). With a 100-pulse train of 5-ms step depolarization from -120 to 0 mV at 5-ms intervals, deltamethrin (1 μM) induced a large tail current, as expected for the $BgNa_v1$-1a channel (Fig. 4.3A). BTG 502 antagonized the effect of deltamethrin by reducing the amplitude of the tail current in a concentration dependent manner (Fig. 4.3A). Consistent with the earlier finding (Ottea, Payne et al. 1989), DAP 1855 did not affect the peak current of $BgNa_v1$-1a channels (data not shown), but it antagonized the action of deltamethrin (Fig. 4.3B).

Amino acid substitution at S^{3i15}, F^{3i17}, L^{3i19}, and F^{4i15} abolished BTG 502 antagonism of deltamethrin action. Substitutions $S^{3i15}P$, $L^{3i19}A$, and $F^{4i15}A$ completely abolished BTG 502 antagonism of deltamethrin action (Fig. 3C), whereas substitutions $I^{3i12}A$, $G^{3i14}A$, $F^{3i16}A$, and $N^{3i20}A$ did not (Fig. 4.3D). At 10 μM, BTG 502 reduced the activity of deltamethrin on $BgNa_v1$-1a channels by 50%. Similar levels of antagonism were observed for substitutions $I^{3i12}A$, $G^{3i14}A$, $F^{3i16}A$ and $N^{3i20}A$. Because the $F^{3i17}I$ and $F^{3i17}A$ channels are completely insensitive to

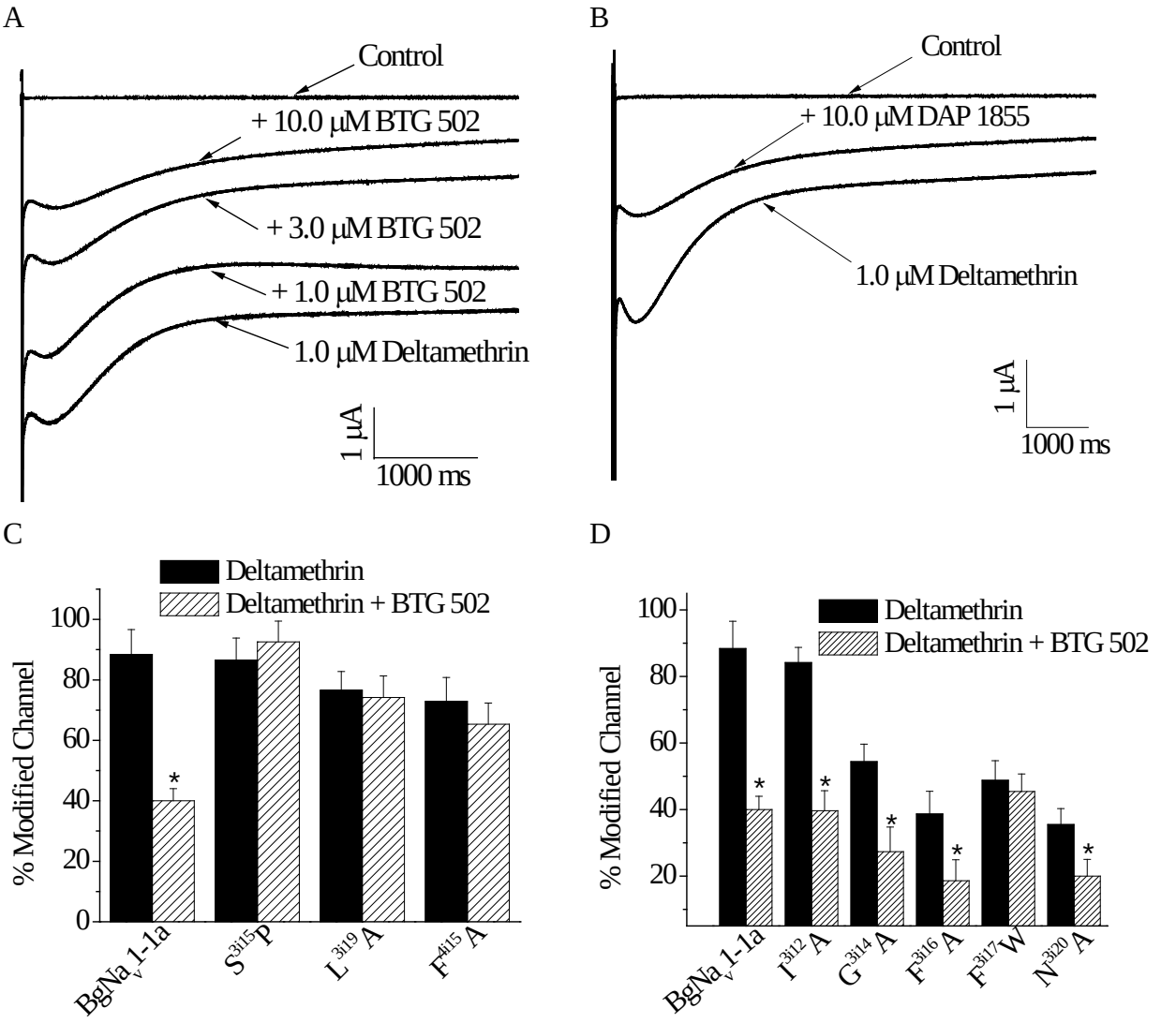

FIGURE 4.3. Effects of BTG 502 and DAP 1855 on the action of deltamethrin on BgNa$_v$1-1a and mutant channels. A and B, Inhibition of deltamethrin-induced tail currents by BTG 502 (A) and DAP 1855 (B). C, Substitutions at the pore-facing positions S^{3i15}P, L^{3i19}A and F^{4i15}A abolished BTG 502 antagonism of deltamethrin activity. D, Antagonism of BTG 502 on the action of deltamethrin is abolished by mutation F^{3i17}W, but not by alanine substitutions of I^{3i12}, G^{3i14}, F^{3i16}, and N^{3i20}. Percentage of channel modification by deltamethrin before (solid bar) and after (stripe bar) the application of 10 μM BTG 502 were calculated using the equation $M = [I_{tail}/(E_h - E_{Na})]/[I_{Na}/(E_t - E_{Na})]$ x 100 . The deltamethrin-induced tail current was recorded after a 100-pulse train of 5-ms step depolarizations from -120 to 0 mV with 5-ms interpulse intervals with a 20 ms test pulse to 0 mV. For the F^{3i16}A, F^{3i17}W and N^{3i20} A channels which were 10- to 20-fold more resistant to deltamethrin than the BgNa$_v$1-1a channel (Tan et al., 2005; Du et al., 2009),10 μM of deltamethrin was used . For the I^{3i12}A channel which was 10-fold more sensitive to deltamethrin than the wild-type (Du et al., 2009), 0.1 μM was used. For the rest of the mutant channels, 1.0 μM was used. The asterisks indicate significant differences after BTG 502 antagonize the action of deltamethrin ($p<0.05$).

pyrethroids and no tail current could be detected (Tan, Liu et al. 2005), we used the $F^{3i17}W$ mutant, which is about 10-fold less resistant to deltamethrin than the $F^{3i17}A$ mutant, for this experiment. Unlike other pyrethroid-sensing residues in IIIS6, the $F^{3i17}W$ mutation abolished the BTG 502 antagonism of deltamethrin activity (Fig. 4.3D).

Docking BTG 502 in the open channel. Mutational studies show that BTX binds in the inner pore, contacts the inner helices from all four repeats (Wang, Mitchell et al. 2006; Wang, Tikhonov et al. 2007; Wang, Tikhonov et al. 2007), and may adopt an ion-permeable "horseshoe" conformation within the channel as we recently proposed (Du et al., 2011a). In contrast, pyrethroids including deltamethrin are proposed to bind in the lipid-exposed interface between the linker-helix IIS4-S5, the outer helix IIS5, and the inner helix IIIS6 (O'Reilly, Khambay et al. 2006; Du, Lee et al. 2009). Our data that both BTX-sensing and pyrethroid-sensing residues are critical for the action of BTG 502 indicate that a part of the BTG 502 molecule may bind at the interface between domains II and III, interact with deltamethrin-sensing residues, and also interact with residues that face the inner pore.

We used the above data from our mutational and toxin-binding experiments as distance constraints to dock BTG 502 in the channel model. We sampled many combinations of distance constraints (Table S4.1) and MC-minimized the complex with and then without the distance constraints. The calculations predicted an energetically preferable binding mode, which is most consistent with the experimental data. In this binding mode, BTG 502 wraps around the IIIS6 helix (Fig. 4.4). The amide group of the toxin forms a hydrogen bond with S^{3i15}. The isopropyl group protrudes into the II/III repeat interface where it interacts with I^{3i12} and F^{3i16}. The naphthalene ring also protrudes into the III/IV repeat interface where it interacts with L^{3i19} and forms π-stacking contacts with F^{3i17} and F^{4i15}. The lipophilic bromine atom faces a hydrophobic

site between IIIS6 and IIIS5. The flexible linker of BTG 502 is exposed to the central pore where it interacts with L^{3i19} (Fig. 4.4C, D, E). Thus BTG 502 makes direct contacts with all the known BTG 502 sensing residues except the gating-hinge G^{3i14}. Using this binding mode we performed further computations to rationalize more experimental observations.

In addition to the BTG 502 binding mode described above, our constraints-driven docking calculations predicted an alternative binding mode in which BTG 502 wraps around IIIS6 from the lipid side (not shown). This binding mode appears unlikely as described in legend to Supplementary Figure S4.1.

Docking BTG 502 in the closed channel. The agonistic effect of BTG 502 when it is applied to sodium channels in combination with scorpion toxin (Ottea, Payne et al. 1989) suggests that BTG 502 stabilizes the open conformation of Na^+ channels. Our data that BTG 502 had no effect without a train of depolarizing prepulses (Du, Khambay et al. 2011) indicates preferable binding to open channels. To suggest a possible cause of this state-dependent action, we docked BTG 502 into the KcsA–based homology model of closed $BgNa_v1.1$ channels. We imposed toxin- channel distance constraints to mimic the BTG 502 binding mode in the open channel. MC-minimizations yielded a high-energy complex in which the inner helices were bent at the site where the aromatic ends of BTG 502 protruded into the domain interfaces (Figure S4.2 A, B). These results suggested that the channel would not close until the toxin leaves the binding site. Unconstrained MC-minimization of the above complex displaced BTG 502 from the horizontal, IIIS6-wrapping mode to a binding mode in which the toxin extended along the pore (Figure S4.2 C, D). These calculations suggested that BTG 502 would not bind in the closed channel in the same way as in the open channel.

A

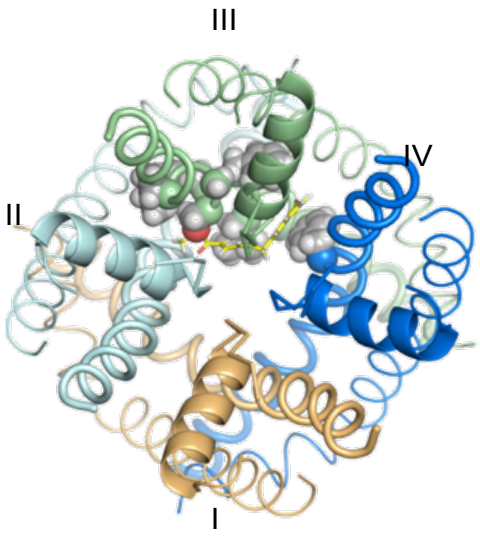
III
IV
II
I

B

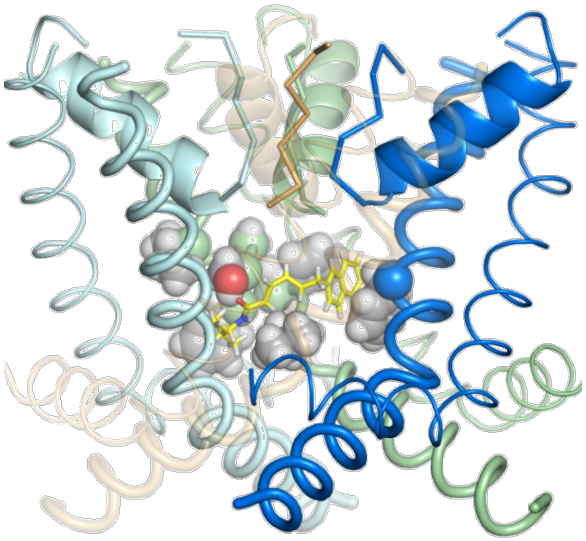

C

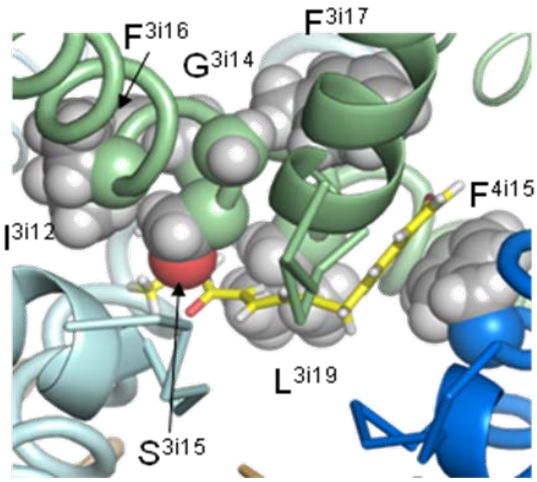
F3i16
F3i17
G3i14
F4i15
I3i12
L3i19
S3i15

D

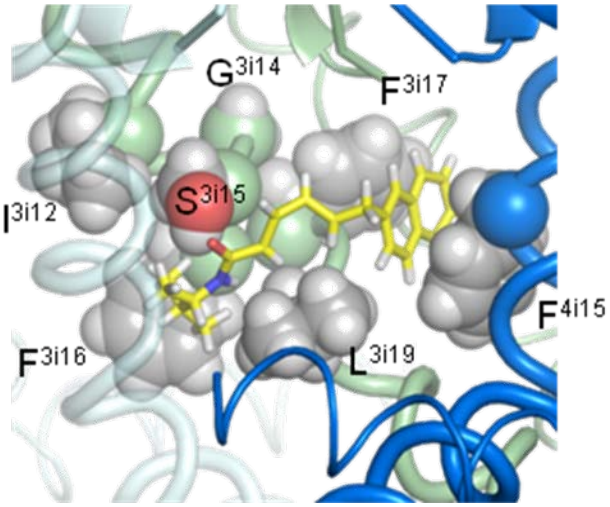
G3i14
F3i17
S3i15
I3i12
F4i15
F3i16
L3i19

E

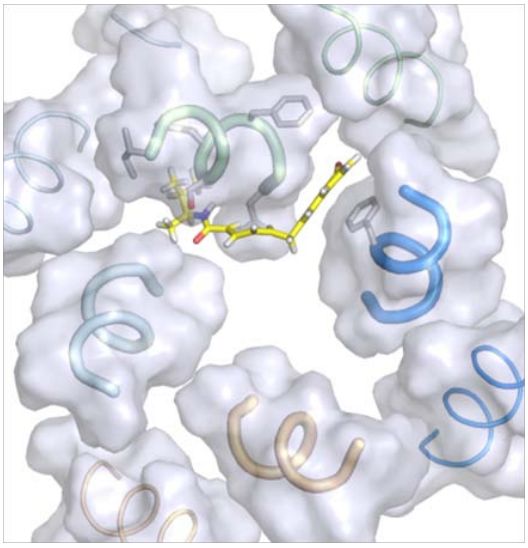

FIGURE 4.4. BTG-502 in the pore domain of BgNav1.1. Repeats I, II, III, and IV are colored brown, gray, green, and blue, respectively. S5s, P-helices, and S6s are shown as thin, intermediate-size, and thick helices, respectively. The ascending limbs are shown as thin C alpha tracings. The ligand (rendered by sticks with yellow carbons) wraps around IIIS6 and exposes its termini into the II/III and III/IV domain. Shown are top (A) and the side (B) views and their zoomed images (C and D). Panel E is the top view of the pore domain in which parts of the transmembrane helices at the level of the bound BTG-502 are shown by transparent surfaces. In the proposed binding mode, BTG-502 would partially obstruct the ion permeation by the hydrophobic linker exposed into the pore (A,C, E). The isopropyl group of BTG 502 contacts residues I^{3i12} and F^{3i16}, which do not face the pore, while the amide oxygen accepts an H-bond from S^{3i15} (C). L^{3i19} is below the hydrophobic linker (D). The naphthalene ring of BTG 502 protrudes in the interface between domains III and IV where it is flanked by F^{3i17} and F^{4i15} and forms π-stacking interactions with these residues (C, D).

DISCUSSION

BTG 502, an N-alkylamide insecticide, reduces peak sodium currents of the $BgNa_v$ channel and antagonizes the action of BTX (Du, Khambay et al. 2011) and deltamethrin, two sodium channel agonists. Using mutational analysis, we found in this study that seven residues in the $BgNa_v$ channel, which are essential for the action of BTG 502. These are three key BTX-sensing residues, S^{3i15} and L^{3i19} in IIIS6 and F^{4i15} in IVS6, two deltamethrin-sensing residues I^{3i12} and F^{3i17} in IIIS6 and two BTX/deltamethrin-sensing residues, G^{3i14}, and F^{3i16} in IIIS6. We used these data to create an atomistic model of BTG 502 binding to the $BgNa_v$ channel. In this model, BTG 502 wraps around the transmembrane segment IIIS6 and exposes its flexible linker between the bulky ends into the channel pore. This model also shows the interaction of BTG 502 with the pore-facing BTX-sensing residues S^{3i15}, L^{3i19}, and F^{4i15}, a deltamethrin-sensing residue I^{3i12}, a BTX/deltamethrin-sensing residue F^{3i16} in the II/III interface, and a pyrethroid-sensing residue F^{3i17} in the III/IV interface. Thus, our results delineate a unique receptor site for BTG 502 on the sodium channel and show that the BTG 502 receptor site overlaps with two receptor sites of BTX and deltamethrin.

BTX, veratridine, aconitine and grayanotoxin are classified as site 2 toxins. These toxins share common characteristics in their actions on sodium channels: they bind to the sodium channel in its open state and toxin-modified channels lack fast inactivation and activate at more negative potentials, resulting in persistent channel activation (Wang and Wang, 2003). Studies of the action of BTG 502 on sodium channels in mouse brain synaptoneurosomes using [^{3}H]batrachotoxinin A-20-α-benzoate (BTX-B) binding and $^{22}Na^+$ influx assays (Ottea, Payne et al. 1989) and toxin competition experiments in oocyte-expressed insect sodium channels (Du, Khambay et al. 2011) showed that BTG 502 antagonizes the action of BTX, suggesting that BTG

502 acts at site 2 . However, instead of enhancing channel activation as site 2 neurotoxins do, BTG 502 reduces the amplitude of sodium currents, behaving as an antagonist (Du et al., 2011b). The discovery of BTG 502-sensing residues that are either identical to or distinct from BTX-sensing residues and our model of BTG 502 binding in this study can now explain both common and distinct aspects of the binding and action of BTX and BTG 502. Like BTX, BTG 502 binds to open channels, probably entering from the cytoplasmic side. The agonistic effect of BTG 502 when applied to sodium channels in combination with scorpion toxin (Ottea, Payne et al. 1989) suggests that BTG 502 stabilizes the open conformation of Na^+ channels. Whereas BTX induces persistent activation by providing a hydrophilic path for the permeating ions (Du, Garden et al. 2011), the hydrophobic linker between the naphthalene and alkylamide ends of BTG 502 protrudes in the pore lumen (Fig. 4.4) thus obscuring the ion conducting path and reducing the amplitude of peak sodium current (Fig. 4.2D). Interestingly, BTG 502 increased the amplitude of peak current of several mutant channels (Fig. 4.2E, F). These results suggest that BTG 502 can bind to the $F^{3i17}A$ and $L^{3i19}A$ mutant channels without obstructing the pore lumen. Further mutational analysis and molecular modeling of BTG 502 with the mutants will be needed to investigate the molecular basis of this agonistic effect.

Our model also provides an explanation for the antagonism of the action of deltamethrin by BTG 502 and suggests direct competition between the two toxins for their overlapping receptor sites. It appears that occupation of the receptor site of BTG 502 is sufficient for the antagonism of the activity of deltamethrin because DAP 1855, an inactive analog of BTG 502, also antagonized the action of deltamethrin (Fig. 4.3B). Interestingly, of the three residues important for pyrethroid activity which are predicted to make contact with BTG 502, only F^{3i17}, and not I^{3i12} or F^{3i16}, is essential for antagonism of the action of deltamethrin by BTG 502.

Similarly, residues S^{3i15}, L^{3i19}, and F^{4i15}, which face the pore and contribute to BTX binding, are all required for BTG 502 to antagonize the deltamethrin action. These results suggest that F^{3i17}, S^{3i15}, L^{3i19}, and F^{4i15} are essential for the binding of BTG 502, whereas I^{3i12} or F^{3i16} may play accessory roles in BTG 502 binding and/or action.

According to our model, the putative gating hinge residue G^{3i14} in the middle of IIIS6 is not located within any of the predicted receptor sites for pyrethroids, BTG 502 or BTX. However, it is intriguing that G^{3i14} is critical for actions of three sodium channel toxins, BTG 502 (this study), deltamethrin (Du, Lee et al. 2009) and BTX (Du, Garden et al. 2011). Previously we showed that G^{3i14}A substitution caused a positive shift in the voltage-dependence of activation (Du, Lee et al. 2009), indicating that the mutant channel prefers closed states and that greater depolarization is needed to activate the channel. We speculate that this gating alteration could provide a basis for the observed involvement of G^{3i14} in the actions of BTX, deltamethrin, and BTG 502, because all three toxins require open channels for action. The mutation G^{3i14}A could alter the positions of other toxin-sensing residues forming a high affinity receptor site. Alternatively, the mutation of the gating hinge may affect the coupling of toxin binding and subsequent gating modifications induced by the toxin.

In summary, using a combination of mutational analyses and computer modeling our study provides insights into the molecular action of BTG 502 (a unique partial antagonist) on the sodium channel and its antagonism on the actions of two well-known classes of sodium channel toxins (i.e., BTX and pyrethroids). Our results emphasize the importance of the pore-forming S6 of domain III and its gating hinge in the binding and actions of three distinct classes of sodium channel neurotoxins.

Supplementary Data

Batrachotoxin, Pyrethroids and BTG 502 Share Overlapping Binding Sites On Insect Sodium Channels

Yuzhe Du*, Daniel Garden*, Bhupinder Khambay, Boris S. Zhorov and Ke Dong

Table S4.1. **Distance constraints that were used for BTG 502 docking** to impose proximity of experimentally determined BTG 502 sensing residues with indicated BTG 502 moieties.

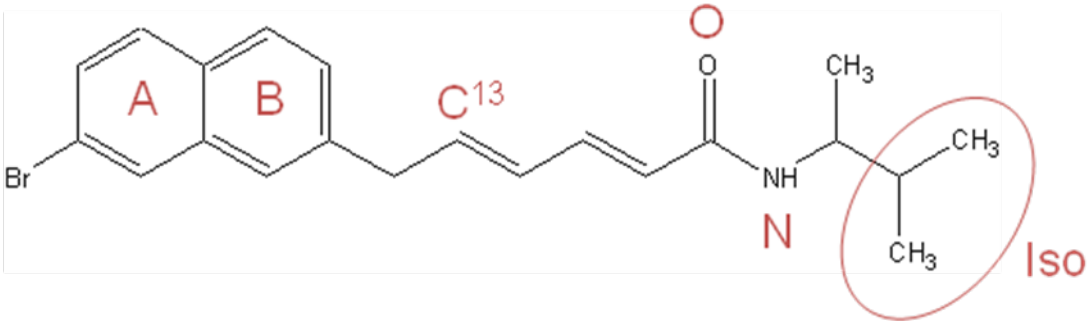

Binding Mode	BTG sensing residue						
	I^{3i12}	G^{3i14}	S^{3i15}	F^{3i16}	F^{3i17}	L^{3i19}	F^{4i15}
1	Iso						
2	A						
3	B						
4				Iso			
5				A			
6				B			
7					A		
8					B		
9							A
10							B
11						C13	
12	Iso						A
13	Iso						B
14	Iso				A		
15			N				
16			O				
17			N		A		
18			O				A
19	Iso		O				
20	Iso		N				
21	Iso					C13	
22						Iso	
23				A		Iso	
24	A					Iso	
25	A		O				
26				A		C13	
27							Iso
28				A			Iso
29	A						Iso
30	A				Iso		

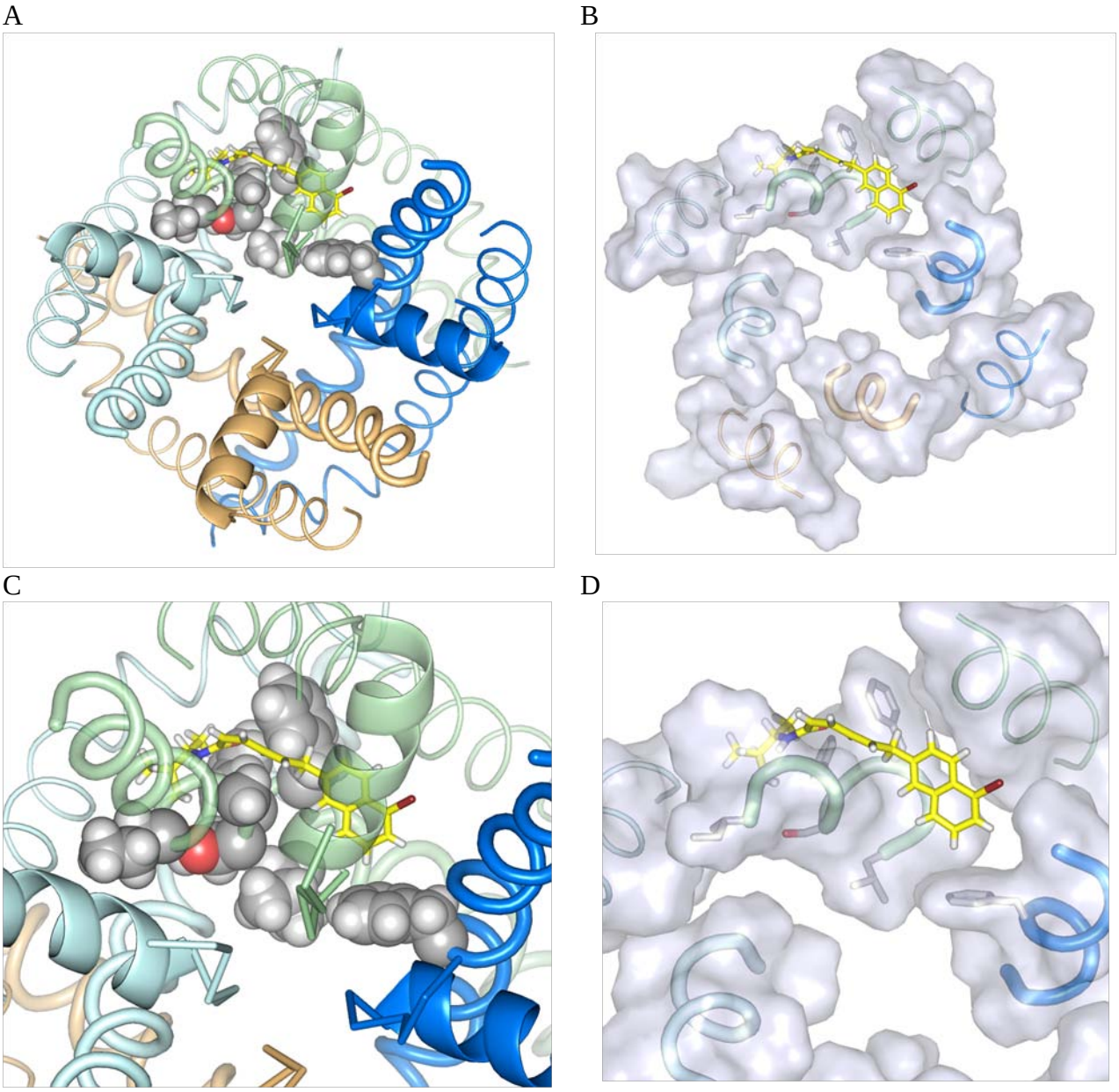

FIGURE S4.1. (***A, B***) **An alternative binding mode of BTG 502**. The toxin wraps around the IIIS6 helix, exposes its linker towards the lipids, and established contacts with all known BTG 502 sensing residues, except S^{3i15}. However, the toxin-channel binding energy in this mode is lower than in the binding mode shown in Fig. 4.4 where BTG 502 wraps around IIIS6 and exposes its linker to the inner pore. (***C, D***) The zoomed views. The bulky naphthalene ring binds between helices IIIS5 and IIIS6 and the isopropyl group binds between IIS5 and IIIS6.

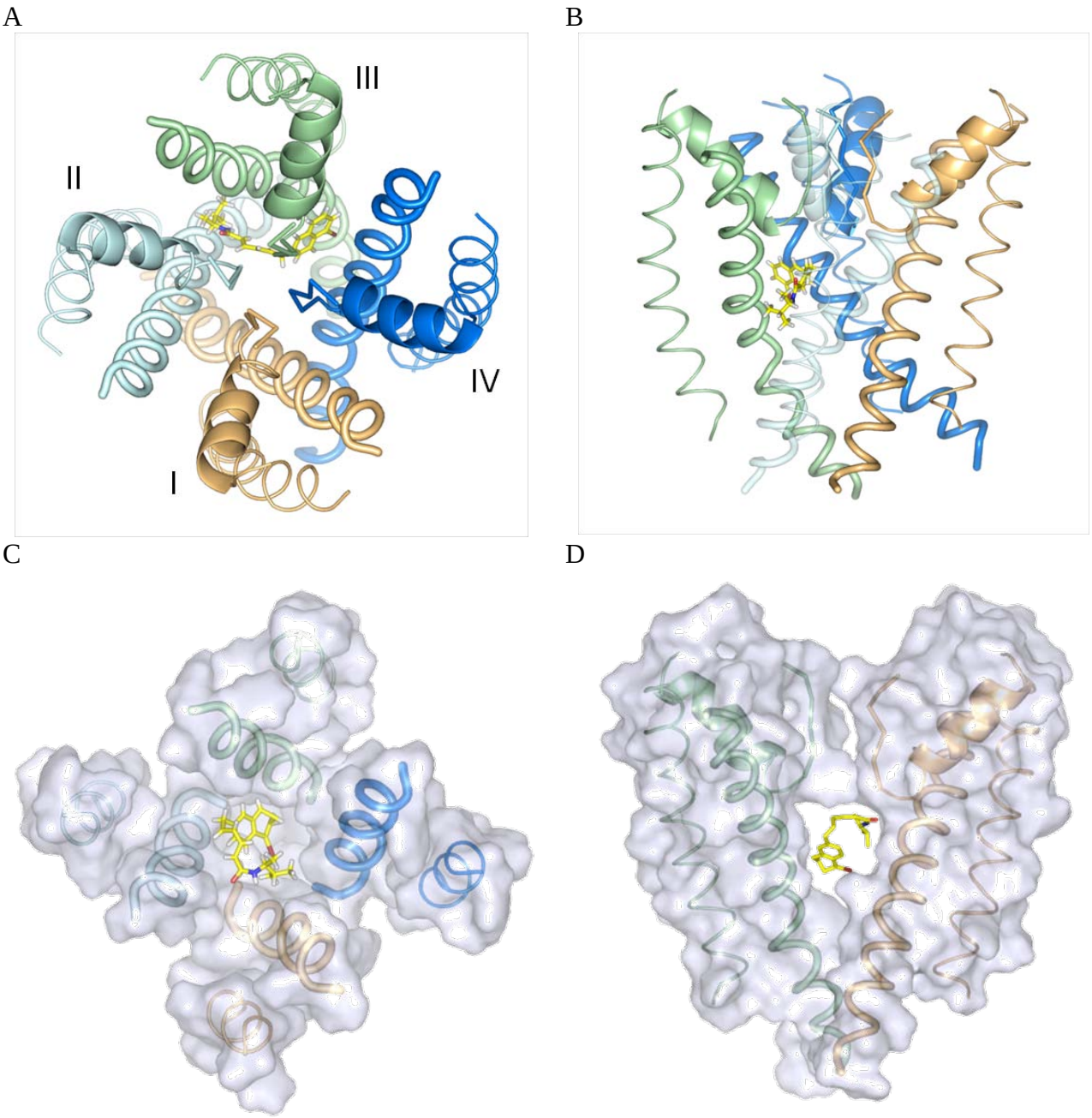

FIGURE S4.2. **The closed-channel KcsA-based models of BgNav1.1 with BTG 502.** (***A***) When ligand-channel constraints were applied to keep BTG 502 in the binding mode predicted for the open channel (Fig. 4.4), strong toxin-channel repulsions were found indicating that the toxin in this binding mode would resist the channel deactivation. (***B***) In the MC-minimized structure with the constrained ligand, helix IIIS6 (green) bent significantly as compared to IS6 (orange) to accommodate the ligand. (***C, D***) Top and side views at the BTG 502 binding modes predicted by MC-minimizations in the absence of channel-toxin constraints. The ligand relocated from the starting position (A) to the central cavity and adopted a folded conformation.

CHAPTER FIVE

SUMMARY AND PERSPECTIVE

Voltage gated ion channels are pharmaceutically important drug targets for treating pain, epilepsy and other disorders related to the nervous system. As well, many of the most potent toxins known have evolved to irreversibly block/activate these channels. Although these compounds have been studied in great detail, the atomistic mechanisms of action of many drugs and toxins are poorly understood. This study used molecular modeling techniques to explore how three compounds, BTX, BTG 502 and deltamethrin, bind to a voltage gated Na^+ channel, modify the channel kinetics and the interactions between the compounds themselves.

Developing docking methodology

The first attempt at large scale, unbiased, flexible ligand docking on an examining set of 60 high resolution crystal structures yielded a success rate lower than was anticipated. Evaluating the energetics of the x-ray structure compared to the best predicted structure revealed a large discrepancy between the desolvation and electrostatic energies. Traditional electrostatic energy calculations employ a Distance-Dependent Dielectric function ($\varepsilon = kr$), causing the interaction energy to vary only with respect to the distance between the charges. We found this to be an oversimplification and that the environment of the charges should be accounted for in the dielectric function. This prompted the development of our Solvent Exposure- and Distance-Dependent Dielectric function, which varies the dielectric between a lower ($2r$) and higher ($8r$) limit depending on the degree of exposure of the 2 charges. Docking the examining set using the SEDDD function resulted in an absolute increase of 20% in the success rate over the best performing DDD function. A final success rate of 58.3% was achieved for unbiased flexible ligand docking and a success rate of 78.3% when the library of ligand conformers was enriched with the ligand conformation taken from the x-structure of the respective ligand-protein

complex. This indicates that if the library of ligand conformers contains at least one "biologically active" conformer, the success rate can be further improved by another ~20%. Therefore, the next major goals should be directed towards accurately predicting biologically active ligand conformations in the absence of the protein.

Predicting the binding site and mode of batrachotoxin (BTX)

Batrachotoxin, a Na^+ channel agonist, is the most potent animal toxin currently known. Due to its irreversible binding, BTX is a commonly used tool in electrophysiology to study the kinetics of ion channels. In this work, we proposed a novel binding mode for BTX, using a homology model of BgNav1-1, our docking protocol and distance constraints derived from existing experimental data and novel data provided by our collaborators. In the model, BTX adopts a horseshoe conformation in the center of the pore and is able to form specific interactions with all the known BTX sensing residues. In this conformation, BTX oxygen atoms face towards the pore axis, while the hydrophobic steroidal core contacts the inner cavity walls. Thus, BTX creates a ring similar to the selectivity filter, which is wide enough to allow for Na^+ ions to pass through. The most noteworthy ligand-channel contact is the cation-π interaction between F^{3i16} and the quaternary ammonium group from BTX, which allows the positively charged group to be bind in the DII/DIII interface. Without this, the positive charge would likely position itself in the center of the cavity to allow for favourable interactions with water, however would be in the permeation pathway of the positively changed Na^+ ions as well. This binding mode also explains the mechanism of persistent activation of the channel by BTX. Since the channel-free conformation of BTX is a bit wider than the inner pore, the bound toxin imposes centrifugal

forces on inner helices of the channel. In addition, electrostatic repulsion between the inward facing oxygen atoms of BTX resists closure of the BTX-bound channels.

Exploring the mechanism of a partial agonist BTG 502

We further studied toxin action on the Nav channel BgNav1-1, exploring the binding mode and mechanism of action of the state-dependent, partial agonist BTG 502 and its interaction with a pyrethroid agonist, deltamethin. Our collaborators identified several BTG 502 sensing residues in IIIS6. Interestingly some of these residues contribute to the receptors for BTX and deltamethrin. The binding site for BTG 502 was predicted using our docking methodology with distance constraints, which were derived from experimental data. BTG 502 was proposed to wrap around the IIIS6 helix and extend its distal ends into the II/III and III/IV domain interfaces. This binding mode was able to account for specific contacts of the ligand with residues, which are buried in domain interfaces as well as with residues which face the inner pore. Comparing the predicted binding sites of BTX and BTG 502, the high degree of their overlap would preclude both toxins from binding simultaneously, which is consistent with experimental data from our collaborators. Deltamethrin is proposed to bind in the IIL45-IIS5-IIIS6 cavity between domains II and III, and the overlap of the deltamethrin binding site with that of BTG 502 is significantly smaller than between BTG 502 and BTX. Deltamethrin is able to reach from the lipid exposed side of the pore domain and expose its terminal bromine group in to water filled inner cavity. In a sodium channel first treated by deltamethrin followed by BTG 502, BTG 502 would be unable to extend one arm into the II/III interface and thus would re-orient back towards the pore axis. Unlike the channel-bound BTX whose oxygen atoms faced towards the pore axis, the pore-exposed groups of the channel-bound BTG 502 are primarily

hydrophobic; they would resist the current of Na ions. This explains the partial-antagonist behavior of BTG 502 applied to the channels in combination with deltamethrin. To explain the agonistic behavior of BTG 502, we forced the channel to transition towards its closed conformation while pinning BTG 502 in its open-state bound conformation. The terminal groups of BTG 502 wrapped around IIIS6, prevented the narrowing of the adjacent S6 helices resisting the activation-gate closure. As a result, kinking of in IIS6, IVS6 and most notably IIIS6 were observed during our *in-silico* deactivation of the BTG 502 bound channel. Another experiment on *in-silico* channel deactivation without pinning BTG 502 to the channel, forces-out the toxin from its binding site; the ligand adopted a folded conformation in the center of the pore and was trapped in the close state.

Perspective Studies

Ion channels activate in response to changes in membrane potential and allow ions to pass through the channel across the membrane. Several K+ channels have been crystallized in either the open or closed state. This raises questions about the conformations of the non-crystallized state. Currently only NaK has been crystallized in both states, however, large parts of the channel were truncated to crystallize it in the open conformation (Shi, Ye et al. 2006; Alam and Jiang 2009). As well, there are several KcsA crystal structures available, which are believed to represent intermediate states towards the open conformation. For the remaining channels, in the absence of experimental data, homology modeling can be used in an attempt to simulate the large scale conformational transitions upon the gating.

I have performed preliminary *in-silico* gating of K+ channels using available x-ray structures (KcsA, MthK, KvAP, Kv1.2 and NaK). For ligand-gated channels (NaK, KcsA and

MthK), centripetal or centrifugal forces were applied to the C-terminal C^{α} of M2 (inner helix) to open or close the channel respectively. For voltage-gated channels (KvAP and Kv1.2), clockwise or counter-clockwise torque forces were applied to the N-terminal C^{α} atom of the S4-S5 linker (Garden, Bruhova et al. 2010).

The gating simulations were able to predict destination structures with low RMSD versus experimental structures. We observed significant and reproducible (in simulations with different random number seeds) differences in the energy of the open and closed conformations. Voltage gated channels appear to favour the open state, and conversely, ligand gated channels favour the closed state. This is consistent with the state in which the channels were crystallized. Partitioning energy of the closed and open channels by individual residues may suggest mutations, that would stabilize or destabilize a particular state and thus help crystallize a channel in different conformations. For example, partitioning the KcsA channel energy in both states by individual residues predicted that His25 in the outer helix experiences the largest energy change during gating and thus plays a critical role in gating. In the open conformation, it is involved in a series of hydrogen bonds with Glu118 and Glu120 residues on the cytoplasmic side of the inner helix. Upon channel closing, the inner helices straighten, breaking these interactions. These results are consistent with experiments in which mutations of His25 or Glu118 and Glu120 deprive the pH sensitivity of the channels and yield constitutively active channels (Thompson, Posson et al. 2008).

Continuation of this study should reveal similar residues in other channels, which will be proposed to collaborators as potential mutations that may affect the probability and stability of the open/closed states.

Conclusion

The work described in this thesis presents the opportunity to explore the effect of other state-dependent ligands on the gating kinetics of various ion channels through molecular modeling. The initial progress with *in-silico* activation and deactivation has yielded gating models for several K^+ channels. These models can be tested by mutating residues which stabilize or destabilize particular states. The thoroughly tested docking protocol can be applied to model drugs binding to different channel conformations, including intermediate states.

REFERENCES

Abagyan, R. and M. Totrov (2001). "High-throughput docking for lead generation." Curr Opin Chem Biol **5**(4): 375-82.

Ahern, C. A. and R. Horn (2004). "Stirring up controversy with a voltage sensor paddle." Trends Neurosci **27**(6): 303-7.

Alam, A. and Y. Jiang (2009). "High-resolution structure of the open NaK channel." Nat Struct Mol Biol **16**(1): 30-4.

Alam, A. and Y. Jiang (2009). "Structural analysis of ion selectivity in the NaK channel." Nat Struct Mol Biol **16**(1): 35-41.

Augspurger, J. D. and H. A. Scheraga (1996). "An efficient, differentiable hydration potential for peptides and proteins." J Comput Chem **17**(13): 1549-58.

Behrens, M. I., A. Oberhauser, et al. (1989). "Batrachotoxin-modified sodium channels from squid optic nerve in planar bilayers. Ion conduction and gating properties." J Gen Physiol **93**(1): 23-41.

Berman, H. M., J. Westbrook, et al. (2000). "The Protein Data Bank." Nucleic Acids Res **28**(1): 235-42.

Bezanilla, F. (2000). "The voltage sensor in voltage-dependent ion channels." Physiol Rev **80**(2): 555-92.

Bezanilla, F. (2002). "Voltage sensor movements." J Gen Physiol **120**(4): 465-73.

Bezanilla, F. (2005). "Voltage-gated ion channels." IEEE Trans Nanobioscience **4**(1): 34-48.

Blanchet, J., S. X. Lin, et al. (2005). "Mapping of steroids binding to 17 beta-hydroxysteroid dehydrogenase type 1 using Monte Carlo energy minimization reveals alternative binding modes." Biochemistry **44**: 7218-7227.

Bloomquist, J. R. (1996). "Ion channels as targets for insecticides." Annu Rev Entomol **41**: 163-90.

Bockris, J. O. and A. K. N. Reddy (1977). Modern Electrochemistry. New York, Plenum Press.

Brooks, B. R., R. E. Bruccoleri, et al. (1983). "CHARMM: a program for macromolecular energy minimization and dynamics calculations." J Comput Chem **4**: 187–217.

Brooks, C. L., B. M. Pettitt, et al. (1985). "Structural and energetic effects of truncating long ranged interactions in ionic polar fluids." J Chem Phys **83**: 5897-5908.

Brown, G. B. (1988). "Batrachotoxin: a window on the allosteric nature of the voltage-sensitive sodium channel." Int Rev Neurobiol **29**: 77-116.

Bruhova, I., D. B. Tikhonov, et al. (2008). "Access and binding of local anesthetics in the closed sodium channel." Mol Pharmacol **74**(4): 1033-45.

Bruhova, I. and B. S. Zhorov (2007). "Monte Carlo-energy minimization of correolide in the Kv1.3 channel: possible role of potassium ion in ligand-receptor interactions." BMC Struct Biol **7**: 5.

Bruhova, I. and B. S. Zhorov (2010). "A homology model of the pore domain of a voltage-gated calcium channel is consistent with available SCAM data." J Gen Physiol **135**(3): 261-74.

Bursulaya, B. D., M. Totrov, et al. (2003). "Comparative study of several algorithms for flexible ligand docking." J Comput Aided Mol Des **17**(11): 755-63.

Canutescu, A. A., A. A. Shelenkov, et al. (2003). "A graph-theory algorithm for rapid protein side-chain prediction." Protein Sci **12**(9): 2001-14.

Catterall, W. A. (1977). "Activation of the action potential Na+ ionophore by neurotoxins. An allosteric model." J Biol Chem **252**(23): 8669-76.

Catterall, W. A. (1986). "Molecular properties of voltage-sensitive sodium channels." Annu Rev Biochem **55**: 953-85.

Catterall, W. A. (2000). "From ionic currents to molecular mechanisms: the structure and function of voltage-gated sodium channels." Neuron **26**(1): 13-25.

Catterall, W. A. (2001). "Physiology. A one-domain voltage-gated sodium channel in bacteria." Science **294**(5550): 2306-8.

Cavasotto, C. N. and R. A. Abagyan (2004). "Protein flexibility in ligand docking and virtual screening to protein kinases." J Mol Biol **337**(1): 209-25.

Cavasotto, C. N., A. J. Orry, et al. (2003). "Structure-based identification of binding sites, native ligands and potential inhibitors for G-protein coupled receptors." Proteins **51**(3): 423-33.

Chanda, B., O. K. Asamoah, et al. (2005). "Gating charge displacement in voltage-gated ion channels involves limited transmembrane movement." Nature **436**(7052): 852-6.

Chandy, K. G. and G. A. Gutman (1993). "Nomenclature for mammalian potassium channel genes." Trends Pharmacol Sci **14**(12): 434.

Cheng, R. C., D. B. Tikhonov, et al. (2009). "Structural model for phenylalkylamine binding to L-type calcium channels." J Biol Chem **284**(41): 28332-42.

Cordero-Morales, J. F., V. Jogini, et al. (2007). "Molecular driving forces determining potassium channel slow inactivation." Nat Struct Mol Biol **14**(11): 1062-9.

Correa, A. M., R. Latorre, et al. (1991). "Ion permeation in normal and batrachotoxin-modified Na+ channels in the squid giant axon." J Gen Physiol **97**(3): 605-25.

Daly, J. W., B. Witkop, et al. (1965). "Batrachotoxin. The active principle of the Colombian arrow poison frog, Phyllobates bicolor." J Am Chem Soc **87**(1): 124-6.

Davies, T. G., L. M. Field, et al. (2007). "DDT, pyrethrins, pyrethroids and insect sodium channels." IUBMB Life **59**(3): 151-62.

Dewar, M. J., E. G. Zoebisch, et al. (1985). "Development and use of quantum mechanical molecular models. 76. AM1: a new general purpose quantum mechanical molecular model." J. Amer. Chem. Soc. **107**(13): 3902-3909.

Dewar, M. J. S., E. G. Zoebisch, et al. (1985). "AM1: A New General Purpose Quantum Mechanical Model." J. Am. Chem. Soc. **107**: 3902-3909.

Dominy, B. N. and C. L. Brooks (1999). "Development of a Generalized Born Model Parametrization for Proteins and Nucleic Acids." J Phys Chem **103**(18): 3765-3773.

Dong, K. (2007). "Insect sodium channels and insecticide resistance." Invert Neurosci **7**(1): 17-30.

Doyle, D. A., J. Morais Cabral, et al. (1998). "The structure of the potassium channel: molecular basis of K+ conduction and selectivity." Science **280**(5360): 69-77.

Doyle, D. A., J. Morais Cabral, et al. (1998). "The structure of the potassium channel: molecular basis of K+ conduction and selectivity." Science **280**(5360): 69-77.

Du, Y., D. Garden, et al. (2011). "Identification of new batrachotoxin-sensing residues in segment IIIS6 of sodium channel." J. Biol. Chem. **Submitted**.

Du, Y., B. Khambay, et al. (2011). "An important role of a pyrethroid sensing residue F1519 in IIIS6 in the action of an alkylamide insecticide BTG 502 on the cockroach sodium channel." Insect Biochem. Molec. Biol. **Sumbitted**.

Du, Y., J. E. Lee, et al. (2009). "Identification of a cluster of residues in transmembrane segment 6 of domain III of the cockroach sodium channel essential for the action of pyrethroid insecticides." Biochem J **419**(2): 377-85.

Durell, S. R., I. H. Shrivastava, et al. (2004). "Models of the structure and voltage-gating mechanism of the shaker K+ channel." Biophys J **87**(4): 2116-30.

Egan, W. J., W. P. Walters, et al. (2002). "Guiding molecules towards drug-likeness." Curr Opin Drug Discov Devel **5**(4): 540-9.

Elliott, M. (1977). Synthetic pyrethroids. Washington, DC, In Synthetic Pyrethroids (ACS Symposium Series No. 42).

Ertel, E. A., K. P. Campbell, et al. (2000). "Nomenclature of voltage-gated calcium channels." Neuron **25**(3): 533-5.

Ewing, T. J., S. Makino, et al. (2001). "DOCK 4.0: search strategies for automated molecular docking of flexible molecule databases." J Comput Aided Mol Des **15**(5): 411-28.

Feng, G., P. Deák, et al. (1995). "Cloning and functional analysis of TipE, a novel membrane protein that enhances Drosophila para sodium channel function." Cell **82**(6): 1001-11.

Ferrara, P., H. Gohlke, et al. (2004). "Assessing scoring functions for protein-ligand interactions." J Med Chem **47**(12): 3032-47.

Finkelstein, A. V. and O. Ptitsyn (2002). Protein physics, Academic Press

Fogolari, F., P. Zuccato, et al. (1999). "Biomolecular electrostatics with the linearized Poisson-Boltzmann equation." Biophys J **76**(1 Pt 1): 1-16.

Friesner, R. A., J. L. Banks, et al. (2004). "Glide: a new approach for rapid, accurate docking and scoring. 1. Method and assessment of docking accuracy." J Med Chem **47**(7): 1739-49.

Gandhi, C. S. and E. Y. Isacoff (2002). "Molecular models of voltage sensing." J Gen Physiol **120**(4): 455-63.

Garber, S. S. and C. Miller (1987). "Single Na+ channels activated by veratridine and batrachotoxin." J Gen Physiol **89**(3): 459-80.

Garden, D. P., I. Bruhova, et al. (2010). "In-Silico Activation and Deactivation of the Pore Domains of Voltage- and Ligand-Gated Ion Channels." Biophys J **98**(3): 1.

Garden, D. P. and B. S. Zhorov (2010). "Docking flexible ligands in proteins with a solvent exposure- and distance-dependent dielectric function." J Comput Aided Mol Des **24**(2): 91-105.

Garrett M. Morris, D. S. Goodsell, et al. (1998). "Automated docking using a Lamarckian genetic algorithm and an empirical binding free energy function." J Comput Chem **19**(14): 1639-1662.

Gelpi, J. L., S. G. Kalko, et al. (2001). "Classical molecular interaction potentials: improved setup procedure in molecular dynamics simulations of proteins." Proteins **45**(4): 428-37.

Gilson, M. K. (1995). "Theory of electrostatic interactions in macromolecules." Curr Opin Struct Biol **5**(2): 216-23.

Gilson, M. K. and H. X. Zhou (2007). "Calculation of protein-ligand binding affinities." Annu Rev Biophys Biomol Struct **36**: 21-42.

Gohlke, H. and G. Klebe (2002). "Approaches to the description and prediction of the binding affinity of small-molecule ligands to macromolecular receptors." Angew Chem Int Ed Engl **41**(15): 2644-76.

Goldin, A. L., R. L. Barchi, et al. (2000). "Nomenclature of voltage-gated sodium channels." Neuron **28**(2): 365-8.

Goodsell, D. S., G. M. Morris, et al. (1996). "Automated docking of flexible ligands: applications of AutoDock." J Mol Recognit **9**(1): 1-5.

Guy, H. R. and P. Seetharamulu (1986). "Molecular model of the action potential sodium channel." Proc Natl Acad Sci U S A **83**(2): 508-12.

Hassan, S. A. (2007). "Liquid-structure forces and electrostatic modulation of biomolecular interactions in solution." J Phys Chem B **111**(1): 227-41.

Heginbotham, C. (1994). "Some versions of joint commissioning." Bmj **309**(6949): 215-6.

Heginbotham, L., Z. Lu, et al. (1994). "Mutations in the K+ channel signature sequence." Biophys J **66**(4): 1061-7.

Heinemann, S. H., H. Terlau, et al. (1992). "Calcium channel characteristics conferred on the sodium channel by single mutations." Nature **356**(6368): 441-3.

Hille, B. (2001). Ion Channels of Excitable membranes. Sunderland, MA, USA., Sinauer Associates Inc.

Honig, B. and A. Nicholls (1995). "Classical electrostatics in biology and chemistry." Science **268**(5214): 1144-9.

Hopfinger, A. J. and R. D. Battershell (1976). "Application of SCAP to drug design. 1. Prediction of octanol-water partition coefficients using solvent-dependent conformational analyses." J Med Chem **19**(5): 569-73.

Huang, L. Y., W. A. Catterall, et al. (1979). "Comparison of ionic selectivity of batrachotoxin-activated channels with different tetrodotoxin dissociation constants." J Gen Physiol **73**(6): 839-54.

Huang, L. Y., N. Moran, et al. (1984). "Gating kinetics of batrachotoxin-modified sodium channels in neuroblastoma cells determined from single-channel measurements." Biophys J **45**(1): 313-22.

Jiang, Y., A. Lee, et al. (2002). "Crystal structure and mechanism of a calcium-gated potassium channel." Nature **417**(6888): 515-22.

Jiang, Y., A. Lee, et al. (2002). "The open pore conformation of potassium channels." Nature **417**(6888): 523-6.

Jiang, Y., A. Lee, et al. (2003). "X-ray structure of a voltage-dependent K+ channel." Nature **423**(6935): 33-41.

Jiang, Y., V. Ruta, et al. (2003). "The principle of gating charge movement in a voltage-dependent K+ channel." Nature **423**(6935): 42-8.

Jones, G., P. Willett, et al. (1997). "Development and validation of a genetic algorithm for flexible docking." J Mol Biol **267**(3): 727-48.

Jorov, A., B. S. Zhorov, et al. (2004). "Theoretical study of interaction of winter flounder antifreeze protein with ice." Protein Sci **13**(6): 1524-37.

Kaczorowski, G. J. and M. L. Garcia (1999). "Pharmacology of voltage-gated and calcium-activated potassium channels." Curr Opin Chem Biol **3**(4): 448-58.

Keynes, R. D. and F. Elinder (1999). "The screw-helical voltage gating of ion channels." Proc Biol Sci **266**(1421): 843-52.

Khodorov, B. I. and S. V. Revenko (1979). "Further analysis of the mechanisms of action of batrachotoxin on the membrane of myelinated nerve." Neuroscience **4**(9): 1315-30.

Khodorov, B. I., E. A. Yelin, et al. (1992). "Comparative analysis of the effects of synthetic derivatives of batrachotoxin on sodium currents in frog node of Ranvier." Cell Mol Neurobiol **12**(1): 59-81.

Laskowski, R. A., E. G. Hutchinson, et al. (1997). "PDBsum: a Web-based database of summaries and analyses of all PDB structures." Trends Biochem Sci **22**(12): 488-90.

Lazaridis, T. and M. Karplus (1999). "Effective energy function for proteins in solution." Proteins **35**(2): 133-52.

Lecar, H., H. P. Larsson, et al. (2003). "Electrostatic model of S4 motion in voltage-gated ion channels." Biophys J **85**(5): 2854-64.

Lee, S. Y., A. Lee, et al. (2005). "Structure of the KvAP voltage-dependent K+ channel and its dependence on the lipid membrane." Proc Natl Acad Sci U S A **102**(43): 15441-6.

Li, H. L., D. Hadid, et al. (2002). "The batrachotoxin receptor on the voltage-gated sodium channel is guarded by the channel activation gate." Mol Pharmacol **61**(4): 905-12.

Li, Z. and H. A. Scheraga (1987). "Monte Carlo-minimization approach to the multiple-minima problem in protein folding." Proc Natl Acad Sci U S A **84**(19): 6611-5.

Linford, N. J., A. R. Cantrell, et al. (1998). "Interaction of batrachotoxin with the local anesthetic receptor site in transmembrane segment IVS6 of the voltage-gated sodium channel." Proc Natl Acad Sci U S A **95**(23): 13947-52.

Lipkind, G. M. and H. A. Fozzard (2005). "Molecular modeling of local anesthetic drug binding by voltage-gated sodium channels." Mol Pharmacol **68**(6): 1611-22.

Long, S. B., E. B. Campbell, et al. (2005). "Crystal structure of a mammalian voltage-dependent Shaker family K+ channel." Science **309**(5736): 897-903.

Long, S. B., E. B. Campbell, et al. (2005). "Voltage sensor of Kv1.2: structural basis of electromechanical coupling." Science **309**(5736): 903-8.

Lu, Z., A. M. Klem, et al. (2002). "Coupling between voltage sensors and activation gate in voltage-gated K+ channels." J Gen Physiol **120**(5): 663-76.

Mallik, B., A. Masunov, et al. (2002). "Distance and exposure dependent effective dielectric function." J Comput Chem **23**(11): 1090-9.

McCammon, J. A., P. G. Wolynes, et al. (1979). "Picosecond dynamics of tyrosine side chains in proteins." Biochemistry **18**(6): 927-42.

McInnes, C. (2007). "Virtual screening strategies in drug discovery." Curr Opin Chem Biol **11**(5): 494-502.

Mehler, E. L. and T. Solmajer (1991). "Electrostatic effects in proteins: comparison of dielectric and charge models." Protein Eng **4**(8): 903-10.

Meiler, J. and D. Baker (2006). "ROSETTALIGAND: protein-small molecule docking with full side-chain flexibility." Proteins **65**(3): 538-48.

Momany, F. A., R. F. McGuire, et al. (1975). "Energy parameters in polypeptides. VII. Geometric parameters, partial atomic charges, nonbonded interactions, hydrogen bond interactions, and intrinsic torsional potentials of the naturally occurring amino acids." J Phys Chem **79**: 2361-2381.

Morreale, A., R. Gil-Redondo, et al. (2007). "A new implicit solvent model for protein-ligand docking." Proteins **67**(3): 606-16.

Morris, G. M., D. S. Goodsell, et al. (1996). "Distributed automated docking of flexible ligands to proteins: parallel applications of AutoDock 2.4." J Comput Aided Mol Des **10**(4): 293-304.

Mozhaeva, G. N., A. P. Naumov, et al. (1983). "[Selectivity and sensitivity to blocking by hydrogen ions of batrachotoxin-modified sodium channels in nerve fiber membranes]." Neirofiziologiia **15**(6): 571-9.

Narahashi, T. (2000). "Neuroreceptors and ion channels as the basis for drug action: past, present, and future." J Pharmacol Exp Ther **294**(1): 1-26.

O'Reilly, A. O., B. P. Khambay, et al. (2006). "Modelling insecticide-binding sites in the voltage-gated sodium channel." Biochem J **396**(2): 255-63.

Ottea, J. A., G. T. Payne, et al. (1989). "Activation of sodium channels and inhibition of [3H]batrachotoxinin A-20-alpha-benzoate binding by an N-alkylamide neurotoxin." Mol Pharmacol **36**(2): 280-4.

Perola, E., W. P. Walters, et al. (2004). "A detailed comparison of current docking and scoring methods on systems of pharmaceutical relevance." Proteins **56**(2): 235-49.

Quandt, F. N. and T. Narahashi (1982). "Modification of single Na+ channels by batrachotoxin." Proc Natl Acad Sci U S A **79**(21): 6732-6736.

Rarey, M., B. Kramer, et al. (1996). "A fast flexible docking method using an incremental construction algorithm." J Mol Biol **261**(3): 470-89.

Ren, D., B. Navarro, et al. (2001). "A prokaryotic voltage-gated sodium channel." Science **294**(5550): 2372-5.

Revenko, S. V. and B. I. Khodorov (1977). "[Effect of batrachotoxin on the selectivity of sodium channels in the membrane of a myelinated nerve fiber]." Neirofiziologiia **9**(3): 313-6.

Rubinstein, A. and S. Sherman (2007). "Evaluation of the influence of the internal aqueous solvent structure on electrostatic interactions at the protein-solvent interface by nonlocal continuum electrostatic approach." Biopolymers **87**(2-3): 149-64.

Sato, C., Y. Ueno, et al. (2001). "The voltage-sensitive sodium channel is a bell-shaped molecule with several cavities." Nature **409**(6823): 1047-51.

Shi, N., S. Ye, et al. (2006). "Atomic structure of a Na+- and K+-conducting channel." Nature **440**(7083): 570-4.

Silver, K. S., Y. Nomura, et al. (2009). "Role of the sixth transmembrane segment of domain IV of the cockroach sodium channel in the action of sodium channel blocker insecticides." Neurotoxicology. **30**(4): 613-21.

Soderlund, D. M. (2005). Sodium channels :Comprehensive Molecular Insect Science. New York, Elsevier.

Song, W., Z. Liu, et al. (2004). "RNA editing generates tissue-specific sodium channels with distinct gating properties.
." J Biol Chem **279**(31): 32554-61.

Starace, D. M. and F. Bezanilla (2004). "A proton pore in a potassium channel voltage sensor reveals a focused electric field." Nature **427**(6974): 548-53.

Still, W. C., A. Tempczyk, et al. (1990). "Semianalytical treatment of solvation for molecular mechanics and dynamics." J. Am. Chem. Soc. **112**(16): 6127-6129.

Striessnig, J., M. Grabner, et al. (1998). "Structural basis of drug binding to L Ca2+ channels." Trends Pharmacol Sci **19**(3): 108-15.

Tan, J., Z. Liu, et al. (2002). "Alternative splicing of an insect sodium channel gene generates pharmacologically distinct sodium channels." J Neurosci **22**(13): 5300-9.

Tan, J., Z. Liu, et al. (2002). "Alternative splicing of an insect sodium channel gene generates pharmacologically distinct sodium channels." J Neurosci **22**(13): 5300-9.

Tan, J., Z. Liu, et al. (2005). "Identification of amino acid residues in the insect sodium channel critical for pyrethroid binding." Mol Pharmacol **67**(2): 513-22.

Tatebayashi, H. and T. Narahashi (1994). "Differential mechanism of action of the pyrethroid tetramethrin on tetrodotoxin-sensitive and tetrodotoxin-resistant sodium channels." J Pharmacol Exp Ther **270**(2): 595-603.

Teague, S. J. (2003). "Implications of protein flexibility for drug discovery." Nat Rev Drug Discov **2**(7): 527-41.

Teschke, O., G. Ceotto, et al. (2001). "Interfacial water dielectric-permittivity-profile measurements using atomic force microscopy." Phys Rev E Stat Nonlin Soft Matter Phys **64**(1 Pt 1): 011605.

Thompson, A. N., D. J. Posson, et al. (2008). "Molecular mechanism of pH sensing in KcsA potassium channels." Proc Natl Acad Sci U S A **105**(19): 6900-5.

Tikhonov, D. B., I. Bruhova, et al. (2006). "Atomic determinants of state-dependent block of sodium channels by charged local anesthetics and benzocaine." FEBS Lett **580**(26): 6027-32.

Tikhonov, D. B. and B. S. Zhorov (2005). "Modeling P-loops domain of sodium channel: homology with potassium channels and interaction with ligands." Biophys J **88**(1): 184-97.

Tikhonov, D. B. and B. S. Zhorov (2005). "Sodium channel activators: model of binding inside the pore and a possible mechanism of action." FEBS Lett **579**(20): 4207-12.

Tikhonov, D. B. and B. S. Zhorov (2007). "Sodium channels: ionic model of slow inactivation and state-dependent drug binding." Biophys J **93**(5): 1557-70.

Tikhonov, D. B. and B. S. Zhorov (2007). "Sodium channels: ionic model of slow inactivation and state-dependent drug binding." Biophys J **93**: 1557-1570.

Tombola, F., M. M. Pathak, et al. (2006). "How does voltage open an ion channel?" Annu Rev Cell Dev Biol **22**: 23-52.

Totrov, M. and R. Abagyan (1997). "Flexible protein-ligand docking by global energy optimization in internal coordinates." Proteins **Suppl 1**: 215-20.

Trainer, V. L., G. B. Brown, et al. (1996). "Site of covalent labeling by a photoreactive batrachotoxin derivative near transmembrane segment IS6 of the sodium channel alpha subunit." J Biol Chem **271**(19): 11261-7.

Ulbricht, W. (1969). "The effect of veratridine on excitable membranes of nerve and muscle." Ergeb Physiol **61**: 18-71.

Vedantham, V. and S. C. Cannon (2000). "Rapid and slow voltage-dependent conformational changes in segment IVS6 of voltage-gated Na(+) channels." Biophys J **78**(6): 2943-58.

Venkatarangan, P. and A. J. Hopfinger (1999). "Prediction of ligand-receptor binding thermodynamics by free energy force field three-dimensional quantitative structure-activity relationship analysis: applications to a set of glucose analogue inhibitors of glycogen phosphorylase." J Med Chem **42**(12): 2169-79.

Vijverberg, H. P. and J. van den Bercken (1990). "Neurotoxicological effects and the mode of action of pyrethroid insecticides." Crit Rev Toxicol **21**(2): 105-26.

Wang, J., P. A. Kollman, et al. (1999). "Flexible ligand docking: a multistep strategy approach." Proteins **36**(1): 1-19.

Wang, S. Y., M. Barile, et al. (2001). "Disparate role of Na(+) channel D2-S6 residues in batrachotoxin and local anesthetic action." Mol Pharmacol **59**(5): 1100-7.

Wang, S. Y., J. Mitchell, et al. (2006). "How batrachotoxin modifies the sodium channel permeation pathway: computer modeling and site-directed mutagenesis." Mol Pharmacol **69**(3): 788-95.

Wang, S. Y., C. Nau, et al. (2000). "Residues in Na(+) channel D3-S6 segment modulate both batrachotoxin and local anesthetic affinities." Biophys J **79**(3): 1379-87.

Wang, S. Y., D. B. Tikhonov, et al. (2007). "Irreversible block of cardiac mutant Na+ channels by batrachotoxin." Channels (Austin) **1**(3): 179-88.

Wang, S. Y., D. B. Tikhonov, et al. (2007). "Serine-401 as a batrachotoxin- and local anesthetic-sensing residue in the human cardiac Na+ channel." Pflugers Arch **454**(2): 277-87.

Wang, S. Y. and G. K. Wang (1998). "Point mutations in segment I-S6 render voltage-gated Na+ channels resistant to batrachotoxin." Proc Natl Acad Sci U S A **95**(5): 2653-8.

Wang, S. Y. and G. K. Wang (1999). "Batrachotoxin-resistant Na+ channels derived from point mutations in transmembrane segment D4-S6." Biophys J **76**(6): 3141-9.

Wang, S. Y. and G. K. Wang (2003). "Voltage-gated sodium channels as primary targets of diverse lipid-soluble neurotoxins." Cell Signal **15**(2): 151-9.

Warmke, J. W., R. A. Reenan, et al. (1997). "Functional expression of Drosophila para sodium channels. Modulation by the membrane protein TipE and toxin pharmacology." J Gen Physiol **110**(2): 119-33.

Warmke, J. W., R. A. Reenan, et al. (1997). "Functional expression of Drosophila para sodium channels. Modulation by the membrane protein TipE and toxin pharmacology.
." J Gen Physiol **110**(2): 119-33.

Warnick, J. E., E. X. Albuquerque, et al. (1975). "The pharmacology of batrachotoxin. VII. Structure-activity relationships and the effects of pH." J Pharmacol Exp Ther **193**(1): 232-45.

Warren, G. L., C. W. Andrews, et al. (2006). "A critical assessment of docking programs and scoring functions." J Med Chem **49**(20): 5912-31.

Weiner, S. J., P. A. Kollman, et al. (1984). "A new force field for molecular mechanical simulation of nucleic acids and proteins." J. Am. Chem. Soc. **106**: 765-84.

Weiner, S. J., P. A. Kollman, et al. (1986). "An All Atom Force-Field for Simulations of Proteins and Nucleic-Acids." J. Comput. Chem. **7**(2): 230-252.

Yang, J., P. T. Ellinor, et al. (1993). "Molecular determinants of Ca2+ selectivity and ion permeation in L-type Ca2+ channels." Nature **366**(6451): 158-61.

Zhao, Y., V. Yarov-Yarovoy, et al. (2004). "A gating hinge in Na+ channels; a molecular switch for electrical signaling." Neuron **41**(6): 859-65.

Zhen, X. G., C. Xie, et al. (2005). "Functional architecture of the inner pore of a voltage-gated Ca2+ channel." J Gen Physiol **126**(3): 193-204.

Zhorov, B. (1983). "Vector method for calculating derivatives of the energy deformation of valence angles and torsion energy of complex molecules according to generalized coordinates." J Struct Chem **23**: 649-655.

Zhorov, B. S. (1981). "Vector method for calculating derivatives of energy of atom-atom interactions of complex molecules according to generalized coordiantes." J Struct Chem **22**: 4-8.

Zhorov, B. S. (1981). "Vector method for calculating derivatives of energy of atom-atom interactions of complex molecules according to generalized coordinates." J Struct Chem **22**: 4-8.

Zhorov, B. S. (1983). "Vector method for calculating derivatives of the energy deformation of valence angles and torsion energy of complex molecules according to generalized coordinates." J Struct Chem **23**: 649-655.

Zhorov, B. S. and P. D. Bregestovski (2000). "Modeling chloride channels of glycine and GABA receptors with blockers." Biophys J **78**: A2092.

Zhorov, B. S., E. V. Folkman, et al. (2001). "Homology model of dihydropyridine receptor: implications for L-type Ca(2+) channel modulation by agonists and antagonists." Arch Biochem Biophys **393**(1): 22-41.

Zhorov, B. S. and S. X. Lin (2000). "Monte Carlo-minimized energy profile of estradiol in the ligand-binding tunnel of 17 beta-hydroxysteroid dehydrogenase: atomic mechanisms of steroid recognition." Proteins **38**(4): 414-27.

Zhorov, B. S. and D. B. Tikhonov (2004). "Potassium, sodium, calcium and glutamate-gated channels: pore architecture and ligand action." J Neurochem **88**(4): 782-99.

Zhou, M., J. H. Morais-Cabral, et al. (2001). "Potassium channel receptor site for the inactivation gate and quaternary amine inhibitors." Nature **411**(6838): 657-61.

Zlotkin, E. (1999). "The insect voltage-gated sodium channel as target of insecticides." Annu Rev Entomol **44**: 429-55.